Investigation of infrared hand vein pattern biometrics

Wang, Ling Yu

2008

Wang, L. Y. (2008). Investigation of infrared hand vein pattern biometrics. Doctoral thesis, Nanyang Technological University, Singapore.

https://hdl.handle.net/10356/13583

https://doi.org/10.32657/10356/13583

NANYANG TECHNOLOGICAL UNIVERSITY

INVESTIGATION OF INFRARED HAND VEIN PATTERN BIOMETRICS

WANG LINGYU

SCHOOL OF COMPUTER ENGINEERING

2008

Investigation of Infrared Hand Vein Pattern Biometrics

Wang Lingyu

School of Computer Engineering

A thesis submitted to the Nanyang Technological University
in fulfilment of the requirement for the degree of
Doctor of Philosophy

2008

Acknowledgements

I wish to express my sincere gratitude to my supervisors professor Graham Leedham and professor Siu-Yueng Cho, for their inspiring and knowledgeable guidance, continuous encouragement and patience during the last few years. I am also very grateful to professor Leedham not only for his enormous support in providing the research facilities but also for his valuable advice for my research through out the years. Further more, I would like to give my thanks to professor Leedham and professor Cho for, despite their tight schedule, giving the thesis careful review, detailed comments and valuable advice.

Last but no the least, my thanks go to Ms. Christina Lee, the executive in the Forensics and Security Laboratory, for her kind administrative help and support.

Contents

Acknowledgements i

Abstract vii

List of Figures ix

List of Tables xiii

Acronyms xv

1 Introduction **1**

1.1 Background 1

1.1.1 Properties of Biometrics 1

1.1.2 Operations of a Biometric Identification System (BIS) 2

1.1.3 Evaluation Criteria of BIS 2

1.2 Motivation 5

1.3 Problem Statement 5

1.3.1 Collectibility of Vein Patterns 5

1.3.2 Data Preprocessing 6

1.3.3 Identification of Features 6

1.3.4 The Study on the Discriminative Power of Vein Patterns 7

1.4 Contributions 8

1.5 Publications Resulting from the Research for the Thesis 9

1.6 Organization of this Thesis 11

2 Biometric Technologies **13**

2.1 Physiological Biometrics 14

2.1.1 Face Recognition 14

2.1.2 Fingerprint Recognition 18

2.1.3 Eye Biometrics: Iris and Retina Pattern 21

2.1.4 Hand Geometry 23

2.2 Behaviorial Biometrics 25

2.2.1 Voice Verification 25

2.2.2 Signature Recognition 27

2.3 Other Biometrics 29

2.4 Comparison of Assorted Biometric Technologies 30

2.4.1 A Summary 30

2.4.2 The Developing Trends 31

2.5 Current Development of Vein Pattern Biometrics 33

2.5.1 Overview 33

2.5.2 Data Preparation 34

2.5.3 Processing of the Vein Patterns Images 36

2.5.4 Features Used for Verification 36

2.5.5 Research Issues of Vein Pattern Biometrics 38

2.6 Conclusion and Research Directions 40

2.6.1 Summary and Conclusions 40

2.6.2 Research Directions 40

2.6.3 The Proposed Hand Vein Pattern Biometrics Framework 41

3 Vein Pattern Acquisition Mechanisms **43**

3.1 General Medical Practices 43

3.2 Non-Intrusive Vein Pattern Acquisition 46
3.2.1 Far-Infrared Image Formation 47
3.2.2 Near Infrared Image Formation 52
3.2.3 A Comparison between Far- and Near- Infrared Imaging 56
3.3 The Infrared Hand Vein Pattern Database 58
3.4 Summary 60

4 Preprocessing of Vein Pattern Images 63

4.1 Problem Specification 63
4.2 Defining Region of Interest Invariant to the Size of the Hand 65
4.3 Noise Estimation and Filtering for Vein Pattern Images 67
4.3.1 Sensor Noise 67
4.3.2 Noise Modelling 68
4.3.3 The Local Linear Minimum Mean Square Error Filter 70
4.3.4 The Proposed Filter Parameter Estimation Methodology using Dual Images 73
4.3.5 Experiments with the Proposed Estimation Technique for Image De-noising 75
4.4 Post-processing of the De-noised Vein Pattern Image 81
4.4.1 Image Normalization 81
4.4.2 Skin Features Removal in NIR Images Using Morphological Top-Hat Operation 84
4.5 Summary 85

5 Vein Pattern Shape Estimation 87

5.1 Skeleton-based Versus. Contour-based Shape Descriptor 87

5.2 Binary-based Vein Pattern Skeletonization 89
5.2.1 Image Binarization with Local Adaptive Thresholding 89
5.2.2 Binary Based Skeletonization 93
5.2.3 Discussion 94
5.3 Gray-Scale Skeletonization using Watershed Algorithm 95
5.3.1 The watershed principle 95
5.3.2 Watersheds Algorithmic Skeletonization for Both Gray-scale and Binary Objects 97
5.3.3 Watershed Algorithm for the Vein Pattern Skeletonization . . . 101
5.4 Summary 103

6 Vein Pattern Features and Matching 106

6.1 Salient Point Features 107
6.1.1 Salient Points Extraction 107
6.1.2 Salient Points Evaluation 109
6.1.3 Similarity Measure of the Salient Point Features with the Modified Hausdorff Distance 112
6.1.4 Tolerance to Errors 114
6.2 The Line Edge Maps 117
6.2.1 Building the Line Edge Map 118
6.2.2 The Line Segment Hausdorff Distance with Line Edge Maps . . 121
6.2.3 Tolerance to Errors 125
6.3 Summary 128

7 An Initial Study of Vein Pattern Biometrics for Identical Twins 132

7.1 Identical twin studies 132

7.2 Additional Issues of Vein Pattern Biometrics 138

7.3 Summary 139

8 Conclusions and Future Research **140**

8.1 Summary 140

8.2 Future Research 145

References **148**

A Infrared Vein Pattern Image Data Collection Protocol **156**

A.1 Overview 156

A.2 Data Collection Procedures 157

A.2.1 The Venue 157

A.2.2 The Time 157

A.2.3 The Sample 157

A.2.4 Instruments 158

A.2.5 Time Frame for Data Collection 159

Abstract

Thesis Title *: Investigation of Infrared Hand Vein Pattern Biometrics.*

Author *: Wang Lingyu.*

Supervisors *: Prof. Graham Leedham & Asst. Prof. Siu-Yeung Cho.*

The increasing public awareness of security issues has led to a massive rise in demand for high accuracy and reliable personal identification systems. Many biometric systems have been developed to meet the requirements. Many human surface features such as the faces and fingerprints have been studied extensively to identify a person for a number of years. Whilst these features can offer relatively high accuracy, their tolerance to forgery is moderate. There is a recent developing trend of studying the unique interior features (e.g. iris, retina etc.) of the human body for biometric purposes. Amongst those interior features, human vein patterns offer the potential for robust performance, and, have not been fully investigated previously by researchers.

This thesis investigates the potential of the hand vein patterns serving as a biometric feature. Several major research issues are identified and investigated regarding the hand vein patterns as biometrics. These research issues are: (i). Collectibility of the vein pattern images; (ii). Processing of the vein pattern images; (iii). Identification of features for matching the vein patterns; (iv). The study of the discriminating power of vein patterns in biometric applications.

In order to carry out the study, a model is proposed with five independent stages

for the vein pattern biometric system, namely, *Data Acquisition*, *Preprocessing*, *Vein Pattern Segmentation*, *Skeletonization* and *Matching*.

Various imaging technologies are reviewed before the Infrared imaging technique is selected to construct a hand vein pattern image database. Several novel image processing algorithms are proposed to enhance the image quality and extract the vein pattern skeleton from the raw images. A novel feature, the Line Edge Maps, is proposed to analyze the vein patterns, and achieved encouraging results in the application of personal verification.

Further study was carried out on the similarity of vein patterns between identical twins. With limited data, the experiment found the hand vein patterns between identical twins can be genetically independent; and they are distinguishable both visually and computationally.

Overall, the study provides evidence demonstrating the vein pattern image data is obtainable in a non-intrusive manner; and some unique computational features can be extracted from the vein pattern images after appropriate pre-processing, and these features are capable of providing strong discriminating power in the context of biometric applications.

List of Figures

1.1 Decision Distributions of BIS 3

1.2 Receiver Operating Characteristics (ROC) Curve of BIS 4

2.1 The flow of the Eigenfaces approach for face recognition. (Source: "http://cnx.rice.edu/content/m12531/latest") 17

2.2 A typical fingerprint image (The dots are the Minutiae) 20

2.3 The framework of the hand vein pattern biometric system. 42

3.1 A coronary angiogram (an X-ray with radio-opaque contrast in the coronary arteries) that shows the left coronary circulation. (Source: http://en.wikipedia.org/wiki/Angiography) 44

3.2 Image of carotid artery. (a) jugular vein, (b) right common carotid artery (Source: http://www.radiologyinfo.org) 45

3.3 The visible light region in the electromagnetic spectrum 46

3.4 Far Infrared Vein Pattern Image Acquisition System Setup 49

3.5 FIR images of the back of four different hands taken in a normal office environment 50

3.6 Far-Infrared images of the palm and wrist taken in a normal office environment 50

3.7 FIR images of the back of the hands in an outdoor environment, where veins are not clearly visually discernable 51
3.8 Far-Infrared image of the same hand taken a few weeks apart 52
3.9 The near-infrared imaging System used to capture images 54
3.10 Typical NIR images for the palm and wrist 56
3.11 Typical NIR images of the back of the hand 56

4.1 Extracting the Hand Contour 66
4.2 Defining the Region of Interest 68
4.3 Region of Interest Images. 69
4.4 De-noising results for the image corrupted with a signal-dependent noise 78
4.5 De-noising results for the 3 standard images corrupted with signal-dependent noise 80
4.6 De-noising results for the FIR vein pattern images using LLMMSE filter with parameters derived with 2 images. (Upper row: the original noisy images; Lower row: the filtered images.) 81
4.7 De-noising results for the NIR vein pattern images using LLMMSE filter with parameters derived with 2 images. (Upper row: the original noisy images; Lower row: the filtered images.) 82
4.8 Post-processing results for the vein pattern image. 83

5.1 Vein Pattern Segmentation using Global Thresholding. 90
5.2 Vein Pattern Segmentation using local thresholding with global reduction. 92
5.3 Skeletons of the vein pattern using binary-based skeletonization, where the shape of the vein pattern is overall well preserved, but the false branches (in the circled area) are also numerous. 94

5.4 The simulated immersion process for the watershed algorithm. (source: "http://cmm.ensmp.fr/ beucher/wtshed.html") 96
5.5 Watershed algorithm applied to gray scale skeletonization 99
5.6 Skeletonization using the watershed algorithm for a binary image . . . 100
5.7 The Euclidian distance transform (right) of a binary image (left). . . . 101
5.8 Skeletonization using the watershed algorithm 102
5.9 Additional experiments for the watershed algorithmic skeletonization with vein pattern images 103
5.10 Situation where the watershed algorithm fails to extract the proper skeletons: the vein patterns have a floating end point 104

6.1 Skeleton and Salient Points of the Vein Pattern 109
6.2 Distribution of the Number of Bifurcation and Ending Points 110
6.3 Distribution of the Total Number of Salient Points (Mean=13) 111
6.4 Error Rate Curves for Salient Point Features Recognition Using the Original Form of Hausdorff Distance (EER=7.2% where the threshold is observed to be 25) 114
6.5 Error Rate Curves for Salient Point Features Recognition Using the Modified Hausdorff Distance (EER=0% where the threshold is 10) . . . 115
6.6 Tolerance of the Salient Point Features Against Errors 117
6.7 An example of Hough Line Transform on detecting the longest line segment on a curve 120
6.8 The Line Edge Maps (e)-(h) Extracted from vein pattern skeleton images (a)-(d) 122
6.9 Line Displacement Measure. (Source: Gao & Leung 2002) 123

6.10 The rotation effect of two lines. (a) The original line pair. (b) Rotate the shorter line. (c) Rotate the longer line. (d) Rotate both lines with half of their angle difference in opposite directions. Solid lines represent lines before rotation. Dashed lines represent lines after rotation. (Source: Gao & Leung 2002) 124

6.11 Cases where $d_{\|}(m,t) = 0$. (Source: Gao & Leung 2002) 124

6.12 Distribution of genuine and intruder accesses against similarity measure H' for the FIR image data 126

6.13 An vein pattern skeleton image occluded by an image mask 127

6.14 Error Rate Curves for the LEMs Occluded by a Random Image Mask . 127

6.15 Error Rate Curves for the LHD Measurement of LEMs with Random Geometrical Displacement ($-10^\circ \leq \theta \leq 10^\circ$, and offsets lie between -5 to 5 pixels) 129

7.1 Vein Pattern Images for the Left and Right Hands of Twin Pair 1 . . . 134

7.2 Vein Pattern Images for the Left and Right Hands of Twin Pair 2 . . . 135

7.3 Vein Pattern Images for the Left and Right Hands of Twin Pair 3 . . . 136

A.1 The user interface of the meta data recording program. 160

A.2 The consent form to be filled by the participants before enrollment. . . 161

List of Tables

2.1 Measurement Criteria for Various Biometrics Technologies 31

3.1 A Comparison of FIR and NIR Imaging of Hand Vein Patterns 58

3.2 Participant Distribution Against Race Groups for the NIR Images Database 59

3.3 Participant Distribution Against Age Groups for both FIR and NIR Image Databases 60

4.1 Estimated Values of σ_f^2 using two image instances against the change of the (γ, σ_n^2) pairs, where the variance of the noise-free "Lena" image is $\sigma_f^2 = 2.295 \cdot 10^3$. (Horizontal is σ_n^2 and vertical is γ, and the predicted value is in the power of $\cdot 10^3$). 76

4.2 The Peak Signal-to-Noise Ratio (in *db*) of Wiener2 filter and our proposed method to de-noise Signal Dependent Noise. 77

4.3 Comparison of the performance of the LLMMSE filter constructed by estimating the (γ, σ_n^2) pair (Aiazzi's approach) and by directly deriving the σ_f^2 (our approach). The performance are measured based on the Peak Signal-to-Noise Ratio in *db*. 79

4.4 De-noising results for 3 standard testing images corrupted with synthetic signal-dependent noise. The performance are measured based on the Peak Signal-to-Noise Ratio in *db*. 79

6.1 Salient Point Feature Evaluation Using Modified Hausdorff Distance . . 111

7.1 Intra-Class Distance for Each Twin Individual with the Salient Point Features 135

7.2 Inter-Class Distance for Each Twin Individual with the Salient Point Features 136

7.3 Intra-Class Distance for Each Twin Individual with the LEM Features . 137

7.4 Inter-Class Distance for Each Twin Individual with the LEM Features . 137

Acronyms

AR Autoregressive.

BIS Biometric Identification System.

CN Cross Number.

DNA Deoxyribose Nucleic Acid.

EEG Electroencephalogram.

EER Equal Error Rate.

FAR False Acceptance Rate.

FIR Far-Infrared.

FPN Fixed Pattern Noise.

FPVP Feature Points of Vein Patterns.

FRR False Rejection Rate.

FTIR Frustrated Total Internal Reflection.

LEM Line Edge Map.

LHD Line-segment Hausdorff Distance.

LLMMSE Local Linear Minimum Mean Square Error.

LMMSE Linear Minimum Mean Square Error.

MHD Modified Hausdorff Distance.

MMSE Minimum Mean Square Error.

MSE Mean Square Error.

NIR Near-Infrared.

PCA Principle Component Analysis.

PIN Personal Identification Number.

PSNR Peak Signal-to-Noise Ratio.

ROI Region of Interests.

ROC Receiver Operating Characteristics.

SAR Synthetic Aperture Radar.

SDN Signal Dependent Noise.

SPF Salient Point Features.

TIFF Tagged Image File Format.

Chapter 1

Introduction

1.1 Background

Associating an identity with an individual is called personal identification. Uniquely identifying oneself is an increasingly common procedure in our modern networked and security conscious society. Examples range from access control to restricted areas, ATM / banking verification systems to international border control and law enforcement etc. Ever since the "$9 \cdot 11$" terrorist event in 2001, public awareness of security issues have been greatly heightened. This has led to a massive rise in demand for personal identification systems. Traditional methods make use of smart cards or Personal Identification Numbers (PIN) to identify a person. However, as smart cards can be lost or stolen, and PINs can be forgotten or guessed by intruders, these methods only offer limited security and are usually unreliable. To overcome these disadvantages, a more secure and cost-effective technology is required. Over the past few years, various biometric systems have been developed to meet these requirements.

1.1.1 Properties of Biometrics

Biometrics is the science of identifying a person using physiological or behavioral features (Ratha et al., 2001). These features range from physical traits like fingerprints,

face, retina etc. to personal behaviors (such as signature, keystroke, gait etc.). For those human characteristics to qualify as biometric, they must have the following properties (Clarke, 1994): (i) *universality*, which means that every person should have the characteristic, (ii) *uniqueness*, which indicates that no two persons should be the same in terms of the characteristic, (iii) *permanence*, which means that the characteristic should be invariant with time or at least over a reasonably long period. Compared to traditional methods, biometric features are much harder for intruders to copy or forge, and it is very rare for them to be lost. Hence, for identification systems making use of biometric features, they offer greater security and reliable performance.

1.1.2 Operations of a Biometric Identification System (BIS)

The BIS can operate in two modes: verification (or authentication) and identification. Verification refers to the problem of confirming or denying a person's claimed identity (Am I who I claim I am?), whereas identification (Who am I?) refers to the problem of establishing a subject's identity (Nanavati et al., 2002). For both operation modes, there are two stages when using the BIS. The first stage is the enrollment stage, where the system captures individual biometric features, which are digitally represented by means of feature vector templates or prototypes. The second stage is the individual accessing the BIS, where the newly captured features are compared with the templates from the storage.

1.1.3 Evaluation Criteria of BIS

Different applications have different requirements of the BIS. A military security system may be required to deny impostor accesses as many times as possible, whilst a restaurant payment system may need to approve genuine payments as many times as possible. However, there are a set of criteria characterizing different BISs, and they

provide a standard measurement on how a BIS fits a specific application domain. This set of criteria are (Luis-Garcia et al., 2003): (i) *Accuracy*, (ii) *User Acceptance*, (iii) *Ease of Use*, (iv) *Ease of Implementation*, and (v) *Cost*. Amongst those measurements, accuracy of performance is the most important and critical issue. Measuring of the accuracy of a BIS is a difficult task. Generally speaking, a BIS makes two types of decisions during the identification process: a genuine individual or an imposter individual. These two decisions can be represented by two statistical distribution called genuine distribution and imposter distribution respectively, as shown in Figure 1.1.

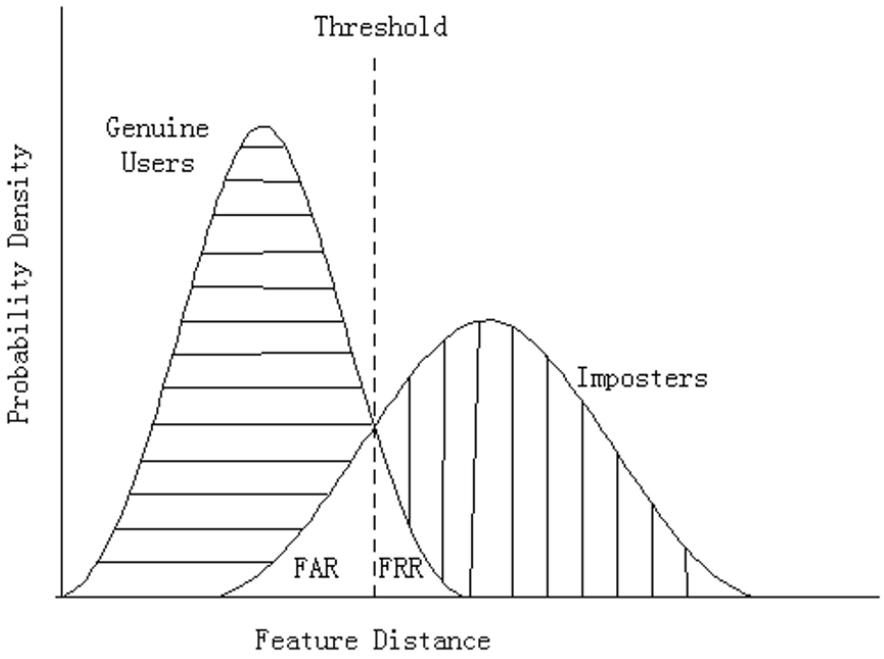

Figure 1.1: Decision Distributions of BIS

When BIS is making the decision based on a certain feature distance threshold value, there can be four possible outcomes: (i) a genuine individual is accepted, (ii) a genuine individual is rejected, (iii) an imposter is accepted, (iv) an imposter is rejected. The accuracy measurement of the BIS is defined by two error rates which occur under situations (ii) and (iii). The false acceptance rate (FAR) is the probability of accepting the user when an impostor is on the system. The false rejection rate (FRR) is the probability of rejecting the user when a genuine user is on the system.

Mathematically, they are defined as:

$$FAR = \frac{\text{number of false acceptance}}{\text{number of intrusion attempts}} \tag{1.1}$$

$$FRR = \frac{\text{number of false rejection}}{\text{number of genuine attempts}} \tag{1.2}$$

As can be seen in the decision distribution graph of a biometric system, the relationship between FAR and FRR is inversely proportional, as illustrated in Figure 1.2.

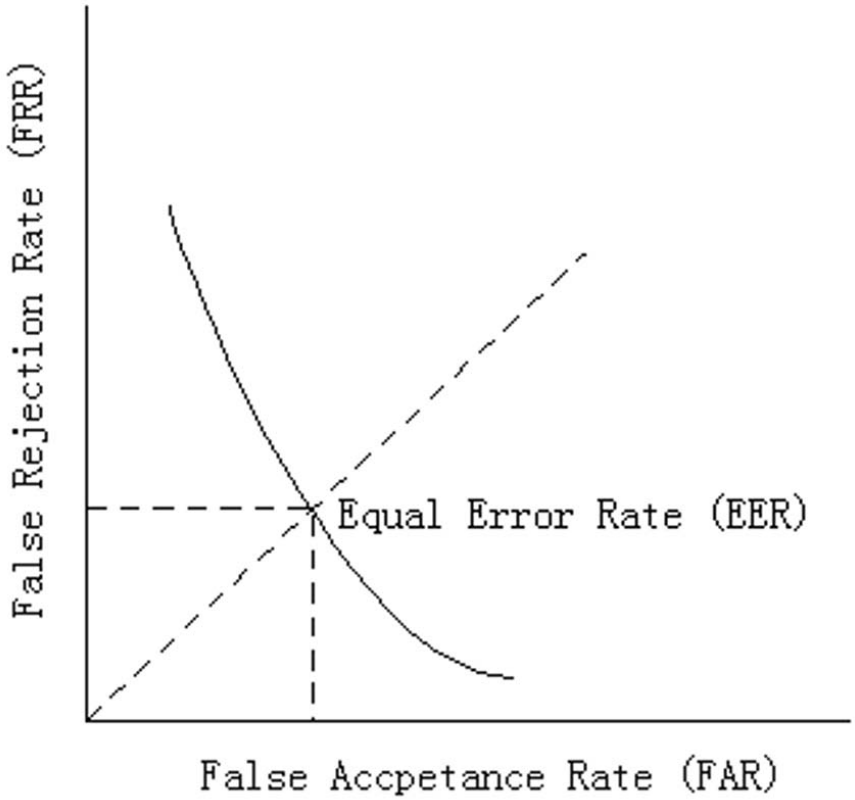

Figure 1.2: Receiver Operating Characteristics (ROC) Curve of BIS

Each point on the Receiver Operating Characteristics (ROC) curve defines the system's FRR and FAR for a given threshold of the feature distance. The value of a location on the ROC curve where FRR equals FAR is commonly known as the Equal Error Rate (EER), which is a statistic used to show the biometric performance. In general, the lower EER, the higher the accuracy of the biometric system. Ideally it is

zero.

1.2 Motivation

In order to build a highly acceptable biometrics system, the biometric features must have high accuracy performance and ease of use. Meanwhile, tolerance to forgery is another increasing key concern about the biometric features. Amongst many biometrics features, human vein patterns have been shown by earlier research (Sweeney, 1998) to be a stable and unique personal trait, and its strong immunity to forgery and high level of user acceptance make it a potentially good solution for human identification. In addition, vein pattern biometrics has not been fully investigated previously. Hence, this project is motivated to investigate the uniqueness of the vein pattern in certain parts of the human body as a biometric feature and to propose techniques and algorithms to process and analyze the vein patterns.

1.3 Problem Statement

The research problem may be stated as: to investigate the potential of the hand vein patterns in the application of person verification. We have identified and investigated the following 4 major issues in the thesis:

1.3.1 Collectibility of Vein Patterns

The veins are hidden underneath the skin, and are mostly invisible to naked eyes. It is therefore a challenging task to acquire any image data of the vein patterns. Whilst the traditional visual imaging systems have difficulties in capturing the vein pattern images, it is worthwhile to look into other imaging mechanisms and attempt to capture the vein patterns in various parts of the human body. The purpose is

to determine the optimum image acquisition techniques for acquiring vein patterns in the context of biometric applications. Another issue on the collectibility of vein patterns is to analyze the factors that can affect the image data quality for the chosen imaging techniques.

1.3.2 Data Preprocessing

The performance of a feature extraction algorithm relies heavily on the quality of the input image data. In practise, due to variations in environmental conditions, skin conditions, acquisition devices and non-cooperative attitude of subjects, etc., some of the acquired vein pattern images are of poor quality. The vein structure in these poor-quality vein pattern images is not always well defined, and hence cannot be correctly detected. This leads to a significant number of false features as well as missing features, which will degrade the performance at the vein pattern matching stage. To ensure the performance of the feature extraction algorithm with respect to the quality of the input image data, an enhancement algorithm which can improve the clarity of the vein pattern structure is necessary.

1.3.3 Identification of Features

In most pattern recognition problems, selection of features from the raw data is considered the most vital issue. Correct selection of features can best represent the data itself, and can provide the highest discriminating power. Meanwhile, raw data is usually corrupted due to numerous factors, which leads to variations in extracting the features. Good features should be sufficiently flexible to cater for such variations so that accuracy will not be adversely affected significantly at the feature matching stage. In vein pattern biometrics, there are scant research studies addressing the issue of selection of features that can provide strong discriminating power and robustness

against preprocessing errors. Therefore, it is one of the major tasks for this research to identify the potential unique and robust features for the vein patterns as well as the corresponding matching algorithms so as to establish a solid scientific basis for the vein patterns to be used in biometric applications.

1.3.4 The Study on the Discriminative Power of Vein Patterns

One of the major problems with vein pattern biometrics is to test the hypothesis about vein pattern distinctiveness. We studied the discriminating power of the hand vein patterns through assessing the general person verification accuracy on our database of hand vein pattern images.

However, suppose the aim is to test the hypothesis for some population which is a subset of the world population (this can be a population of a country, or a population of people speaking the same language). This imposes a requirement on the database that the vein pattern samples should be representative of the population in a statistical sense, i.e. if there is a possibility that the race group difference can influence the vein patterns, then the database should contain the same percentage of samples for each race group as in the real population. In practices, the factors that affect the vein patterns are still unknown, and it is impossible to take all the potential factors into consideration. Therefore, it is more reasonable to make some assumptions about the factors which could possibly affect the vein patterns. In the thesis, the factors we take into consideration whilst constructing our vein pattern image database include:

1. race group;
2. age;
3. gender;

4. occupation.

If the uniqueness study of vein patterns is to be carried out, it requires a more comprehensive analysis on more advanced issues, and some of the important ones are identical twins study, hereditary study, temporal study etc. Whilst it is impossible to cover all of these issues in this project at the current stage, it is necessary to carry out an initial analysis on one of the most important ones. This is the identical twins study included as chapter 7.

1.4 Contributions

The work presented in this thesis makes several major original contributions in the following areas:

1. In Section 3.2: The mechanisms for non-intrusive acquisition of hand vein pattern images are analyzed in detail; and the data acquisition process and system setup are carefully designed.
2. In Section 3.3: A hand vein pattern image database was constructed, which includes images of the vein patterns in various parts of the hand, captured by both Far- and Near- Infrared cameras.
3. In Section 4.3: An algorithm is proposed to remove the signal-dependent noise in the infrared vein pattern images. The method derived the Kuan filter parameters from two image instances automatically without the need to know the noise parameters. The proposed method can also be used for noise removal of generic images.
4. In Section 5.3: A watershed based gray-scale skeletonization algorithm is proposed to extract the skeletons from the vein pattern images.

5. In Section 6.2: A new feature set: the Line Edge Maps, is proposed to represent the vein patterns, which provides strong discriminating power and high tolerance to preprocessing errors compared to the conventional features (such as minutiae) used in other biometrics.
6. In Chapter 7: An initial study on the similarity of vein patterns amongst identical twins was carried out.

1.5 Publications Resulting from the Research for the Thesis

This research has in many parts been shaped by reviewers' comments and suggestion regarding many of the publications (both journal articles and conference presentation) listed below:

Journal Articles:

1. **Wang Lingyu**, Graham Leedham, & Siu-Yeung Cho, "Minutiae Feature Analysis for Infrared Vein Pattern Biometrics", *Pattern Recognition*, 41(3), pp. 920-929, 2008;
2. **Wang Lingyu**, Graham Leedham,& Siu-Yeung Cho, "Automatic Signal-Dependent Noise Removal for Infrared Vein Pattern Images", *Machine Vision and Applications*, 2008 (under review);
3. **Wang Lingyu**, Graham Leedham, & Siu-Yeung Cho, "Infrared Imaging of Hand Vein Patterns for Biometric Purposes", *IET Computer Vision*, 1(3-4), pp. 113-122, 2007;

Book Chapters:

1. **Wang Lingyu** & Graham Leedham, "A Watershed Algorithm Approach for Gray-scale Skeletonization in Thermal Vein Pattern Biometrics", *Lecture Notes in Artificial Intelligence* , Springer, Vol 4456, pp. 935-942, 2007;
2. **Wang Lingyu** & Graham Leedham, "A thermal vein pattern verification system", In *Pattern Recognition and Image Analysis, Lecture Notes in Computer Science 3687*, Springer, Sameer Singh, Maneesha Singh, Chid Apte, Petra Perner (Eds.), pp. 58-65, 2005.
3. **Wang Lingyu**, Graham Leedham, & Siu-Yeung Cho, "Feature Analysis of the Physiological Hand Vein Pattern for Personal Identification", *Computer Forensics - Methods, Applications and Challenges in Computer-Assisted Criminal Investigations*, Editors: Katrin Frank, Slobodan Petrovic, & Ajith Abraham, Springer, 2007 (Under Review);
4. Sui-Yueng Cho, Nanda-Pwint Tin, & **Wang Lingyu** "An Investigation of Concealed Weapon Detection and Visualization by Image Analysis", *Computer Forensics - Methods, Applications and Challenges in Computer-Assisted Criminal Investigations*, Editors: Katrin Frank, Slobodan Petrovic, & Ajith Abraham, Springer, 2007 (Under Review);

Conference Papers:

1. **Wang Lingyu**, Graham Leedham, & Siu-Yeung Cho "Deriving Filter Patermeters Using Dual-Images For Image De-Noising", in Proceedings of *The IEEE 2007 International Symposium on Intelligent Signal Processing and Communication Systems (ISPACS 2007)* , Xiamen, China, Nov 28-Dec 1, 2007;
2. **Wang Lingyu** & Graham Leedham, "An improved smoothed watershed algorithm for gray-scale skeletonization of thermal vein patterns", in Proceedings

of *the Tenth International Workshop on Advanced Image Technology (IWAIT 2007)*, pp. 405-410, Bangkok, Thailand, January 8-9, 2007;

3. **Wang Lingyu** & Graham Leedham, "Near- and far- infrared imaging for vein pattern biometrics", in *Proceedings of the IEEE International Conference on Advanced Video and Signal based Surveillance (AVSS 2006)*, Sydney, NSW, Australia, 22-24 November, 2006;
4. **Wang Lingyu** & Grahma Leedham, "Gray-scale skeletonization of thermal vein patterns using the watershed algorithm in vein pattern biometrics", in *Proceedings of the IEEE International Conference on Computational Intelligence and Security (CIS2006)*, pp. 1597-1620, Guangzhou, China, 3-6 November, 2006;
5. **Wang Lingyu** & Graham Leedham, "A thermal vein pattern verification system", in *Proceedings of the Third International Conference on Advances in Pattern Recognition (ICAPR 2005)*, pp. 58-65, Bath, UK, 22-25 August, 2005.

1.6 Organization of this Thesis

This thesis comprises 8 chapters. It is organized as the following:

Chapter 2 presents a literature review of various biometric technologies. In the first part of the chapter, six mainstream and some other esoteric biometric technologies are surveyed. The chapter then focuses on the current status of the vein pattern biometrics. With the review of the current development of the biometric technologies, the research direction and the major research issues are identified.

Chapter 3 concentrates on the mechanisms of vein pattern acquisition as well as the analysis of the factors affecting the image quality. In this chapter, two major imaging methods are then studied: Far-Infrared (FIR) imaging and Near-Infrared

(NIR) imaging. Two infrared hand vein pattern image databases are constructed and reported in this chapter. The databases are built based on FIR and NIR imaging techniques respectively.

Chapter 4 is an elaboration of the vein pattern preprocessing process, which consists of the region of interest selection and image de-noising. In this chapter, a technique that defines the region of interest invariant to hand sizes is presented. Then a noise removal algorithm is also proposed in the chapter to remove the signal dependent noise in the image.

Chapter 5 discusses the work done to extract the skeleton representation form for the vein patterns from the images. In the first part of the chapter, the traditional binary based skeletonization method is studied. Then a new gray-scale skeletonization algorithm based on the watershed concept is proposed and presented in the second part of the chapter.

Chapter 6 focuses on identifying the features used to match the vein patterns. Two types of features are investigated, namely the salient point features and the line edge maps. The steps involved to extract these two types of features are presented in details. Two matching algorithms based on the two different feature types were proposed. Experiments on the two feature types were carried out and the results are reported in the chapter together with the analysis of their tolerance against errors.

Chapter 7 reports an initial study on the analysis of the similarity of vein patterns between twins. Some experimental results are reported in this chapter.

Finally, Chapter 8 summarizes the thesis. It outlines the contribution that the work has made, and it also identifies the remaining research issues and possible research direction for further study in the future.

Chapter 2

Biometric Technologies

In the past few decades, biometric technologies have been one of the most active research areas. Many researchers have carried out extensive studies on utilizing various biometric features (both physiological and behavioral) for personal identification, and some of them have successfully implemented their technologies into commercial biometric products that have become widely adopted and used in numerous applications. Amongst those biometric features, the most popular ones are fingerprints, faces, and iris for physiological biometrics, as well as signature, and voice for behavioral biometrics. These biometric features are widely used by today's security systems; however they yield different characteristics, and have both advantages and disadvantages (Luis-Garcia et al., 2003). Therefore, it is a necessary step to assess the current commonly available biometrics to identify the developing trend of the biometric technologies. Meanwhile, It is important to study the current state of the art of the vein pattern biometrics. Lastly, by reviewing the various biometric technologies, inspiration can be obtained for the vein pattern biometrics from the currently well established biometric technologies.

Hence, in the first part of this chapter, six mainstream biometrics (namely, *face*, *fingerprint*, *eye*, *hand geometry*, *voice* and *signature*) are studied and compared in

depth, together with some other esoteric biometric technologies. The major aspects of these biometrics which we are interested in include:

1. The general principles of the technology,
2. Data acquisition mechanisms and the available databases,
3. Features used for recognition and recognition accuracy,
4. Current challenges faced by the technology.

In the second part of this chapter, a thorough review is carried out on the current status of vein pattern biometrics, and through which, the research direction is identified.

2.1 Physiological Biometrics

Definition 1 *Physiological Biometrics is the measurement of the distinct human physical traits which are usually dictated by the person's genetics. It is based on the data directly measured from a part of human body.*

2.1.1 Face Recognition

Face recognition is the most natural way of personal identification for humans. Computerized face recognition is to identify one or more persons from still images or a video image sequence of a scene by comparing input images with template faces stored in a database. Because of its naturalness, computerized face recognition is one of the most user-acceptable biometric technologies, and is of particular interest for a large variety of application areas, ranging from security access control, and video surveillance to law enforcement. Due to its possible popularity, over the past few decades, many efforts have been put into the research of computerized recognition of human

faces, and a wide variety of approaches to machine recognition of faces has been published in the literature (Brunelli & Falavigna, 1993; Phillips, 1999; Chellappa et al., 1995).

Data Acquisition:

The environment surrounding a face recognition system has great influence on its data acquisition process. It can be a well-controlled environment or a totally uncontrolled one. Face recognition systems can have a wide variety of image acquisition modes. NIST (National Institute of Standards and Technology) has proposed a recommended set of guidelines for face image acquisition (NIST, 2000):

- Single Image: Optical methods include digitizing hard-copy documents using optical scanners. Generally images are taken cooperatively and under well-controlled lighting conditions.
- Video sequence: Surveillance cameras acquire video sequences that include face images. However, this type of regular camera is not very useful for face recognition due to its low spatial resolution. Even with hyper resolution techniques, the performance of surveillance cameras does not increase significantly. This is because the frame rates are generally quite low (1-4 frames per second) and hence very few good images of a face are acquired from a moving target (Bolle et al., 2004).
- 3D images: This technique makes use of skin and skull geometric information and other 3D features of the faces instead of still 2D images. This is a relatively new approach to face image acquisition.
- Near Infrared: This technique aims to tackle the problem of poor lighting conditions during the face image acquisition process. Low-power infrared illumination can be used to supplement face detection process.

Amongst those face image acquisition modes, the use of CCD cameras to acquire still images has the longest history and widest applications currently. Recently, because of the tremendous interest in face recognition in academia, a plethora of university face databases is emerging, such as:

- The Olivetti (ORL, now AT&T) database (Samaria & Harter, 1994),
- FRVT 2002 (http://www.dodcounterdrug.com/facialrecognition),
- NIST Mugshot Identification Database (http://www.nist.gov/srd/mistsd18.htm),
- The MIT database (ftp://whitechapel.media.mit.edu/pub/images/),
- The CMU database(http://www.ri.cmu.edu/projects/project_418.html),
- The Yale database
- The Purdue database (http://rvl1.ecn.purdue.edu/aleix/aleix_face_DB.html) etc.

Feature Selection:

There are two particularly popular approaches in face recognition research. The first one is the eigen-face approach that was proposed by Turk & Pentland (Turk & Pentland, 1991). The technique applies the Karhunen-Loeve transform, now known as Principle Component Analysis (PCA), to the images to obtain the eigenfaces. Then each individual face can be represented as a weighted combination of eigenfaces. Finally a classifier, such as an artificial neural work, is trained to classify the faces. Figure 2.1 shows the logic flow of the eigen-face approach.

The second approach is to classify the face images based on face features (Chellappa et al., 1995). A Gabor filter, for example, can be applied to the face images to obtain the filter response as the features that can be used by the classifier in the subsequent stage. Some other methods recognize faces using compact face features like Line Edge Map (LEM) proposed by Gao & Leung (Gao & Leung, 2002a), in which the LEM is obtained by applying a polygonal line fitting process to the binary face

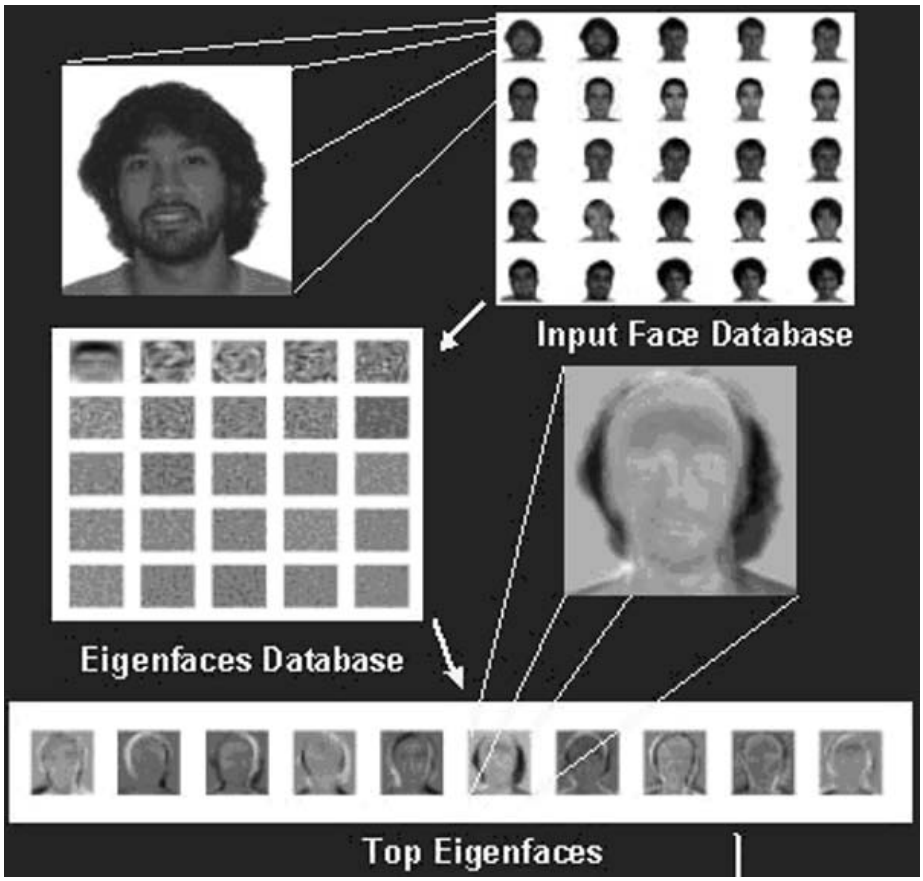

Figure 2.1: The flow of the Eigenfaces approach for face recognition. (Source: "http://cnx.rice.edu/content/m12531/latest")

edge map obtained using the Sobel edge detection algorithm. This approach, the authors claimed, is less sensitive to the variation of face conditions such as illumination, facial expression and poses etc.

Challenges:

Though it seems to be simple for human beings to recognize each other by faces, it is a very difficult task for computers. Despite all the work done, face recognition is not yet sufficiently accurate to accomplish the large-population identification tasks tackled with fingerprint or iris recognition. Bolle et al. (Bolle et al., 2004) categorize the challenges facing by the face recognition systems into 4 types of variation: (i) Physical appearance. These include changes in facial expression, personal appearance changes (such as wearing make-up and glasses, changing hair style etc.) as well as slow appearance changes due to aging. (ii) Acquisition geometry. This refers to the

unknown location, unknown size of a face in the image, together with the rotation of a face in depth (i.e., facing the camera in profile or obliquely). (iii) Imaging conditions. Lighting of a human face have large effects on the images. Uneven illumination due to some external factors such as side-positioned lighting leads to the changes of appearance of faces in the images. (iv) Compression artifacts. For the purpose of optimizing transmission and storage, image compression and subsequent decompression are common in many applications. This process normally leads to degradation in image quality which could has significant impacts on the performance of most face recognition algorithms. Currently, no face recognition system can effectively handle all these problems (Bolle et al., 2004). These problems leave automatic face recognition with great challenges ahead for all the future research in this area.

2.1.2 Fingerprint Recognition

There is archaeological evidence that fingerprints as a form of identification have been used at least since the third century B.C. by the ancient Assyrians and Chinese (Woodward et al., 2003). But it was not until the late 19th century that the Home Ministry Office of the UK, first accepted that no two individuals have the same fingerprints (Jain et al., 2001) in a criminal trial. Ever since then, extensive studies have been carried out for the suitability of fingerprints as a stable source of biometrics. In the late 1990s, the introduction of inexpensive fingerprint capturing devices boosted the development of fingerprint biometric technology. Today, fingerprint identification is the most widely used system not only in law enforcement agencies, but also in other security control sectors.

Data Acquisition:

The most traditional fingerprints acquisition technique is via inking. However, the

involvement of ink causes inconvenience in the subsequent digitization and segmentation stages. It is also a problem to make this an automatic process. Another type of fingerprint capturing devices with a long history are the optical devices (Harrick, 1962). These devices operate on the principle of frustrated total internal reflection (FTIR). They are still the most commonly used fingerprints capturing devices till now. A recent fingerprint acquisition technology is ultrasonic scanning (Bicz et al., 1995): an ultrasonic beam is scanned across the fingerprint surface and the receiver captures the echo signal that measures the depth of the ridges. This technology is less affected by the oil and dirt on the fingerprint surface and thus can better represent the fingerprint topology.

Feature Selection:

A fingerprint image consists of a number of ridges (the lines flowing in various patterns across fingerprints) and valleys (the spaces between ridges). A fingerprint can be well represented by a number of critical points in the image (Jain et al., 1997): the ridge endings and ridge bifurcations. An ending is a feature where a ridge terminates. A bifurcation is a feature of a ridge branch point as shown in Figure 2.2. These critical points are called minutiae, and they are widely used as the sole features to match a pair of fingerprints, and hence to identify a person.

Most of the work of fingerprint identification in the literature is based on the minutiae technique (Ratha et al., 1995; Stosz & Alyea, 1993). However, this approach suffers from several drawbacks according to Jain (Jain et al., 2000): First of all, it is difficult to extract complete ridge structures automatically for a large fraction of the population. Secondly, it is difficult to match two fingerprint representations when they contain a different number of minutiae points. These shortcomings are some of the major challenges faced by the the minutiae approach. Another approach that is

Figure 2.2: A typical fingerprint image (The dots are the Minutiae)

attracting more interest from the researchers in recent years is the texture matching method. In this approach, the flow of ridges at all locations, which can be considered as the texture of the fingerprint, is compared between a pair of fingerprints. Coetzee (Coetzee, 1992) proposed a texture-based technique that makes use of no minutiae features, but performs a correlation in the frequency domain of the binarized fingerprint image. This approach can overcome some of the drawbacks that the minutiae approaches generally have.

Challenges:

Fingerprints are one of the most mature biometrics, however, most of these systems still suffer from several problems in real life situations. One example is the imperfect condition of imaging, which refers to the dirty or oily fingers. Another one is the distortion to the fingerprints such as scars on the fingers etc. Last but not least is the liveness issue: the system can be easily spoofed by the intruders using some artificial fingers, dead fingers or latent fingerprints (Jain et al., 1999). Whilst the first problem can be overcome with the development of image acquisition devices

(such as the ultrasonic scanner mentioned above), the latter two remain an issue that is difficult for the current systems to resolve.

2.1.3 Eye Biometrics: Iris and Retina Pattern

The intricate nature of the human eye provides two of the most accurate biometrics: the iris and the retina pattern.

a). Iris Recognition:

The definition of iris is "the round pigmented membrane surrounding the pupil of the eye, having muscles that adjust the amount of light entering the eye". The iris has patterns that are intricate and richly textured. Ophthalmologists postulate that all irises are unique with no detectable or know genetic dependencies, and they further conclude that the irises are randomly formed prior to birth and under normal health conditions remain stable from early childhood till death (Woodward et al., 2003). Furthermore, the iris is a layer underneath the cornea, which leads to strong immunity to potential forgery. All these characteristics make iris an excellent choice for biometrics.

Data Acquisition:

As an internal and yet externally visible organ of the eye, the iris patterns can be obtained by projecting a near infrared light beam onto the eyeball. The reflection of the IR light is then captured by a CCD camera, which forms the image containing the iris patterns. Most of the iris recognition systems are based on grey-scale images, because it is believed that a grey iris image can provide enough information to identify different individuals (Ali & Hassanien, 2003). Commercial iris scanning works at a focal distance of about 3 to 7 inches. There is an Iris database made publicly available online (URL - "http://iris.di.ubi.pt/", accessed on 16th April 2007) by Portugal's

Universidade da Beira, which contains around 2000 images from around 250 people. A variation of the database is also available on the same web site where the Iris images have more realistic noise factors.

Feature Selection:

The complex pattern of the iris can contain many distinctive features such as arching ligaments, furrows, ridges, crypts, rings, corona, freckles, and a zigzag collarette. Many methods have been proposed to utilize these features for iris recognition. Daugman (Daugman, 2001) used the phase code obtained by Gabor filters in his system. Boles et al. (Boles & Boashash, 1998) used the iris features extracted using zero-crossing representation of 1-D wavelet transform. These methods are reported to have very high performance in the personal identification applications.

Challenges:

Whilst iris recognition is a well established biometrics, it has the restriction of having low user acceptance, as people tend to be very protective to their eyes, which prevents it from being deployed for daily security applications. In addition, the small size of the iris brings signification challenges for long range, noncooperative surveillance applications where image resolution, camera angles, occlusion, and isolation and tracking increasingly become factors (Woodward et al., 2003).

b). Retina Identification:

The retina is located on the back of the eye and normally is not visible. the geometrical arrangement of the retinal blood vessels forms the basis for retinal recognition systems. It is believed that retinal vascular patterns will not be willingly altered or disfigured by any human subject, thus allowing it to have a high level of tolerance to potential forgery.

Data Acquisition and Feature Selection:

Similar to iris, the retina is an internal organ, it is difficult for any imaging device to capture its detail in the visible light spectrum. Typical retinal scanning is accomplished by illuminating the retina with a low-intensity infrared light, and capturing the patterns formed by the major blood vessels.

There are two major representations for the retinal signature, according to Jain et. al. (Jain et al., 1999): The original representation consisted of 40 bytes of contrast information encoded as real and imaginary coordinates in the frequency domain and was generated by the fast Fourier transform; the second representation takes the contrast information in the time domain, which makes it computationally efficient. These frequency/time domain features are then normalized, and the correlation array will be calculated between the template and the testing data for the final matching decision.

Challenges:

Retinal identification has similiar limitations to the Iris recognition. Retinal scanning is considered intrusive to many people. It is also more difficult to use compared to other biometrics, as the user enrollment process requires prolonged concentration and effort. Lastly, retinal scanning usually requires a high-cost sensor, which is not desirable by in many applications.

2.1.4 Hand Geometry

There are no recorded uses of hand geometry to differentiate people prior to the introduction of hand geometry readers in the late 1980s by Recognition Systems, Inc.(RSI). Several biometric systems based on hand geometry have been deployed in various locations throughout the world. Nevertheless, the distinctiveness of hand geometry is still a questionable issue.

Data Acquisition:

A typical hand geometry acquisition system consists of a light source, a CCD camera, a flat surface, and a PC for processing the images. Traditionally, the systems have five pegs fixed on the flat surface serving as controls for appropriate placement of participants' hands. Recently there are also several peg-free hand geometry systems proposed by some researchers (Ong et al., 2003; Oden et al., 2003; Wong & Shi, 2002). These peg-free systems automatically locate the hand positions by finding the key hand landmark points such as fingertips. Usually the hand geometry biometric systems capture the 2D shape of the hands. Some systems also measure the thickness profile of the hand. However, Lay (Lay, 2000) captures the 3D information of the hand using a parallel grating to project onto the back of the hand.

Feature Selection and Challenges:

As the hand geometry biometrics rely on the geometric invariants of the hand, features popularly used for recognition include length and width of the fingers, aspect ratio of the palm or fingers, thickness of the hand etc (Jain et al., 1999; Ong et al., 2003). Jain and Duta (Jain & Duta, 1999) also directly used the contour of the hand as the sole feature and perform recognition by means of deformable matching.

Whilst those works on hand geometry biometrics have claimed they have achieved a reasonable high accuracy for verification applications, the features of hand geometry are not distinctive enough for any identification purposes. Another vulnerability is that spoofing the hand geometry biometrics is not as difficult as other biometric technologies. Meanwhile, the property of permanence for the hand geometry features is a questionable issue according to the research by Newham (Newham, 1995).

2.2 Behaviorial Biometrics

Definition 2 *Behavioral Biometrics is the measurement of the distinct actions that humans take. It measures the characteristics of the human body indirectly.*

2.2.1 Voice Verification

Voice verification is sometimes known as speaker identification. Voice combines elements of physiological and behavioral biometrics. The primary principle behind voice biometrics is that construction of an individual's vocal chords, vocal tract, palate, teeth, sinuses and tissue within the mouth affects the dynamics of speech (Ashbourn, 2000). Meanwhile, a user's behavior determines the motion, manner, and pronunciation of words, which forms the basis for the behavioral aspects of voice biometrics (Woodward et al., 2003). Voice verification usually operates in two ways: constrained mode (text dependent) and unconstrained mode (text independent).

Data Acquisition:

Voice-scan data acquisition is straight forward. In many cases, an individual is prompted to repeat a pass-phrase generated by the system, and an audio capturing device (such as a microphone or telephone handset) is used to record the acoustic wave into an analog signal, which generally will be converted to a digital form for further processing. There are many public speaker databases. Most of the more common ones were designed for telephone applications, and are listed below (Bolle et al., 2004):

- The NIST speaker database.
  (`http://www.nist.gov/speech/tests/skp/index.htm`).
- The TIMIT and NTIMIT database.
  (`http://www.ldc.upenn.edu/catalog/ldc93s2.html`).

- The YOHO database.

  (`http://www.ldc.upenn.edu/catalog/ldc94s16.html`).

- ELRA database, which has the data in non-English languages and non-native English speakers.

  (`http://www.icp.grenet.fr/ELRA/`)

Feature Selection and Challenges:

Voice biometric systems measure varieties of vocal features, which generally are not detectable by human ears. Apart from the fundamental frequency, many algorithms also measure other features such as gain or intensity, short-time spectrum of speech, formant frequencies, linear prediction coefficients, cepstral coefficients, spectograms, and nasal coarticulation. Many of the features are algorithm specific and they are subject to different matching algorithms. Reynolds (Reynolds, 2002) indicates 4 major prevalent speaker modelling techniques: template matching; nearest neighbor; Neural Networks; Hidden Markov Models.

The main strength of voice biometrics is that it relies on a signal that is natural and unobtrusive to produce, and it can be obtained easily without any special equipments or training. Meanwhile, voice biometrics is easy to use, and has low computation requirements, and it has high accuracy provided appropriate constraints are satisfied. However, the flexibility of speech also leads to its weakness. Reynolds (Reynolds, 2002) listed several of the challenges of voice biometrics. First, the behavioral aspect of voice means the speech signal may not be consistently reproduced by a speaker and can be affected by a speaker's health. Second, the various audio capturing devices people use can cause difficulties since most of the systems rely on low-level spectrum features susceptible to transducer/channel effects. Third, the uncontrolled and harsh acoustic environments can stress accuracy. Finally, spoofing of systems is also a strong

challenge for voice biometrics.

2.2.2 Signature Recognition

Another biometrics with a long history is signature verification. It has been in service before the advent of computers. Nowadays, signature verification is still very commonly used in numerous document authentication and transaction authorization applications, such as issuing checks and signing credit card receipts etc. Different from other biometric technologies, signature verification measures the behavioral features of a person. It comes in two forms of verification (Bolle et al., 2004): Offline Signature Verification and Online Signature Verification. These two types of verification differ not only in the data acquisition devices, but also in the feature sets selected for matching.

Data Acquisition:

For Offline Signature Verification, the signatures are generally scanned from paper documents; hence only a standard camera or a high-resolution scanner is required. Whereas for Online Signature Verification, people write their names with a specially designed electronically instrumented device. This type of devices (such as Tablet PC) captures the dynamic information of the signatures. A typical handwriting sensor records a stream of five-dimensional vectors $[x, y, p, \theta_x, \theta_y]$ sampled at equidistant time points, where p is the pressure the pen applies to the writing board, while θ_x and θ_y are the angles of the pen with respect to the $X - Y$ plane.

Feature Selection:

For offline signatures, whilst document examiners have a whole set of predefined features to classify the handwritings, most of them (such as legibility and writing quality etc.) are not yet computational features (those that can be determined algorithmi-

cally) in a sense that they are too subjective to be implemented. For most automatic offline signature verification systems, they utilize a subset of attributes used by expert document examiners, such as line separation, slant, and character shapes etc (Srihari et al., 2002). However, with these limited features, the offline signature verification is very vulnerable to forgery. Compared to offline techniques, in addition to those spatial attributes, online verification has the dynamic information of the signature generation process. With this dynamic information, a feature vector such as pen acceleration, pen tilt angles, and pen pressure etc can be constructed to represent the signature (Nalwa, 1997). Then, different methods can be approached to classify these feature vectors (and hence signatures), including measuring Euclidean distances between pen trajectories, regional correlation matching measures, Hidden Markov Models (Dolfing & Aarts, 1998), and other probabilistic temporal recognizers.

Challenges:

Though it is one of the most widely used biometric technologies in the market, signature verification faces challenges not fewer than other biometric systems. Whilst offline verification has limited information of the signature generation process and is vulnerable to forgery, online techniques can partially solve this problem with its richness of dynamic information. However, online verification requires special hardware to acquire the signature, which adds in extra cost that could be unacceptable for some applications (Luis-Garcia et al., 2003). More importantly, both techniques rest on the hypothesis that each individual has consistent handwriting that is distinct from the handwriting of another individual. However, this hypothesis has not been subjected to rigorous scrutiny with the accompanying experimentation, testing, and peer review (Srihari et al., 2002). Therefore, under certain circumstances such as forensic applications, their admissibility might be questioned.

2.3 Other Biometrics

In addition to the mainstream biometrics discussed in the preceding Sections 2.1 and 2.2, which are commonly available or commercially viable, there are many other biometric technologies that are still in the early research or development stages. Whilst it is impossible to have an exhaustive assessment of all the biometric technologies, these biometrics receive increasing interests from both research and industrial communities.

- *DNA Identification.* The basis of DNA biometrics is the comparison of alternate forms (alleles) of DNA sequences found at identifiable points (loci) in nuclear genetic material. DNA is often considered as the ultimate biometrics because of its advantage of being distinctive throughout the lifetime of each individual. Nevertheless, unlike most of the other biometric technologies which need only images or recording, the DNA biometrics requires actual samples, and analyzing the DNA is not a realtime, but often slow (in terms of minutes to hours), process. A Canadian company called "Spartan Bioscience Inc." recently proposed a product for "real-time" personal DNA analysis. However, it is not realtime in a strict sense as the analysis takes around 30 minutes according to their product specification (Accessed online on 10th September 2007: "http://www.spartanbio.com/assets/DX_Spec_Sheet_20070611.pdf"). Meanwhile, the fact that the identical twins have identical DNA sequence is another problem for DNA biometrics. Currently, most of the DNA identification applications are limited to forensic investigation.
- *Skin Luminescence.* The human skin shows a signature when reflecting light within certain wavelengths, which is referred as *skin luminescence*. This signature is because of individual characteristics of human skins, consisting of multiple layers and different structures, which affect the different wavelengths of light.

The distinctiveness of skin reflectance allows it to be used as a biometric feature for personal identification. This biometric technology is considered relatively new and requires further testing.

- *Electroencephalogram Pattern.* Several research works recently proposed that there are some distinctive features in the electroencephalogram (EEG) signal for each individual, which could possibly be used for biometric purposes. They examined the statistical features such as the coefficients in Autoregressive (AR) models (Paranjape et al., 2001) of the EEG signal, and they concluded there is great potential for EEG signal being used as biometric features. However, these technologies are yet to undergo more rigorous study and testing for them to be accepted by the research and industrial communities.

Some other personal traits are also utilized for biometric purposes, such as *Gait*, *Ear Shape*, *Lip-print*, *Keystroke* etc. Most of these biometrics are still in the early research stages. Whilst they show some potential to become a reliable technology, there are limited researches carried out in these biometrics. Most of them are not yet well established, and have not undergone rigorous testing and peer review. Meanwhile, the lack of publicly available databases limits the potential research activities in these biometric technologies.

2.4 Comparison of Assorted Biometric Technologies

2.4.1 A Summary

As stated in the previous Sections 2.1, 2.2 and 2.3, each and every single biometric technology has its own strengths as well as limitations. To determine whether a

Table 2.1: Measurement Criteria for Various Biometrics Technologies

Group	Type	Measurement Criteria				
		Accuracy	Tolerance to Forgery	Intrusiveness	Ease of Use	Cost
Physiological	Face	Low	Low	Low	High	Low
	Fingerprint	High	Med.	Med.	Med.	Med.
	Iris	High	High	High	Med.	High
	Retina	High	High	High	Low	Med.
	Hand Geometry	Med.	Low	Med.	High	High
Behavioral	Voice	Med.	Med.	Low	High	Low
	Signature	Med.	Low	Low	Med.	Med.

biometric technology fits a specific application domain, the decision has to be made based on the application properties as well as the set of criteria (as explained in section 1.1.5) that characterize different biometric identification systems. Table 2.1 is a general comparison of the current mainstream biometric technologies, which are grouped into two categories, namely physiological and behavioral biometrics.

It is not difficult to conclude from Table 2.1 (Luis-Garcia et al., 2003) that, in general, physiological biometrics have relatively higher level of accuracy than the behavioral ones do, and similarly for the tolerance to forgery. Therefore, under circumstances (such as accessing military facilities), where security concern is critical, the physiological features, such as iris and retina, is more desirable. Whilst for the behavioral biometrics, it is more preferable for applications where usability is critical and the accuracy requirement is moderate. An example is that signature is a better option for making payments in a restaurant.

2.4.2 The Developing Trends

It is further observed from Table 2.1 that none of the above biometrics accomplishes all the requirements of the measurement criteria. Many researchers try to resolve

this problem by combining multiple biometrics and integrate them into a multi-model biometric system. The final matching decision of the system is made based on the information fusion result of the combined features; alternatively, fusion can be carried out on the individual score of each biometric recognition.

Another approach is to further refine the current individual biometric system to improve its robustness. New techniques for data acquisition and processing can compensate the disadvantages of a certain biometrics. As data acquisition plays a vital role in the overall biometric system, more efforts have been put into the improvement of data acquisition devices, as well as attempting alternative acquisition methodologies. An example is the utilization of ultrasonic scanning of fingerprints which increases the tolerance of such biometrics against change of data acquisition environment, as explained in Section 2.1.2.

A third solution is to look for new human traits that can serve as a new biometrics. In order to better meet the measurement criteria, the new trait has to be robust in its nature in terms of distinctiveness, concealment and collectibility. Many human surface features have been studied extensively throughout the years, such as the aforementioned faces and fingerprints. Whilst they can offer relatively high accuracy, their tolerance to forgery is moderate. There is a recent developing trend of studying the unique interior features of the human body for biometric purposes. However, acquirement of these interior features is usually intrusive. Retinal and iris scanning are two examples of having high immunity to forgery and low user acceptance simultaneously. Nevertheless, the vein pattern, which lies directly beneath the skin, can well tackle this problem faced by other subsurface features, and it has not been well investigated previously.

2.5 Current Development of Vein Pattern Biometrics

2.5.1 Overview

In 1991, a system that scanned the back of a clenched fist to determine vein structure for verifying user identity was first reported by MacGregor and Welford (MacGregor & Welford, 1991). Cambridge Consultants Ltd., in collaboration with the British Technology Group (BTG), also studied the vein pattern concept with the aim of developing a commercial system which they called Veincheck, and it was first presented at a seminar in September 1993 (Hawkes & Clayden, 1993). Though this product did not achieve much commercial success, the concept of using vein patterns as a biometric measure attracted an increasing amount of research interest. Three characteristics of vein patterns are the major sources that drive the development of the vein pattern biometrics, namely, *uniqueness*, *stability*, and *tolerance to forgery*.

Anatomically, aside from growth, accidental injury, and surgical intervention, a person's vascular patterns are distinct from person to person. It is believed even identical twins have different vascular network structures (and hence different vein patterns) (Jain et al., 1999). The shapes of vein patterns are also very stable. A person's pattern of blood vessels is "hardwired" into the body at birth, and remains relatively unaffected by aging, except for predictable growth as with fingerprints.

Unlike other biometric systems (such as face recognition systems) that can be easily defeated by intentional disguise, the blood vessels are hidden underneath the skin and are generally invisible to the human eye and other simple visual inspection systems, thus making vein patterns are much harder for intruders to copy. In addition, although it is possible to restructure the patterns of superficial blood flow by surgery,

this attempt faces very high risks of damaging the surrounding tissues and body nerve systems (Jain et al., 1999). Therefore, compared to other biometrics features, vein patterns have much stronger immunity from forgery.

Whilst its high tolerance to forgery is intuitive, the uniqueness and stability of vein patterns has never been proven in a strict scientific sense. Recently, several institutes and companies have carried out research into vein pattern biometric technology.

2.5.2 Data Preparation

There are two major concerns about data preparation. The first is the object of interest, and the second is the acquisition mechanism. Typically, for vein pattern biometrics, the object of interest is selected to be a part of human body that is considered less intrusive. The face, the hand, and the finger are considered most acceptable by the public.

Equinox Corporation (`http://www.equinoxsensors.com/`), a New York headquartered company, constructed a thermal image database for the face. This *Face Thermogram* technology utilizes the vein patterns in the human face as the biometric feature. The vein pattern image is captured using a thermal camera that records the temperature information of the face, and hence is also referred to as a Face Thermogram. These temperature values of a face thermogram are affected by changes in ambient temperature and some physiological conditions such as sinus problems, inflammation etc (Jain et al., 1999). However, when the objective is identification only, the temperature data itself is not used directly. Instead, the thermal data is analyzed to yield the anatomical structure information of the vein, which is constant with regardless of the medical condition variables.

Compared to the face thermogram, acquiring vein patterns in the hand is consid-

ered less invasive and easier to use by many people. In addition to MacGregor and BTG mentioned in section 2.5.1, there are several other research groups and companies investigated the biometrics based on hand vein patterns. A research team (Cross & Smith, 1995) in the Australian Institute of Security and Applied Technology and a Korean research team (Im et al., 2000) both acquire the vein patterns in the back of the hand. Fujitsu Laboratories (Fujitsu-Laboratories-Ltd, 2003) came up with a product that detects the vein pattern in the palm side of the hand. All these works use the active infrared imaging technique to acquire the images. However, the details of the acquisition setups are not revealed in any public publications. Meanwhile, there are no publicly available database for hand vein patterns.

Miura et. al. (Miura et al., 2004) investigated the vein patterns in a finger. They irradiate an infrared light beam and let it pass through the finger, and a camera captures the IR lights and forms an image which contains the vein patterns in the finger.

Though varieties of techniques have been attempted to acquire vein patterns images from various parts of human body, there lacks of detailed design setup information on the data acquisition. In addition, there is no analysis specifically addressing the factors (both internal and external) that affect the data acquisition process and the subsequent impacts on the image quality. Last but not least, for hand vein patterns, to the best of our knowledge, there is no database available to the public research community, and thus limiting the research activities from further investigating the potential of the vein pattern biometrics.

2.5.3 Processing of the Vein Patterns Images

Most of the current works do not provide sufficient preprocessing to the vein pattern images. The selection of region of interests (ROI) is relatively ambiguous. Cross and Smith (Cross & Smith, 1995) use the whole fist as the object of interests, whilst Im et. al. (Im et al., 2000) predefine the ROI manually. Lin and Fan (Lin & Fan, 2004) did not apply any preprocessing to the extracted ROI images, whilst Im et. al. (Im et al., 2000) and Cross (Cross & Smith, 1995) used some standard low pass filters to suppress the high frequency noise. Cross further used some morphological operations to remove some of the defects in the images such as hair and skin pores. Nevertheless, the analysis of the performance and effect of these preprocessing efforts are not reported clearly in their works.

2.5.4 Features Used for Verification

There are two main types of features that have been used as the vein pattern signature. Cross and Smith stored the vein patterns using the medial axis representation as the feature. A library template was constructed from several independently acquired signatures by continuously taking the union of the original template with the next signature that has been translated to have the highest correlation with the original template. Then matching was performed in a two-fold manner: a signature to be verified was matched against the dilated library template (forward match) using constrained sequential correlation, and then the library template was matched against the dilated testing signature (reverse match). The final matching decision was made based on whether both the forward and reverse match percentages were high. Cross examines a data set with 20 individuals, and claimed the features and algorithm used achieved around 5% FRR and 0% of FAR.

Lin & Fan (Lin & Fan, 2004) attempted a second approach by extracting the "Feature Points of Vein Patterns" (FPVP), which essentially are the residues after applying a modified watershed transformation to the vein pattern images. These feature points are represented as a feature vector in 2.1, where x and y are the coordinates, $I = f(x, y)$ is the gray value, $G = [(\partial f/\partial x)^2 + (\partial f/\partial y)^2]^{1/2}$ is the gradient, $\theta = tan^{-1}[(\partial f/\partial y)/(\partial f/\partial x)]$ is the gradient direction, and FP_N is 1 if (x, y) is an FPVP, otherwise 0.

$$FV(x, y) = \left[\begin{array}{cccccc} x & y & I & G & \theta & FP_N \end{array} \right] \tag{2.1}$$

In order to remedy the displacement of the FPVP, Lin and Fan use 3 multi-resolution filters to extract the dominant points by filtering miscellaneous features for each FPVP, and thus obtain the multi-resolution represention of the images. The 3 multi-resolution filters are namely Moment Filter (Equations 2.2 and 2.3), Mean Filter (Equation 2.4), and Count Filter (Equation 2.5) respectively. A hierarchical integrating function is then applied to integrate multiple features and multi-resolution representations. Experiments were carried out on their database containing images from 32 participants, and it was reported that the features and algorithm achieved 2.3% FRR and 2.3% of FAR.

- *Moment Filter*:

$$MDP_I^{(m,n)}(p, q) = mom^n(FPVP_w(x_i, y_i)),\ i \in \{1, 2, ..., 2^m \times 2^m\} \tag{2.2}$$

$$mom^n(ft) = \sum_x \sum_y (x - \overline{x})^k (y - \overline{y})^l ft(x, y) \tag{2.3}$$

where $MDP_I^{(m,n)}(p, q)$ represents the nth moments of I at the mth level resolution whose coordinates are p and q, and $FPVP_w(x_i, y_i)$ indicates the $FPVP$s

inside a $2m \times 2m$ window for the $FPVP(x, y)$.

- *Mean Filter*:

$$M_x(p,q)^{(m)} = mean(FPVP_w(x_i, y_i)),\ i \in \{1, 2, ..., 2^m \times 2^m\} \tag{2.4}$$

where $M_x(p,q)^m$ is the mean value of the x_i coordinates of $FPVP_w(x_i, y_i)$ inside a $2 \times 2m^2$ window in the original images, and $M_y(p,q)^m$ represents the mean value of the y_i coordinates.

- *Count Filter*:

$$C_f^{(m)}(p,q) = count(FPVP_w(x_i, y_i)),\ i \in \{1, 2, ..., 2^m \times 2^m\} \tag{2.5}$$

where $C_f^m(p,q)$ is the number of $FPVP_w(x_i, y_i)$ inside the $2^m \times 2^m$ windows and represents the number of $FPVP$s at the mth-level resolution.

Fujitsu Lab claimed that their systems achieve relatively high level of accuracy (the FRR is 1% whilst FAR is 0.5%), however, their technologies and features used are not revealed in any publication form accessible to the public.

2.5.5 Research Issues of Vein Pattern Biometrics

There are four major research issues remaining unsolved for the vein pattern biometrics.

1. *Uniqueness Validation.* Although as mentioned in Section 2.5.1, the uniqueness of vein patterns can not be proved in a strict scientific sense; however, it is important to study its uniqueness in a statistical significance manner. It is necessary to assess its discriminating power in a computational measure in order for the vein patterns to qualify as another biometrics. In addition, so far, there

is no research addressing the issue of genetic relationship for vein patterns. The correlations between the vein patterns of a pair of twins as well as the members within a family is unknown. It is valuable to find out this genetic relationship of vein patterns by measuring their correlation distances, even though the vein patterns might yield a low level of similarity.

2. *Standard Vein Pattern Image Database.* The lack of a standard vein pattern image database to the public research community is a problem which prevents any research works from bench-marking the performance of their methods or algorithms.

3. *Optimum Data Acquisition and Processing Techniques.* It has been shown that several data acquisition techniques have been applied to acquire vein pattern images. However, there is only little information on the data acquisition system design, and there is scant analysis on the factors that affect the image quality. The data quality plays a critical role in any biometric systems, therefore, finding an optimum data acquisition technique is an important issue for vein pattern biometrics. Meanwhile, additional processing techniques are required to increase image quality for better system performance.

4. *Optimum Feature Sets.* Like other biometric technologies, identifying an optimum feature set is a key and usually difficult problem. Though several feature types have been investigated to represent the vein patterns. There is plenty of room to find more optimum features so as to improve the matching accuracy as well as to encode the vein patterns in a more efficient manner.

Hence, this research is targeting to tackle all these challenges currently faced by vein pattern biometric technology.

2.6 Conclusion and Research Directions

2.6.1 Summary and Conclusions

In this chapter, six mainstream biometric technologies and some other esoteric biometrics have been surveyed. For each of the biometrics, four aspects of the technology were studied, namely: *general principles*, *data acquisition*, *features*, and *current challenges*. Comparison of the various biometrics is made based on the general measurement criteria for biometrics. Then this chapter specifically reviews the current status of the vein pattern biometrics. The same 4 aspects of the vein pattern biometric as other biometrics were studied, and the major 4 research issues remaining for vein pattern biometrics were identified.

Through the study of various biometric technologies, it is apparent that overall, the physiological biometrics outperform the behavioral biometrics, especially in terms of accuracy and tolerance to forgery. However, none of current biometrics meets all the general measurement criteria. Whilst the current individual biometrics nowadays has relatively high recognition accuracy, most of the biometric features have difficulty to achieve high immunity against forgery and low intrusiveness simultaneously. The vein patterns, however, with the properties of being distinct, stable and invisible to naked eyes, depict the potential to become more advantageous over other biometrics. In the meantime, this vein pattern biometrics has not been fully studied, and hence it is worthwhile to investigate its potentials to become another mainstream biometric technology.

2.6.2 Research Directions

This research is aiming to resolve the 4 issues faced by the current vein pattern biometrics, as listed in Section 2.5.5. Therefore, the following research work must be

carried out carefully.

1. To investigate various imaging technologies and determine the optimum method and setups for acquiring vein pattern images.
2. To construct the vein pattern image database and make it available to the public research community.
3. To improve vein pattern image quality by attempting novel preprocessing algorithms.
4. To propose and identify a more optimum features as the vein pattern signature for matching and encoding.
5. To assess the discriminative power of the hand vein patterns by the means of measuring the recognition accuracy in the context of a personal verification application.
6. To study the genetic relations of vein patterns. This mainly refers to the study of the correlations of such patterns between identical twins.

2.6.3 The Proposed Hand Vein Pattern Biometrics Framework

A framework was proposed for the investigation of the hand vein pattern biometrics. This framework is based on the general model of the biometric identification systems (BIS) proposed by Wayman (Wayman, 1997). The system consists of 5 individual processing stages: *Hand Image Acquisition*, *Image Enhancement*, *Vein Pattern Segmentation*, *Skeletonization* and *Matching*, as shown in Figure 2.3. The work in the rest of this thesis studied details of this system framework.

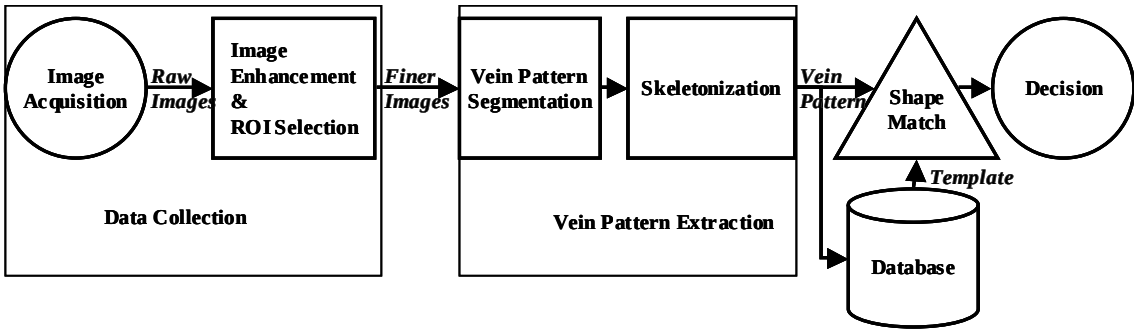

Figure 2.3: The framework of the hand vein pattern biometric system.

Chapter 3

Vein Pattern Acquisition Mechanisms

The data quality for any biometric application is vital. It is therefore critical to find an optimum solution for acquiring vein pattern images. This chapter studies the principles of Far- and Near- Infrared imaging techniques to assess their capability of acquiring vein pattern images. It also presents the designs of the image acquisition system setup, as well as the data collection procedures. Further analysis was performed to evaluate the image data quality and the factors affecting the data quality. Meanwhile, due to lack of a publicly available database, much work has been done to collect infrared hand vein pattern images with the aim to build up a bench-marking database for the research activities in vein pattern biometrics.

3.1 General Medical Practices

As the vein patterns formed by superficial blood vessels lie underneath the skin surface, the invisibility of veins to any traditional visual inspection system makes the successful image acquisition of the vein patterns a technical challenge. As the quality of the images performs a key role in all the subsequent processing stages of the vein pattern

Figure 3.1: A coronary angiogram (an X-ray with radio-opaque contrast in the coronary arteries) that shows the left coronary circulation. (Source: http://en.wikipedia.org/wiki/Angiography)

biometric systems, the image acquisition is critical for the systems. In many medical practices, X-ray and ultrasonic scanning are used to obtain vascular images.

The X-ray film or image of the blood vessels is commonly called an angiogram. As blood has the same radiodensity as the surrounding tissues, a radiocontrast agent (which absorbs X-rays) is added to the blood to make angiography visualization possible. Figure 3.1 shows a coronary angiogram (an X-ray with radio-opaque contrast in the coronary arteries) that shows the left coronary circulation.

Another well known technique is by ultrasonic scanning, also called ultrasound imaging or sonography. It involves exposing part of the body to high-frequency sound waves to produce pictures of the inside of the body. Because ultrasound images are captured in real-time, they can show blood flowing through blood vessels. Ultrasound exams do not use ionizing radiation (x-ray), however, it requires user to apply clear gel to the area of the body to be studied so as to help the transducer make secure

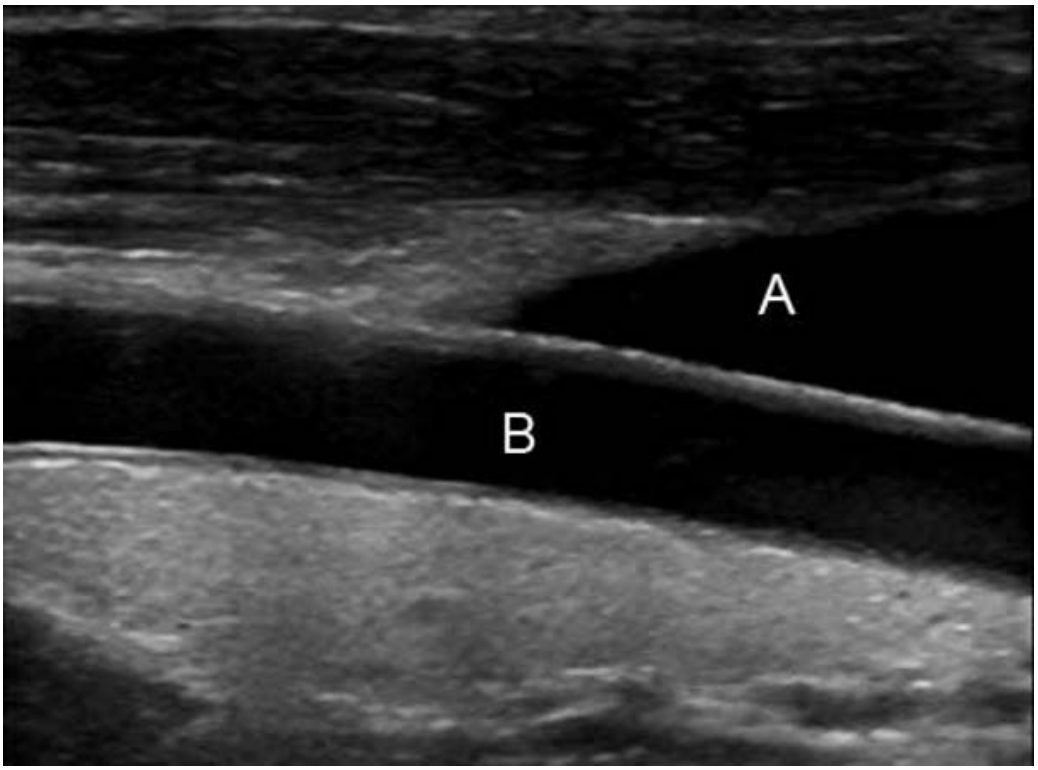

Figure 3.2: Image of carotid artery. (a) jugular vein, (b) right common carotid artery (Source: http://www.radiologyinfo.org)

contact with the body and eliminate air pockets between the transducer and the skin. Figure 3.2 shows an image of carotid artery.

Whilst these methods can produce good quality images of blood vessels, they are an invasive technique (in the case of X-rays) as it requires injection of agents into the blood vessels. In addition, excessive doses of X-ray radiation is dangerous. Ultrasonic imaging is less dangerous but requires the application of a gel to the surface of the skin and the images take several seconds to acquire. Such constraints are not acceptable for general purpose biometric applications in the real-world, and hence they are more commonly used in the medical practices instead. Obtaining the vein pattern images in a non-invasive manner is the key challenge in a vein pattern biometric system.

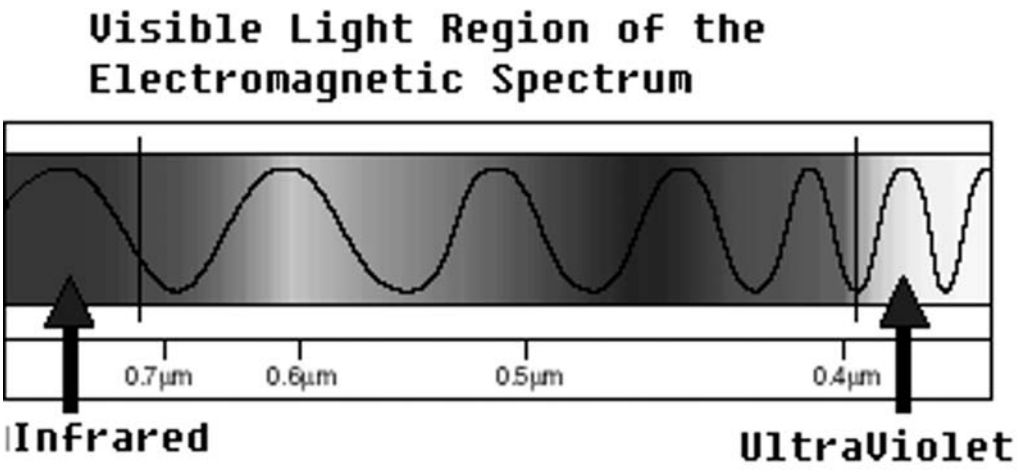

Figure 3.3: The visible light region in the electromagnetic spectrum

3.2 Non-Intrusive Vein Pattern Acquisition

Human eyes can only detect visible light that occupies a very narrow band (approx. 400 - 700 nm wavelength) of the entire electromagnetic spectrum, as shown in Figure 3.3. However, generally speaking, there is much more information contained in other bands of light in the electromagnetic spectrum reflected/emitted by the objects of interest. Imaging objects within different spectral regions involves different physical principles, which requires special imaging devices, and results in images with significantly different properties. Applications like remote sensing use special multi-spectral or hyper-spectral imaging instruments to obtain images in a wide spread of bands within the electromagnetic spectrum.

Similarly, for human vein patterns beneath the skin, their visibility under normal visible light conditions is fairly low, which prevents the visual inspection system from forming images containing clear structures of the patterns. An ideal solution is to inspect the entire electromagnetic spectrum to determine the optimum imaging spectral range. Nevertheless, this attempt requires very expensive and usually specially-manufactured instruments and devices. Since the vein pattern images in this research is targeting for general biometric applications, it is more reasonable to

consider the existing imaging techniques used in other applications, which generally have lower cost. Infrared imaging, is a well established no-contact imaging technique and considered more acceptable to most people.

In the entire electromagnetic spectrum, Infrared refers to a specific region with wavelength typically spanning from $0.75\mu m$ to $1000\mu m$. This region is commonly further divided into four sub-bands: *1. Near Infrared* $(0.75-2\mu m)$*; 2. Middle Infrared* $(2-6\mu m)$*; 3. Far Infrared* $(6-14\mu m)$*; 4. Extreme Infrared* $(14-1000\mu m)$. Due to the constraint of the equipments, this research mainly focuses on vein imaging using two sub-bands of the infrared spectrum: Far-Infrared (FIR) and Near-Infrared (NIR).

3.2.1 Far-Infrared Image Formation

Almost all black body objects emit radiation when they are heated. The Far-Infrared (FIR) imaging technology forms an image passively using the infrared radiation emitted by the human body.

Principles of Imaging

All objects radiate a continuous spectrum of frequencies. The total emissive power ω is described by the Stefan-Boltzmann Law given in Equation 3.1, where ε is the emissivity of the object and $\sigma = 5.6703 * 10^{-8} watt/m^2K^4$ is Stefan's constant. The relationship between the wavelength λ_{max} and black body temperature T is formulated by Wien's Displacement Law based on Planck's energy distribution law as given in Equation 3.2, where the unit of T is in Kelvins (K) which relates to Celsius in Equation 3.3.

$$w = \varepsilon * \sigma * T^4. \tag{3.1}$$

$$\lambda_{max} = 2.9 * 10^{-3}/T. \tag{3.2}$$

$$K =^{\circ} C + 273.15. \tag{3.3}$$

To determine the IR radiation range for the human body, it is firstly assumed that the human body is a black body and the temperature is $37°C$. Then the peak radiant wavelength by the human body can be calculated to be $\lambda_{max} = 9.35\mu m$ using Equations 3.2 and 3.3. More typically, a human body emits infrared radiation with wavelength in the range of 3–14 μm. These infrared waves radiate into the atmosphere and are attenuated according to the infrared transmittance spectrum of the atmosphere, and at the ranges of 3–5 μm and 8–14 μm (Harris, 1992), the radiant emittance of infrared spectrum possesses the highest transmittance rate. Therefore, a thermal camera with detector sensitivity in the range of either 3–5 μm or 8–14 μm, is capable of capturing the radiated IR waves within these ranges, and based on the energy of the IR radiation, calculates the temperature profile of the imaged human body part using Equation 3.1. An image can be further generated by converting the temperature value to the corresponding pixel intensity value, which visually shows the heat distribution of the human body part.

It has been noted by researchers (Lin & Fan, 2004) that human superficial veins generally have higher temperature than the surrounding tissues. Therefore, via thermal imaging, the images containing the heat distribution of body parts can clearly display the structure of the desired vein patterns, as can be seen in Figure 3.5. The advantage for FIR imaging is that it forms images using the infrared radiation emitted from the objects. No external lighting is required. Therefore it does not suffer from illumination problems like many other imaging techniques.

System Setup and Image Acquisition

In this research, an NEC Thermo Tracer TS7302 was used as the FIR image acquisition device. It operates in the spectral range of 8–14 μm, and has a temperature resolution of 0.08°C and spatial resolution of 320(H) x 240(V) pixels. The camera was mounted on a copy-stand and adjusted to a height of approximately 30cm above the base of the copy-stand. A workstation is connected to the camera to receive and process the image data. The overall system setup is shown in Figure 3.4.

(a) NEC Thermotracer

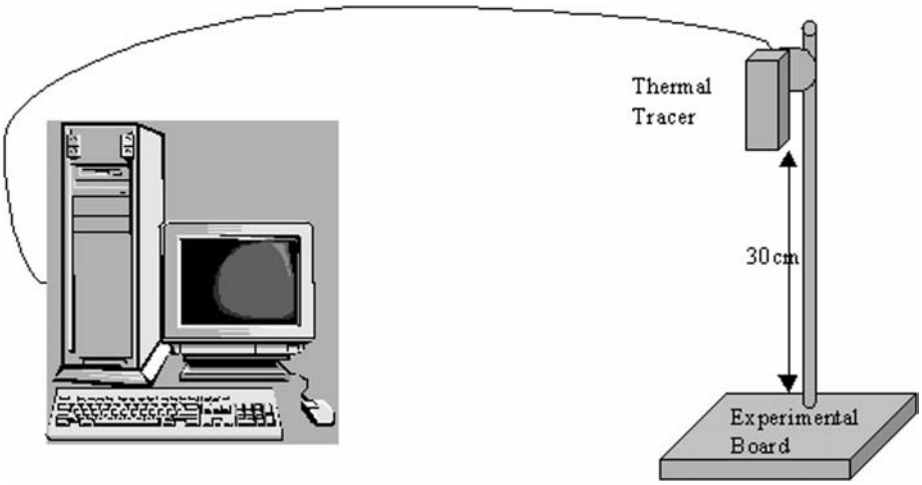

(b) Overview of the System Setup

Figure 3.4: Far Infrared Vein Pattern Image Acquisition System Setup

During the FIR image acquisition, the subject placed one hand on the base of the copystand with the back of the hand facing upwards so that the FIR camera can

capture the temperature profile of the back of the hand and transfer it to the workstation. On the workstation, the thermo analyzer software converts the temperature data into 256 level gray-scale images for analysis in the subsequent stages.

Far-Infrared Vein Image Quality Analysis

Figures 3.5, 3.6(a) and 3.6(b) show some sample vein pattern images captured using this FIR imaging method. From Figure 3.5, it can be seen that the major vascular network in the back of the hand is successfully captured. However, for the palm side (Figure 3.6(a)) and the wrist area (Figure 3.6(b)), there is no meaningful information of the vein patterns contained in the image.

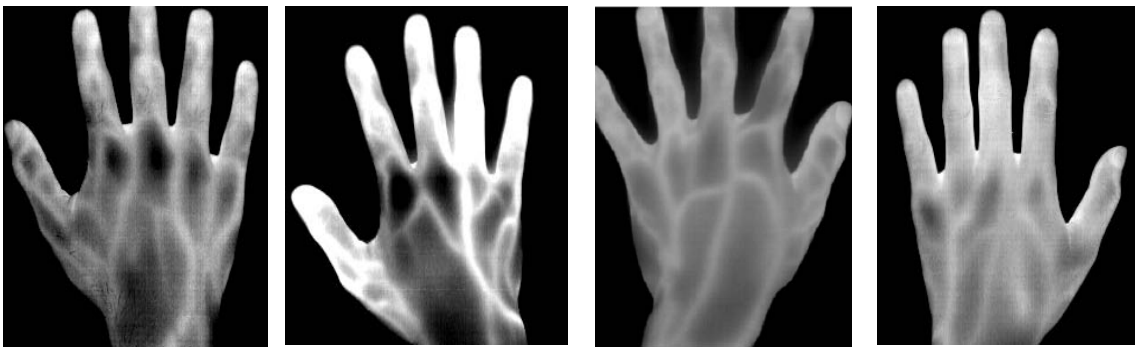

Figure 3.5: FIR images of the back of four different hands taken in a normal office environment

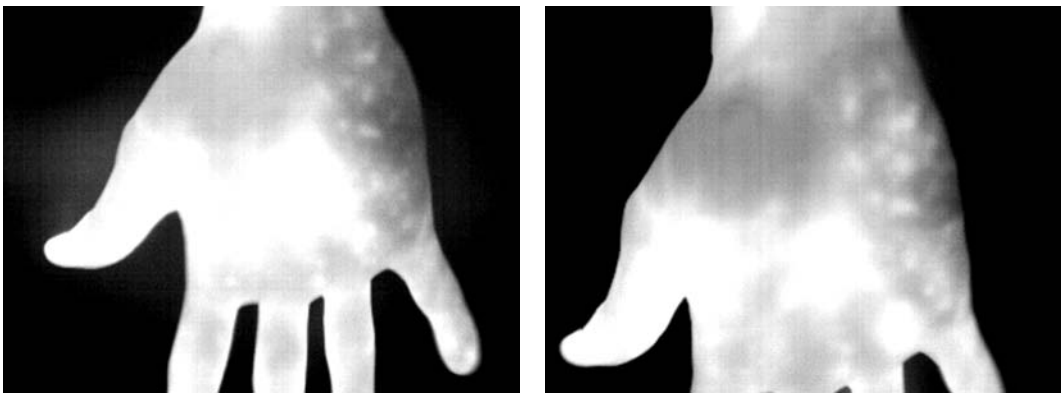

(a) FIR image for palm (b) FIR image for wrist

Figure 3.6: Far-Infrared images of the palm and wrist taken in a normal office environment

The images of four different hands shown in Figure 3.5 were captured in a normal

office environment, where the ambient temperature and humidity were constant and the ambient temperature was at least 10 degrees centigrade less than the human body temperature. Figure 3.7 shows another set of images captured in a tropical outdoor environment ($30 - 34°C$ and $> 80\%$ humidity). It can be seen that the ambient temperature and humidity have a negative impact on the image quality, and the vein patterns in these images are now not easily visually distinguishable. In addition, perspiration on the skin surface will also affects the image quality. Figure 3.8 shows the images of the same hand at two different time instances. Far-Infrared imaging technology is very sensitive to external conditions.

Overall, most of the FIR images obtained have low a level of contrast, which makes it difficult to separate the veins from the background. Also, due to heat radiation, the tissue near the blood vessels has similar temperature (and hence similar gray level in the image) as the vein. This makes it difficult to locate the exact position of the vein. In addition, as the Far-Infrared imaging can only capture the major vein patterns, the information contained in these patterns is limited, which will reduce its uniqueness and thus will prevent it from being used as the only biometric in a large scale person identification task.

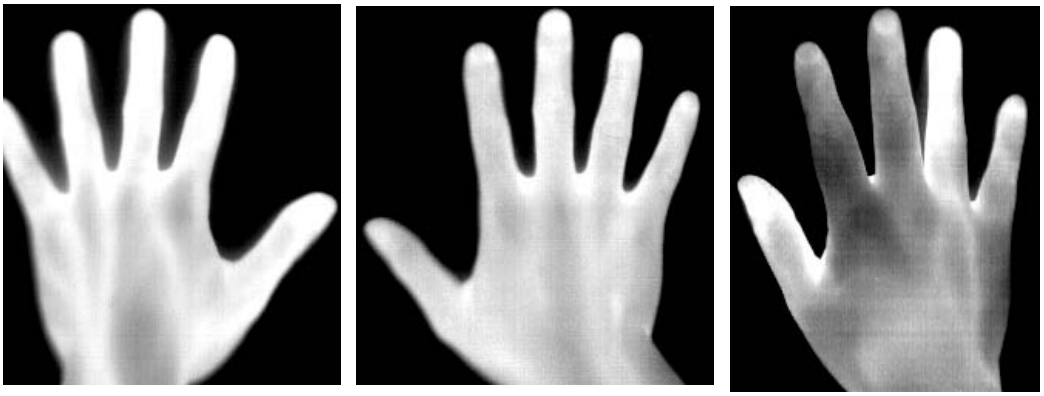

Figure 3.7: FIR images of the back of the hands in an outdoor environment, where veins are not clearly visually discernable

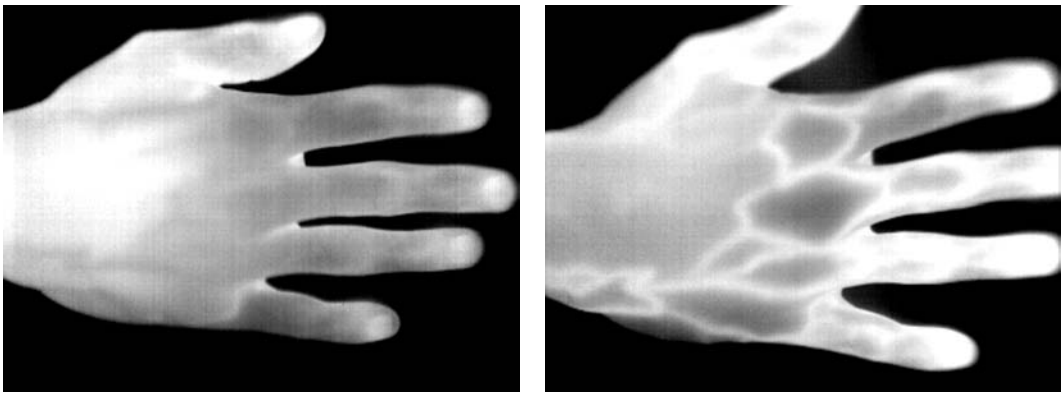

(a) (b)

Figure 3.8: Far-Infrared image of the same hand taken a few weeks apart

3.2.2 Near Infrared Image Formation

Principle of Imaging

Two special attributes of infrared radiation and human veins lead to another method of vein pattern imaging: (i) The incident infrared light can penetrate into the biological tissue of the hand to a depth of approximately $3mm$, and (ii) The reduced hemoglobin in venous blood absorbs more of the incident infrared radiation than the surrounding tissue (Cross & Smith, 1995). Therefore, by shining an infrared light beam at the desired body part, a CCD camera with an attached IR filter can be used to capture an image of veins near to body surface. The vein patterns near the skin surface appear darker than the surrounding parts and are easily discernible.

Biologically, there is a "medical spectral window" which extends approximately from about 700 to 900 nm, where radiation in this spectral window penetrates deeply into tissues, thus allowing for non-invasive investigation (Fantini & Franceschini, 2002). Therefore, for imaging the human body, and features below the skin surface, the wavelength of the infrared light beam coming out from a light source is selected to be within the near infrared region with wavelength around $850nm$. Using this wavelength, it also avoids undesirable interference by the IR radiation (with a wavelength of 3 μm - 14 μm) emitted by the human body and the environment.

System Setup and Data Acquisition Process

In our study, we used two LED array lamps to shine infrared light onto the hand from both sides. The infrared light emitted by the LED lamps peaks at a wavelength of 850nm. In order to form an image with this reflected infrared light from the hand, we need to use a camera whose spectral response also peaks at a wavelength of around 850nm. A Hitachi KP-F2A infrared CCD camera was selected for this purpose. As can be seen from Figure 3.9(a), the spectral sensitivity range of this camera covers well the peak of the infrared light from the LED lamp. To eliminate the effect of visible light, an optical infrared filter was mounted in front of the camera's lens. Three infrared filters with different cutoff wavelength (720nm, 800nm, and 900nm) were experimented with, and it was concluded that the infrared filter with cutoff wavelength of 800nm produced better images. Hence, during our data collection, a Hoya IR80 filter was used. This decision is further supported by the technical specification of the filters, where the spectral sensitivity is much higher for the IR80 filter than the RM90 at the wavelength of 850nm, as shown in Figure 3.9(b).

The camera was mounted on a copy-stand, and adjusted to be approximately $60cm$ above the board. The camera was connected to a computer to capture the images using a frame grabber. The system setup is shown in Figure 3.9(c).

Similar to the far-infrared imaging, participants were required to place their hand at the center of the base of the copy-stand. At first, they placed their hand with the back of the hand facing up at the camera. Three images were then taken of the vein patterns in the back of the hand. Then the participant flipped the hand over with palm side facing up, and three more images were taken of the vein patterns in the palm. Finally, the participant moved the wrist to the center of the board, and another three images were taken of the veins in the wrist area on the underside of the hand.

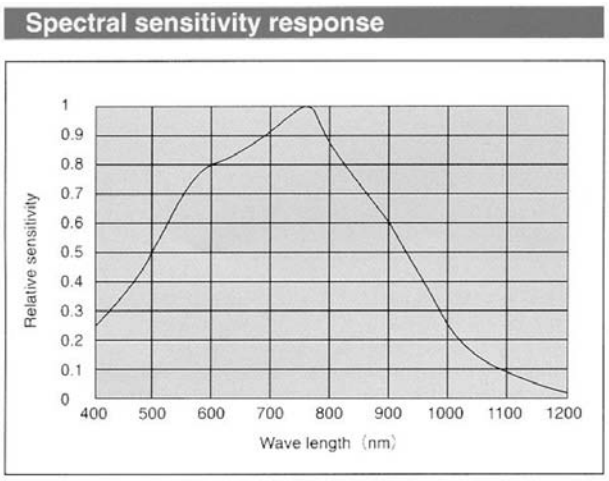

(a) Spectral sensitivity response for the KP-F2A camera (source: Hitachi)

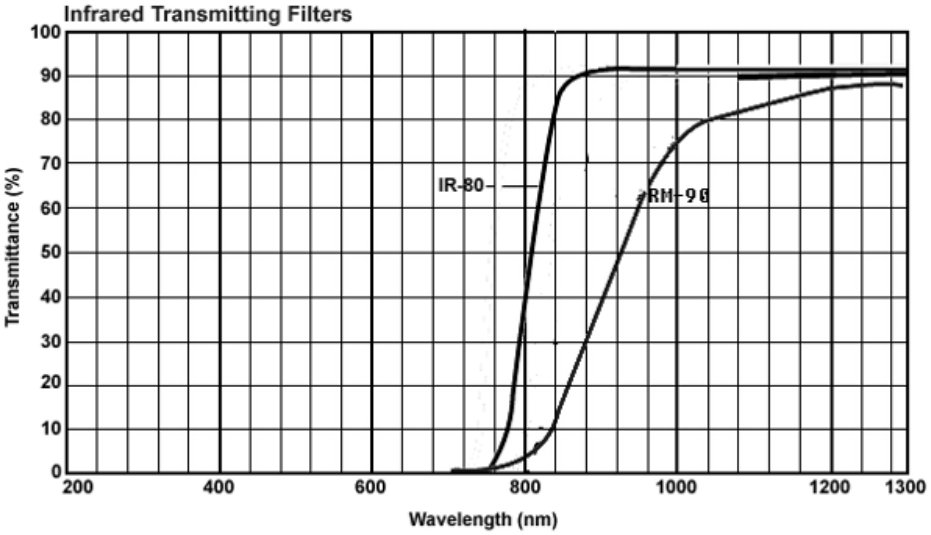

(b) The spectral sensitivity response for the Hoya IR-80 (800nm)/RM-90 (900nm) filter

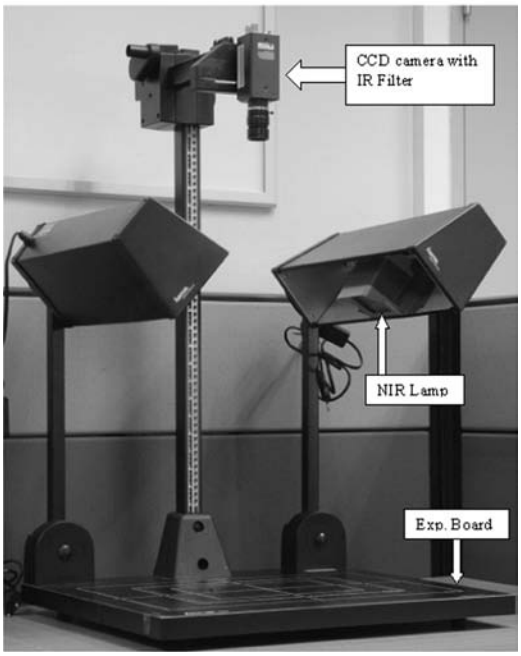

(c) The NIR imaging system setup

Figure 3.9: The near-infrared imaging System used to capture images

Near-Infrared Vein Image Quality Analysis

Figures 3.10 and 3.11 show vein pattern images captured by the NIR camera for the three parts of the hand: the back of the hand; the palm; and the wrist. By inspection, it can be seen from Figure 3.11(a), that the NIR imaging technique can capture the major vein patterns in the back of the hand as effectively as the FIR imaging technique. More importantly, the NIR camera is capable of capturing images of the small veins lying near the skin surface in the palm and wrist areas. Unlike the image of the back of the hand, where only major veins are visible, the vein pattern in the palm is far more complex and contains much more information than the one in the back of the hand. This is important because it significantly increases the potential discrimination power of the vein pattern biometrics when the size of the user group is large.

The NIR imaging technique is more tolerant to the external environment and the subject's medical condition and environmental situation. In our study, the quality of the image does not change significantly for both air-conditioned and outdoor environment. Also, the color of the skin does not affect the visibility of the vein patterns in the image. In our study, it is clear that the white skinned Caucasian and the tan skinned Indian, both have vein patterns that are all clearly visually distinguishable in the images.

However, NIR imaging of vein patterns suffers from the common illumination problem. It can be seen from Figure 3.11(a) that the center of the image is brighter than the border areas due to uneven illumination. Another disadvantage of NIR imaging is that marks and defects on the skin surface are also visible in the image, which occasionally will corrupt the structure of the vein patterns and lead to problems when it comes to the later image processing and pattern recognition stages. Figure

3.11(b) shows confusion in the NIR images caused by hairs on the back of the hand. Also, in Figure 3.10(a), the usual creases on the palm of the hand are difficult to distinguish from the vein patterns. Whilst human beings are capable of distinguishing these defects from the vein patterns in the image with a high degree of accuracy, it is a challenging, and as yet unresolved, task to remove these defects using automatic processing.

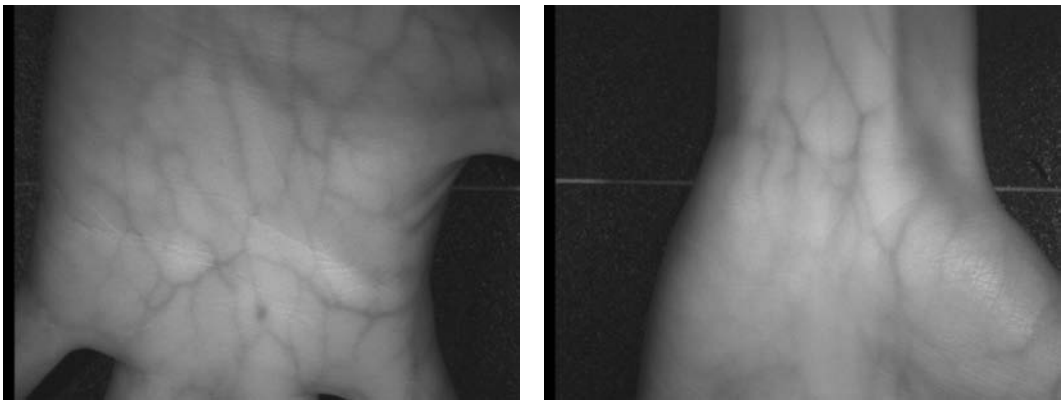

(a) NIR image of palm (b) NIR image of the wrist

Figure 3.10: Typical NIR images for the palm and wrist

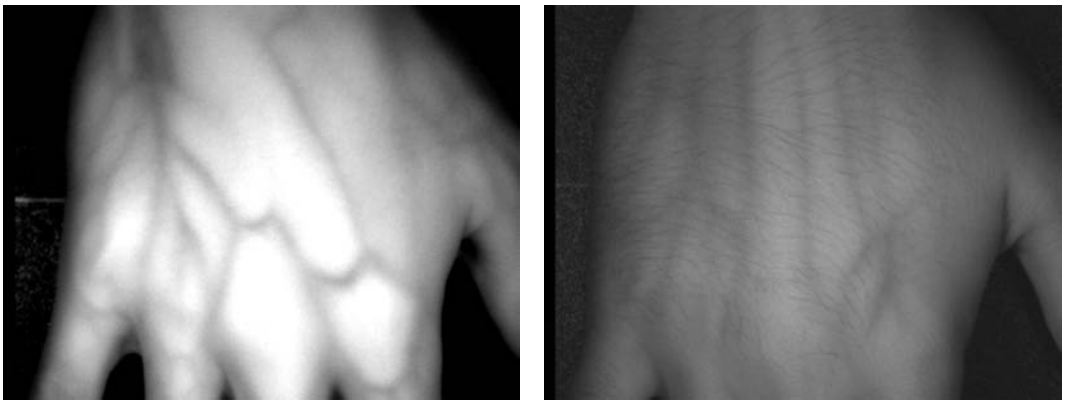

(a) NIR image of back of a hand (b) NIR image of the back of a hand with hair

Figure 3.11: Typical NIR images of the back of the hand

3.2.3 A Comparison between Far- and Near- Infrared Imaging

It can be seen easily from Sections 3.2.1 and 3.2.2 that the principles between FIR and NIR image formation are totally different. This leads to different imaging devices

and system setup, and consequently results in different image properties.

Whilst both imaging techniques are capable of capturing major veins in the hand, FIR imaging is less sensitive to the finer detailed structures formed by small veins. This prevents the FIR imaging from acquiring images in the palm or wrist areas, where the vein structure is more complex and richly textured. In addition, compared to NIR imaging, the FIR images are very sensitive to the external environment, changes of ambient temperature and humidity can easily degrade the visibility of the vein structure in the image. However, FIR imaging is based on the IR radiation from the human body, which makes it immune to illumination problems commonly faced by many other imaging applications.

For NIR imaging, it is capable of capturing the finer details of vein structures, therefore, it outperforms the FIR imaging when the vein patterns in the palm or wrist areas are the objects of interest. NIR imaging is more tolerant to the change of external environment, nevertheless, NIR imaging suffers from the disadvantage of the marks and defects on the skin surface being visible in the image, which in some occasion, will corrupt the structure of the patterns, which leads to problems when automatic separation of vein patterns from the background is needed. In fact, as will be discussed in Chapter 4, many of the NIR images in our database require frequent human intervention to remove the skin features and defects. Therefore, a decision was made that at the current stage, at the matching stage in Chapter 6, only the FIR vein pattern image data would be tested. Further work will be done to propose automatic skin feature removal methods for the NIR images in the future.

Table 3.1 shows a general comparison between Far- and Near- Infrared imaging techniques in the application of hand vein pattern image formation.

Table 3.1: A Comparison of FIR and NIR Imaging of Hand Vein Patterns

	Details Captured	Tolerance to Ext. Conditions	Tolerance to Skin Features	Tolerance to Illumination	Costs
FIR	Moderate	Low	High	High	High
NIR	High	High	Moderate	Moderate	Low

3.3 The Infrared Hand Vein Pattern Database

To the best of our knowledge, there is currently no hand vein pattern database available to the public research community. Therefore, it was necessary to construct a database for preliminary investigation of the vein pattern biometrics. In April 2006, we initiated an infrared hand vein pattern image data collection event that lasted for one week's time. A relatively medium-sized database containing both Far-infrared and Near-infrared vein pattern images was obtained. We set up two data acquisition stations in a public venue, and invited volunteers (both female and male) from the public to participate in our data collection exercise. The participants were of various racial groups, representing the racial mix in Singapore. They were mainly Chinese, Indian, and Caucasian but included other ethnic groups from Asia. The age group of those participants was between 18 to 60 years, and their occupations ranged from university students, professors, and technicians to manual workers such as cleaning ladies and electricians. Table 3.2 shows the distribution of participants against the gender and race for the NIR image database, whilst Table 3.3 shows the age distribution for both FIR and NIR image database. The data collection protocol that is designed and adopted by this project is attached as Appendix A to the end of this thesis, where detailed data collection procedures are reported.

The database of Far-infrared vein pattern images, currently has 47 distinct subjects. Each subject provided 3 images of the vein patterns in the back of their hands, which overall, resulted in a total of 141 Far-infrared images obtained from 47 partici-

Table 3.2: Participant Distribution Against Race Groups for the NIR Images Database

	Chinese	Indian	Caucasian	Others	Total
Female	35	5	2	11	53
Male	55	15	13	14	97
Total	90	20	15	25	150

pants in the database. The images are in 256 level gray-scale of size 320 x 240 pixels and are stored in Bitmap (bmp) format.

For the Near-infrared vein pattern images, we have currently collected images from 150 subjects. The database contains NIR images for the back of the hand (3 images), the palm (3 images), and the wrist (3 images). Images were taken for both the left and the right hands. Hence, there are 2700 images in the database for the 150 subjects (18 images per subject). The NIR images are also in gray-scale of size 644×492 pixels, and they are stored as Tagged Image File Format (tiff).

The reason why the FIR database is much smaller than the NIR database is because the failure rate for acquiring the FIR images containing visually discernible vein patterns is high. During our data collection process, only around 47 out of 150 subjects produced images with good quality, which accounts for around 30% of successful rate. On the contrary, NIR imaging has around 90% of successful rate, which accounts from 150 out of 170 subjects.

Another aspect of both databases is that they both contain images from 3 pairs of twins, which will be used to investigate the hereditary correlation of such vein patterns.

The infrared hand vein pattern database has been made available on the web-site and it is accessible upon request. The database is being extended gradually, and currently contains sufficient data for initial feasibility studies and evaluation to be carried out.

Table 3.3: Participant Distribution Against Age Groups for both FIR and NIR Image Databases

	<20	20-29	30-39	40-49	≥50	Total
FIR	6	25	8	6	2	47
NIR	7	109	21	11	2	150

3.4 Summary

This chapter investigates imaging technologies for acquiring hand vein patterns for biometric purposes. General medical practises such as X-ray angiogram and Ultrasonic scanning are found to be invasive and difficult to use. Two other major imaging methods were then studied: Far-Infrared (FIR) imaging and Near-Infrared (NIR) imaging. It was observed that both imaging techniques are capable of producing the vein pattern images effectively, though the two techniques use different physical phenomena and exhibit differences in image quality and features.

Analysis shows FIR imaging operates by detecting the electromagnetic radiation emitted from the human body in the far infrared wavelength with the peak value found to be $\lambda_{max} = 9.35\mu m$ and discerns the presence of veins near the surface of the skin by exploiting the fact that generally the blood in the veins is warmer than the surrounding tissue and hence there is more FIR radiation emitted from the veins. NIR imaging, on the other hand, operates quite differently by exploiting the fact that the hemoglobin in the blood absorbs incident infrared radiation with wavelength in the 700 to 900 nm range (which is just outside the wavelength of visible light range of 300 to 700 nm). It has been tested that, a system consisting of a NIR sensitive CCD camera mounted with a 800 nm optical filter and two NIR light projecting lamps, can well detect the vein structures within a few millimeters of the skin surface.

It was further observed that far-infrared imaging can capture the large veins in the back of the hand, it is not sufficiently discriminative to capture vein images in

the palm and wrist. FIR imaging is sensitive to ambient temperature and humidity conditions and also the temperature variation of the human body. The temperature difference at the surface of skin near a vein is only of the order of $0.2°C$warmer than the surrounding tissue. The ability to detect this temperature difference is close to the capability of the FIR sensors and the temperature across the hand surface may vary by several degrees centigrade making it impossible to accurately detect all veins in one image. Each image will result in flaring or "white-out" of some parts of the image, as can be seen in Figure 3.5. FIR imaging is difficult and the fact that only 47 of about 150 subjects imaged resulted in images which could be used for biometric comparison illustrates the difficulty in obtaining good FIR images of veins near the surface of the skin.

Near-infrared imaging was observed to perform better than FIR imaging by producing good quality images when capturing vein patterns in the back of the hand, palm, and the wrist. It is more tolerant to the changes in the ambient environmental and body temperature conditions. However, NIR imaging faces the problem of corruption from the skin features such as hair, cuts, external marks and palm prints. FIR does not suffer from this problem as the images are not affected by visible light.

Two infrared hand vein pattern image databases were constructed with the aim of providing bench marking data for vein pattern biometrics research activities. The databases are built based on FIR and NIR imaging techniques respectively, and they have reasonable levels of racial mixture, ages ranges, occupation ranges, and genders difference. FIR image database contains 141 images from 47 subjects, whilst the NIR image database has 2700 images from 150 subjects. This database is used throughout the course of the work, and particular interests are paid to the FIR vein pattern images in the back of the hand.

The work reported in this chapter was reported in the paper (Wang & Leedham, 2006).

Chapter 4

Preprocessing of Vein Pattern Images

In the FIR and NIR images prepared in Chapter 3, the vein patterns are visually discernible. However, in these raw images, the vein patterns only occupy a portion of the image area, and the vein patterns in this subarea of the image are the object of interest, therefore, it is necessary to isolate this subregion from the rest of the image, which is essentially to extract the region of interest. In addition, the quality of the raw images obtained in Chapter 3 is very low and is not suitable for further processing (such as vein pattern extraction) without enhancement. All these fall into the category of vein pattern image preprocessing. In this chapter, several image processing algorithms are proposed and investigated to solve the preprocessing related problems.

4.1 Problem Specification

Two major issues require special attention during the preprocessing.

1. *Region of Interest Selection.* In this research, the object of interest is the vein pattern in the back of the hand. Therefore, choosing a region of interest that

covers the majority and important vein pattern is critical for not missing any significant information that will potentially degrade the discriminating power of the pattern. In most traditional pattern recognition problems (such as palmprint recognition), the ROI is selected to be a fixed size region. However, this is not applicable to the vein pattern biometrics. Human veins grow as the person grows up, but the shapes remain fairly stable. If a fixed sized ROI is chosen for everyone, it will result in comparing vein patterns in different locations and different level of completeness (e.g. a fixed sized region of a child's hand and an adult's hand). This causes errors to the whole system, and hence an alternative approach of selecting region of interests is required that is invariant to the size change of the hand.

2. *Image Quality Enhancement.* It has been discussed in Chapter 3 that the both FIR and NIR images are of low contrast and are noise prone. In addition, for FIR images, due to heat radiation, the veins in the images are heavily coupled with many faint white regions, whilst for the NIR images, the skin features such as hairs and scars, are often visible in the images simultaneously with the veins. All these will lead to errors when trying to extract the shape of the vein patterns from the image. Therefore, preprocessing of the image is necessary. This requires appropriate modelling of the the noise in the image, finding appropriate filters for noise filtering, and automatically estimating the filter parameters for optimum image de-noising. Finally, extra measures have to be taken to suppress the effect of the skin feature residues observed in NIR images.

4.2 Defining Region of Interest Invariant to the Size of the Hand

During the collection of the image database, we restricted the position where the participants place their hands to be a rectangular region immediately below the camera. Therefore, the hand images are consistently aligned to within a few degrees of rotation. These constraints make it relatively easy to define a rectangular region in the hand images that defines the region of interest (ROI) which contains the main vein pattern in the back of the hand. In order to ensure all the ROIs reference to the same region in the hand image regardless of the size of the hands, we firstly locate a number of key landmark points of the hand, and then with the aid of these points, define the region of interest.

Usually, the landmark points of the hand include the 5 fingertips and the 4 valley points between each finger. In this work, we use only the valley points to define the ROI. To automatically find the position of the valley points, one has to firstly extract the contour of the hand.

Figure 4.1(a) shows a thermal FIR image of the back of a hand. It can be easily seen that the temperature of the hand is much higher than the background, and hence the hand appears much whiter in the image (though the gray level within the hand area varies due to uneven distribution of heat), whilst the stand base is much cooler than the hand and appears black in the image. With this attribute, the contour of the hand can be extracted using an edge detector.

The discontinuities of gray scale images can be detected as edge points by calculating the first- and second-order digital derivatives of the images as defined in Equations 4.1 and 4.2 respectively (where f is the original gray-scale image). The second-order derivative operator is more capable to extract small details in the image,

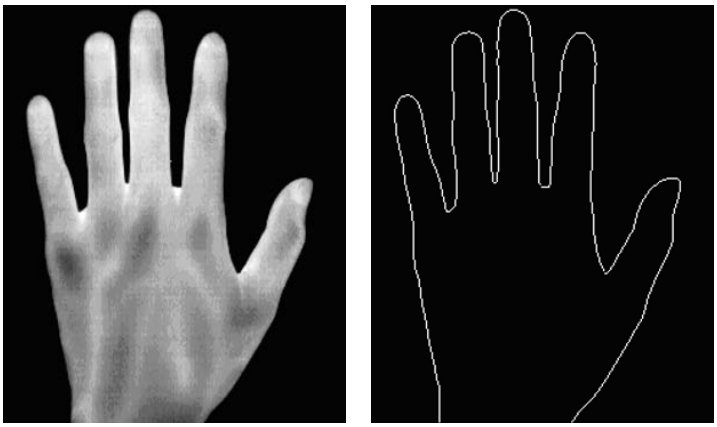

(a) A FIR Hand Image (b) Hand Contour Extracted by a Sobel Edge Detector

Figure 4.1: Extracting the Hand Contour

but it is also sensitive to noise. At this part of the work, only the hand contour is of interest and the small details of gray level variations at the back of the hand can be neglected. Therefore, using first-order derivative edge detector that possesses greater noise immunity is more suitable in this case, and it produces sufficiently good results. This is illustrated in Figure 4.1(b), where the contour is extracted using the Sobel (a variation of the first ordered edge detector).

$$\bigtriangledown f = mag(\bigtriangledown F) = \left[\left(\frac{\partial f}{\partial x}\right)^2 + \left(\frac{\partial f}{\partial y}\right)^2\right]^{1/2} \tag{4.1}$$

$$\bigtriangledown^2 f = \frac{\partial^2 f}{\partial^2 x} + \frac{\partial^2 f}{\partial^2 y} \tag{4.2}$$

After obtaining the contour for the hand, for each point on the hand contour, the Euclidean distance d_t between this point and the mid-point of the wrist is calculated in Equation 4.3, where (x_c, y_c) is the contour point and (x_p, y_p) is the coordinate of the mid-point of the wrist.

$$d_t = \sqrt{(x_c - x_p)^2 + (y_c - y_p)^2} \tag{4.3}$$

These distance values for all the contour points yield a profile as shown in Figure 4.2(c). It is not difficult to tell that the valley points between the fingers correspond to the valleys in this distance profile of the points in the contour. Therefore, by finding the local minima of this distance profile via a sliding window, all the valley points can be obtained. With the 5 valley points, two of them, namely the valley points P_1 (the valley point between the small finger and ring finger) and P_2 (the valley point between the middle finger and the index finger) are used to define the ROI as a rectangular region $R_{P_1P_2P_4P_3}$, where $l_{P_1P_3} = 1.4 * l_{P_1P_2}$. The process of defining the ROI is illustrated in Figure 4.2. Defining the ROI in this manner is because this ensures all the ROIs reference to the same region in the hand image and it covers major part of the vein patterns in the back of the hand; in addition to that, these ROIs are variables depending on the size of the hands. The image in Figure 4.3(a) shows the result of the extracted ROI for the hand image in Figure 4.2(a).

This technique of defining ROI can also be applied to the NIR images. Figure 4.3(b) shows the extracted ROI image from the NIR image.

4.3 Noise Estimation and Filtering for Vein Pattern Images

4.3.1 Sensor Noise

Like many imaging applications, both the NIR and FIR vein pattern images are corrupted by noise, this is because the output of the CCD sensor of the NIR imaging system and the micro-bolometer image sensor of the FIR imaging system not only carries the useful signal but it also includes a variety of noise components such as photon noise, fixed-pattern noise (FPN), and amplifier noise (Healey & Kondepudy,

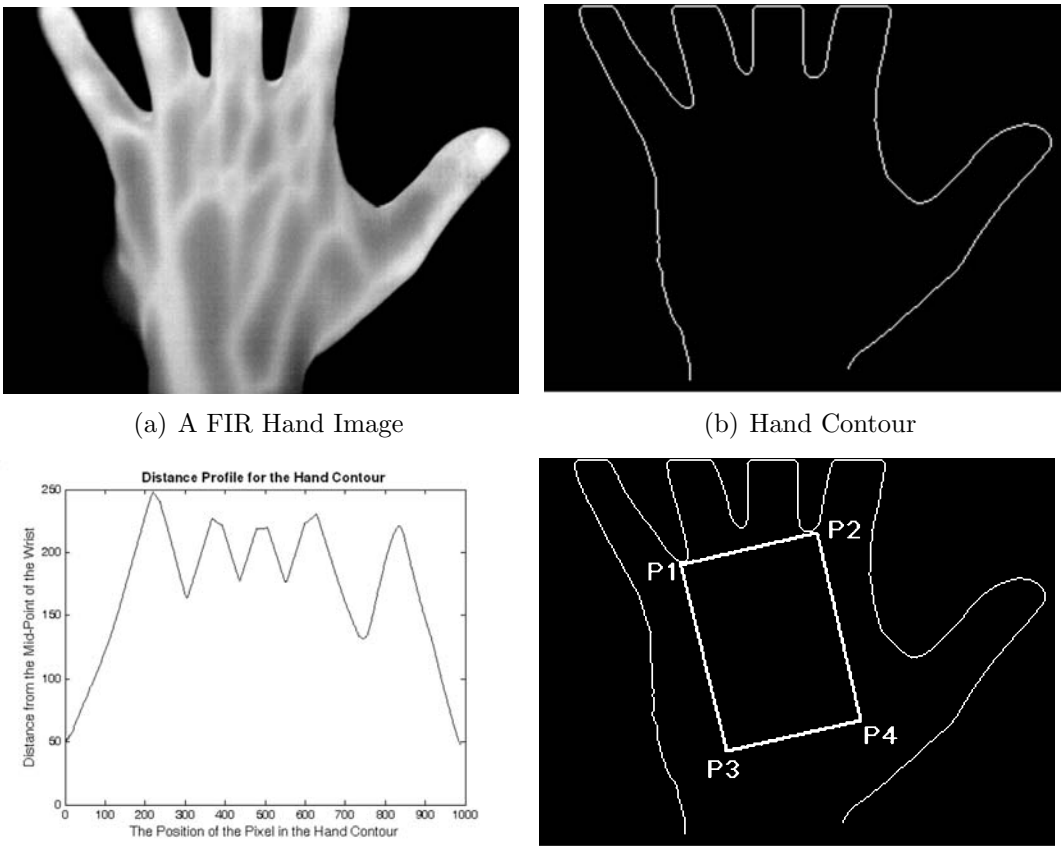

(a) A FIR Hand Image

(b) Hand Contour

(c) Distance Profile Between the Contour Points and the Mid-Point of the Wrist

(d) Locating the Region of Interest

Figure 4.2: Defining the Region of Interest

1994; Janesick, 2001; Faraji & MacLean, 2006). Photon noise is due to the random fluctuation of photon flux arriving at the sensor, and it follows Poisson statistics. FPN is due to differences in individual pixels' responsibilities. This type of noise is more prominent at higher intensities and is signal dependent. Its statistics are proportional to the original signal. Readout noise is introduced to the signal during the process of measuring the signal, and is usually modelled as white noise.

4.3.2 Noise Modelling

In some image de-noising applications, the noise is assumed to be additive and independent to the signal. However, as indicated in Section 4.3.1, real camera noise is not simply additive; it is strongly dependent on the image intensity level. Therefore, it is more reasonable to consider the noise model for the vein pattern image as signal

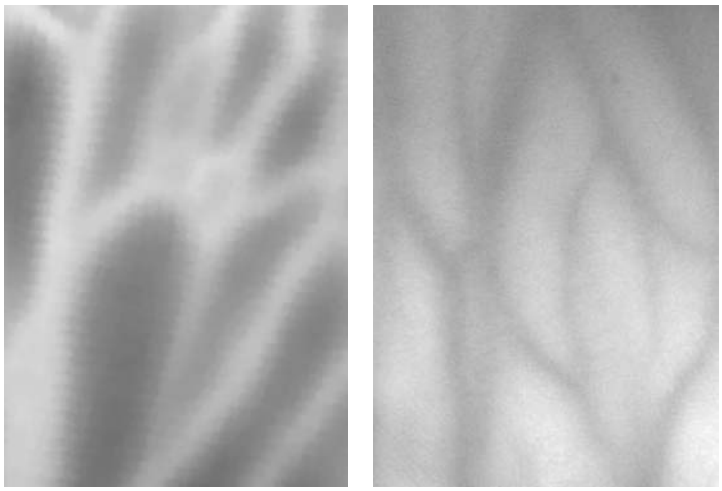

(a) Extracted ROI from a FIR image (b) Extracted ROI from a NIR image

Figure 4.3: Region of Interest Images.

dependent in our work (and likewise for most other real-life images). Jain (Jain, 1989), Pratt (Pratt, 1991) and other researchers (Curlander & McDonough, 1991; Burckhardt, 1978) have listed several other examples of signal-dependent noise (SDN) occurring in images, such as film-grain noise as well as speckling noise in Synthetic Aperture Radar (SAR) and Ultrasonic images.

Most of the signal dependent noise can be expressed in a perimetrically multiplicative form in Equation 4.4, which is then added to the original noise-free image $f(i,j)$. Equation 4.5 shows the general model (Jain, 1989) for signal-dependent noise, where $\mathcal{N}(i,j)$ is a stationary, zero-mean, and signal independent random process with variance σ_n^2, whilst $g(i,j)$ is the observed image. γ is the characteristic value for the specific imaging technique, which varies from application to application. It has been shown that the value of γ lies in the range of $[0,1]$, typically with values of 1 and 1/3 for SAR and photographic film images respectively; in the case of γ equals to 0, the noise is then essentially plain additive signal-independent noise.

$$\eta(i,j) = f^{\gamma}(i,j) * \mathcal{N}(i,j) \tag{4.4}$$

$$g(i,j) = f(i,j) + \eta(i,j) \tag{4.5}$$

It is apparent in Equations 4.4 and 4.5 that the noise term $\eta(i,j)$ varies with different parameters γ and the noise $\mathcal{N}$. Therefore, most of the filtering algorithms require *a priori* knowledge (or assumption) of γ and $\mathcal{N}$ (typically its variance σ_n^2). However, these parameters are not always available.

Several adaptive linear filters, including the Frost (Frost et al., March, 1982), Lee (Lee, May 1986), and Kuan (Kuan et al., 1985) filters are capable of removing the signal dependent noise. In particular, the Kuan filter, also known as the *Local Linear Minimum Mean Square Error* (LLMMSE) filter has been widely accepted that it displays superior performance in smoothing the SDN in the images whilst preserving important image features such as edges. Nevertheless, like other filters, the Kuan Filter requires knowledge of the parameters γ and σ_n^2. This part of the research will look into the use of the Kuan filter in removing the SDN in the vein pattern images, and a novel technique is proposed to construct the Kuan filter by estimating the filter parameters without the need to know γ and σ_n^2, which is elaborated in the following two sections.

4.3.3 The Local Linear Minimum Mean Square Error Filter

Given an observed image g, the *minimum mean square error* (MMSE) estimate of the original image f is its expectation conditional to g. That is:

$$\widehat{f}_{MMSE} = E[f|g], \tag{4.6}$$

where $E[\bullet]$ is the expectation operator. The linear MMSE (LMMSE) estimator, however, is an improved estimator that requires only signal and noise statistics up to

the second order and is given in Equation 4.7.

$$\widehat{f}_{LMMSE} = E[f] + C_{fg}C_g^{-1} \cdot [g - E(g)], \tag{4.7}$$

where the matrices C_g and C_{fg} are the covariance of g and the cross-covariance between f and g respectively.

According to Argenti et. al. (Argenti et al., May 2002), Equation 4.7 imposes a global mean square error (MSE) minimization over the whole image. When it is assumed that the noise η in Equation 4.5 is zero-mean and uncorrelated, and f is also uncorrelated (i.e. $C_f = E[f - E(f)][f - E(f)]^T$ is a diagonal matrix), the global minimization corresponds to a local minimization in the neighborhood of each sample. Let $\sigma_f^2(n)$ and $\sigma_g^2(n)$ denote the variances of f and g at the n^{th} sample position, the covariance matrices C_{fg} and C_g in Equation 4.7 become

$$C_g = diag[\sigma_g^2(1), \sigma_g^2(2), \ldots, \sigma_g^2(N)] \tag{4.8}$$

and

$$C_{fg} = C_f = diag[\sigma_f^2(1), \sigma_f^2(2), \ldots, \sigma_f^2(N)]. \tag{4.9}$$

Substituting C_{fg} and C_g into Equation 4.7, we will have the Local Linear Minimum Mean Square Error (LLMMSE) estimator for f (Kuan et al., 1985; Aiazzi et al., 1997), as given by Equation 4.10, where $\widehat{f}(i,j)$ is the estimate of the pixel $f(i,j)$, μ_f and σ_f^2 are the mean and variance of the local neighborhood of f; whilst $g(i,j)$ and σ_g^2 are the pixel value at position (i,j) and the variance of the same neighborhood region of the observed image g respectively.

$$\widehat{f}(i,j) = \left(1 - \frac{\sigma_f^2}{\sigma_g^2}\right) \cdot \mu_f + \frac{\sigma_f^2}{\sigma_g^2} \cdot g(i,j). \tag{4.10}$$

When applying the LLMMSE filtering, given the image region g, in order to find the estimated value $\widehat{f}(i,j)$, one has to obtain the values of μ_f, σ_f^2 and σ_g^2. As $\mu_f = E[f]$, by taking the expectation operation on both sides of Equation 4.5, we have

$$E[g] = E[f] + E[f^\gamma \cdot \mathcal{N}]. \tag{4.11}$$

Since $\mathcal{N}$ is a zero-mean, independent noise as stated previously, we then will have the unbiased version of μ_f

$$\mu_f = E[f] = E[g] - E[f^\gamma] \cdot E[\mathcal{N}] = E[g]. \tag{4.12}$$

σ_g^2 is obtained by its definition:

$$\sigma_g^2 = E[g^2] - E^2[g]. \tag{4.13}$$

To obtain σ_f^2, we can expand the right side of Equation 4.13 by substituting Equations 4.5 and 4.12 into it, then we have

$$\begin{aligned} \sigma_g^2 &= E\left[(f + f^\gamma \cdot \mathcal{N})^2\right] - E^2[f] \\ &= E\left[f^2\right] - E^2[f] + 2 \cdot E[f] \cdot E\left[f^\gamma\right] \cdot E[\mathcal{N}] \\ &\quad + E\left[f^{2\gamma}\right] E\left[\mathcal{N}^2\right] \\ &= \sigma_f^2 + \sigma_n^2 \cdot E\left[f^{2\gamma}\right] \end{aligned}. \tag{4.14}$$

$E\left[f^{2\gamma}\right]$ can be estimated by using the Taylor series expansion where

$$E\left[f^{2\gamma}\right] \approx \mu_f^{2\gamma} + \gamma(2\gamma - 1)\mu_f^{2\gamma-2}\sigma_f^2. \tag{4.15}$$

Substituting Equation 4.15 to 4.14, we have the estimate for the variance σ_f^2 of f.

$$\sigma_f^2 = \frac{\sigma_g^2 - \sigma_n^2 \mu_f^{2\gamma}}{1 + \gamma(2\gamma - 1)\mu_f^{2\gamma-2}\sigma_n^2}. \tag{4.16}$$

Therefore, the final LLMMSE filter can be expressed as ((Argenti et al., May 2002; Faraji & MacLean, 2006))

$$\widehat{f}(i,j) = \frac{\left(1 - \sigma_n^2 \cdot \frac{\mu_g^{2\gamma}}{\sigma_g^2}\right)(g(i,j) - \mu_g)}{1 + \gamma(2\gamma - 1)\mu_g^{2\gamma-2}\sigma_n^2} + \mu_g. \tag{4.17}$$

Kuan et. al. (Kuan et al., 1985) used this LLMMSE filter to smooth various types of signal-dependent noise with various values of σ_n^2 and γ (such as the film-Grain Noise having $\gamma = 1/3$), and achieved encouraging results. However, it is apparent from Equation 4.17 that given an observed image g, the LLMMSE filter is determined by the value of γ and noise variance σ_n^2. Whilst these two values are generally not available, Aiazzi et. al. (Aiazzi et al., 1997) estimate them by analyzing several homogeneous non-textured regions in the image. However, detecting uniform image regions in the noisy image is challenging (Faraji & MacLean, 2006) and usually requires user interaction (Sijbers et al., 1998). Therefore, we propose a technique to estimate the parameters for the LLMMSE filter by using two image instances of the noisy scene.

4.3.4 The Proposed Filter Parameter Estimation Methodology using Dual Images

It is easy to see from Equation 4.10 that $\widehat{f}(i,j)$ is determined by μ_f, σ_f^2 and σ_g^2. Since μ_f and σ_g^2 can be calculated using Equations 4.12 and 4.13 ($E[g]$ and $E[g^2]$ can be estimated by taking the spatial average of g and g^2 respectively), σ_f^2 is the only parameter to be determined.

If two image instances g_1 and g_2 of the same scene f were taken in a short interval, it can be assumed that both images follow the same model in Equation 4.5. For

simplicity, by dropping the index (i, j), we have

$$g_1 = f + f^{\gamma} \cdot \mathcal{N}_1 \tag{4.18}$$

$$g_2 = f + f^{\gamma} \cdot \mathcal{N}_2. \tag{4.19}$$

Since $\mathcal{N}$ is a stationary process as stated in Section 1, $\mathcal{N}_1$ and $\mathcal{N}_2$ would have the same values of mean ($\mu_n = 0$) and variance (σ_n^2).

In order to obtain σ_f^2, we firstly take the average of g_1 and g_2 to get g_a.

$$g_a = \frac{g_1 + g_2}{2} = f + f^{\gamma} \cdot \frac{\mathcal{N}_1 + \mathcal{N}_2}{2}. \tag{4.20}$$

Then by taking the second moment for both sides of Equation 4.20, and since $\mathcal{N}_1$ and $\mathcal{N}_2$ are independent zero-mean noise with common variance σ_n^2, we will have

$$\begin{aligned} E[g_a^2] &= E\left[\left(f + f^{\gamma} \cdot \tfrac{\mathcal{N}_1+\mathcal{N}_2}{2}\right)^2\right] \\ &= E\left[f^2 + f^{1+\gamma} \cdot (\mathcal{N}_1 + \mathcal{N}_2) + f^{2\gamma} \cdot \left(\tfrac{\mathcal{N}_1+\mathcal{N}_2}{2}\right)^2\right] \\ &= E\left[f^2\right] + E\left[f^{1+\gamma}(\mathcal{N}_1 + \mathcal{N}_2)\right] + E\left[\tfrac{f^{2\gamma}(\mathcal{N}_1+\mathcal{N}_2)^2}{4}\right] \\ &= E\left[f^2\right] + \tfrac{\sigma_n^2}{2} \cdot E\left[f^{2\gamma}\right] \end{aligned} . \tag{4.21}$$

Similarly, when we calculate the second moment for g_1 defined in Equation 4.18, we will have

$$E[g_1^2] = E\left[f^2\right] + \sigma_n^2 \cdot E\left[f^{2\gamma}\right]. \tag{4.22}$$

It is observed that both Equations 4.21 and 4.22 have the term $\{\sigma_n^2 \cdot E\left[f^{2\gamma}\right]\}$, hence, $E\left[f^2\right]$ can be found by solving the two equations by eliminating the common term $\{\sigma_n^2 \cdot E\left[f^{2\gamma}\right]\}$. That yields

$$E\left[f^2\right] = 2 \cdot E\left[g_a^2\right] - E\left[g_1^2\right]. \tag{4.23}$$

Since

$$\sigma_f^2 = E\left[f^2\right] - \mu_f^2, \tag{4.24}$$

substituting Equations 4.23 and 4.12 to Equation 4.24, we will have the unbiased value for σ_f^2 where

$$\sigma_f^2 = 2 \cdot E\left[g_a^2\right] - E\left[g_1^2\right] - E^2[g_1]. \tag{4.25}$$

Finally, we can obtain the expression for $\widehat{f}(i,j)$, which is the estimate of original noise free image f, by substituting Equation 4.25 to 4.10, as is given in Equation 4.26.

$$\widehat{f}(i,j) = E[g_1] + (g_1(i,j) - E[g_1]) \cdot \frac{2E\left[g_a^2\right] - E\left[g_1^2\right] - E^2[g_1]}{E\left[g_1^2\right] - E^2[g_1]}. \tag{4.26}$$

By now, we have the unbiased expression for the LLMMSE filter that is independent of the parameter γ and noise $\mathcal{N}$. It is purely determined by an image instance g_1 and an average image g_a. All the expectation terms $E[\bullet]$ in Equation 4.26 can be estimated by directly taking the spatial average of the corresponding $\langle\bullet\rangle$.

4.3.5 Experiments with the Proposed Estimation Technique for Image De-noising

Validation of the Proposed Method

Since the key effort of this work is to estimate the variance σ_f^2, we firstly carried out experiments to verify the accuracy of our method in predicting the signal variance σ_f^2 from a noisy image. The gray-scale image of "Lena" (with variance $\sigma_f^2 = 2.295 \cdot 10^3$) was used as the testing image. The noisy images were simulated using Equation 4.5, where $\mathcal{N}$ was chosen to be zero-mean Gaussian noise with variance σ_n^2, and for each pair of (γ, σ_n^2), two image instances were generated. Multiple combinations of γ and σ_n^2 have been tested, and it can be seen from Table 4.1 that our method can estimate the

Table 4.1: Estimated Values of σ_f^2 using two image instances against the change of the (γ, σ_n^2) pairs, where the variance of the noise-free "Lena" image is $\sigma_f^2 = 2.295 \cdot 10^3$. (Horizontal is σ_n^2 and vertical is γ, and the predicted value is in the power of $\cdot 10^3$).

(γ, σ_n^2)	1	9	49	121	400	2500
$\gamma = 0$	2.295	2.295	2.298	2.293	2.293	2.304
$\gamma = 0.1$	2.296	2.296	2.291	2.283	2.291	2.365
$\gamma = 0.2$	2.294	2.291	2.298	2.292	2.311	2.333
$\gamma = 0.3$	2.297	2.297	2.284	2.299	2.355	2.397
$\gamma = 0.5$	2.289	2.294	2.334	2.208	2.429	2.498
$\gamma = 0.8$	2.295	2.306	3.023	2.405	2.405	2.663

signal variance very accurately. It is also observed that the estimated value towards the bottom right of the table deviate away from the actual value. This is because, though Equation 4.25 gives the unbiased representation of σ_f^2, during the calculation, the expectation terms $E[\bullet]$ were estimated by calculating the spatial average of the corresponding $\langle \bullet \rangle$, which introduces errors especially when the noise level increases substantially (the (γ, σ_n^2) pair moves to the bottom right in our case).

SDN Removal for Generic Images

When using this proposed method for de-noising Signal-Dependent Noise with LLMMSE, two image instances of the same noisy scene are used to provide two versions of the neighborhood for each pixel to estimate the local variance based on Equation 4.25, which will then be used to estimate the filtered value for that pixel by Equation 4.26. Experiments were carried on the "Lena" image with various levels of synthetic signal-dependent noise. To evaluate its performance, we compare the Peak Signal-to-Noise Ratio (PSNR) before and after the filtering process. The PSNR is the ratio between the maximum possible power of a signal and the power of corrupting noise that affects the fidelity of its representation, and is defined in Equations 4.27 and 4.28.

$$MSE = \frac{1}{mn} \sum_{i=0}^{m-1} \sum_{j=0}^{n-1} \| f(i,j) - g(i,j) \|^2, \tag{4.27}$$

Table 4.2: The Peak Signal-to-Noise Ratio (in *db*) of Wiener2 filter and our proposed method to de-noise Signal Dependent Noise.

Noisy Image	Wiener2	our proposed method
10.57	19.19	22.58
13.51	22.01	25.42
17.94	26.03	28.07

$$PSNR = 10 \cdot \log_{10}\left(\frac{MAX_f^2}{MSE}\right) = 20 \cdot \log_{10}\left(\frac{MAX_f}{\sqrt{MSE}}\right), \tag{4.28}$$

where MSE stands for *mean square error* for the monochrome image f and its noisy version g, while MAX_f is the maximum pixel value of the image f.

Table 4.2 shows the PSNR of the image before and after noise filtering. It can be seen that the Peak Signal-to-Noise Ratio (PSNR) of the image has increased significantly after applying our method. Even compared with the Wiener filter with the same window size, our method outperforms it by $2-3db$ in terms of PSNR. This can be further observed visually in Figure 4.4.

Further experiments were carried out to compare performance of the LLMMSE filters constructed by Aiazzi's approach (Aiazzi et al., 1997) (estimating the values of γ and σ_n^2 through analyzing several homogenous regions in the noisy image) and our proposed approach (directly deriving the σ_f^2 from two noisy images). Table 4.3 shows that the LLMMSE filter constructed using our method has better performance in filtering the SDN in the images. Meanwhile, unlike other approaches that estimate filter parameters through several empirically selected background regions, the our method estimates the filter parameters automatically, which is another major advantage.

More experiments were carried out on other standard generic images with randomly selected noise parameters. These images include the standard "Peppers", "Airplane", and "Mandril", which are commonly used in the image processing field. The experimental results showed that the performance of the LLMMSE filter constructed

(a) Lena Image

(b) Image corrupted with a signal dependent noise ($PSNR = 13.51$)

(c) Wiener2 Filtering ($PSNR = 22.01$)

(d) LLMSE filtering with parameter estimated from two images ($PSNR = 25.42$)

Figure 4.4: De-noising results for the image corrupted with a signal-dependent noise

Table 4.3: Comparison of the performance of the LLMMSE filter constructed by estimating the (γ, σ_n^2) pair (Aiazzi's approach) and by directly deriving the σ_f^2 (our approach). The performance are measured based on the Peak Signal-to-Noise Ratio in *db*.

Original (γ, σ_n^2)	Noisy Image	Aiazzi's Approach	Our Approach
$(0.5, 4)$	21.486	26.5427	29.378
$(0, 400)$	21.6703	24.658	28.9307

by our approach remains quite efficient in noise removal, which is shown in Table 4.4. The experimental results showed that the performance of the LLMMSE filter constructed by our approach remains quite efficient in noise removal, which is further shown visually in Figure 4.5.

Table 4.4: De-noising results for 3 standard testing images corrupted with synthetic signal-dependent noise. The performance are measured based on the Peak Signal-to-Noise Ratio in *db*.

Image	Original $(\gamma, \sigma_n^2, \sigma_w^2)$	Noisy Image	Our Approach
Peppers	$(0.2, 900, 0.02)$	9.6959	21.9533
Airplane	$(0.1, 200, 0.02)$	20.0482	26.7392
Mandril	$(0.3, 100, 0.02)$	14.6406	20.1372

Noise Removal for Infrared Vein Pattern Images

Finally, experiments were carried out to test the proposed method with real-life images: the infrared vein pattern images in our work. During the testing, two types of infrared (both far- and near- infrared respectively) hand vein pattern images of the back of the same hand were used to estimate the signal variance σ_f^2, which was then used by the LLMMSE filter. Since it is impossible to have the original noise-free vein pattern images, it is difficult to measure the noise-removal performance in terms of the PSNR. Nevertheless, the performance of the proposed method can be evaluated visually. The result shown in Figure 4.6 clearly shows that our approach is effective in removing signal-dependent noise in the FIR vein pattern images. A similar approach was applied to the NIR images, and it is also observed that the noise in the image is

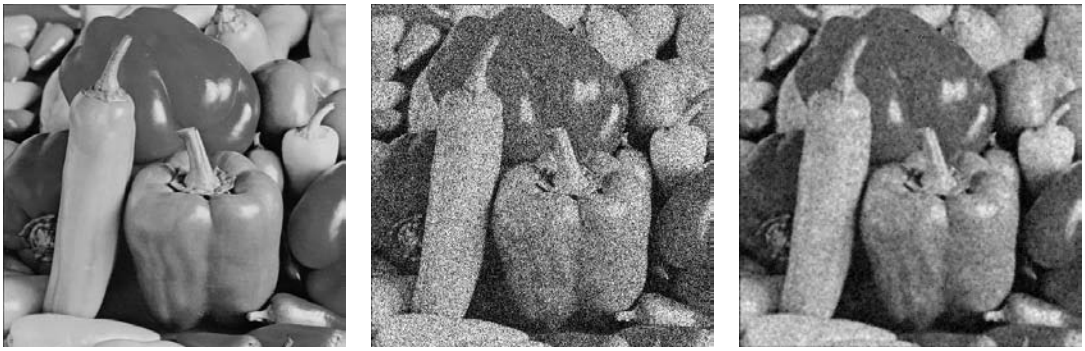

(a) Peppers Image

(b) Image corrupted with synthetic signal dependent noise where $\gamma = 0.2$,$\sigma_n^2 = 900$, and $\sigma_w^2 = 0.02$ ($PSNR = 9.6959$)

(c) LLMMSE filtering with Our Approach ($PSNR = 21.9533$)

(d) Airplane Image

(e) Image corrupted with synthetic signal dependent noise where $\gamma = 0.1$,$\sigma_n^2 = 200$, and $\sigma_w^2 = 0.02$ ($PSNR = 20.0482$)

(f) LLMMSE filtering with Our Approach ($PSNR = 26.7392$)

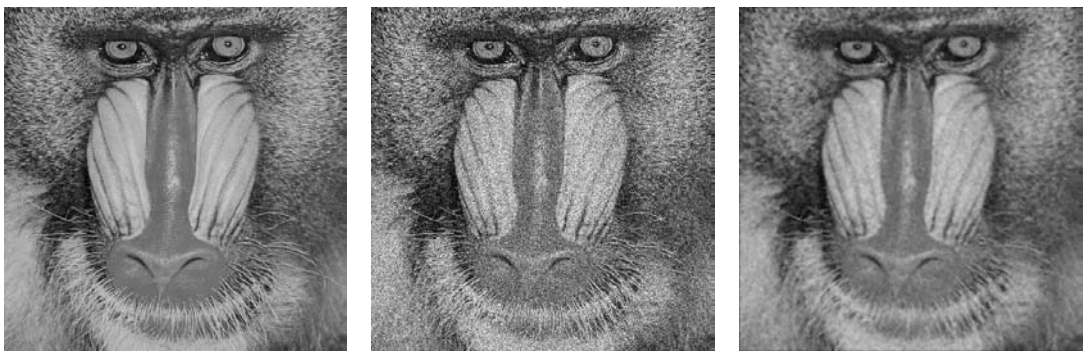

(g) Mandril Image

(h) Image corrupted with synthetic signal dependent noise where $\gamma = 0.3$,$\sigma_n^2 = 100$, and $\sigma_w^2 = 0.02$ ($PSNR = 14.6406$)

(i) LLMMSE filtering with Our Approach ($PSNR = 20.1372$)

Figure 4.5: De-noising results for the 3 standard images corrupted with signal-dependent noise

suppressed significantly as shown in Figure 4.6. The experiments further prove our approach is effective in removing the signal-dependent noise in the images.

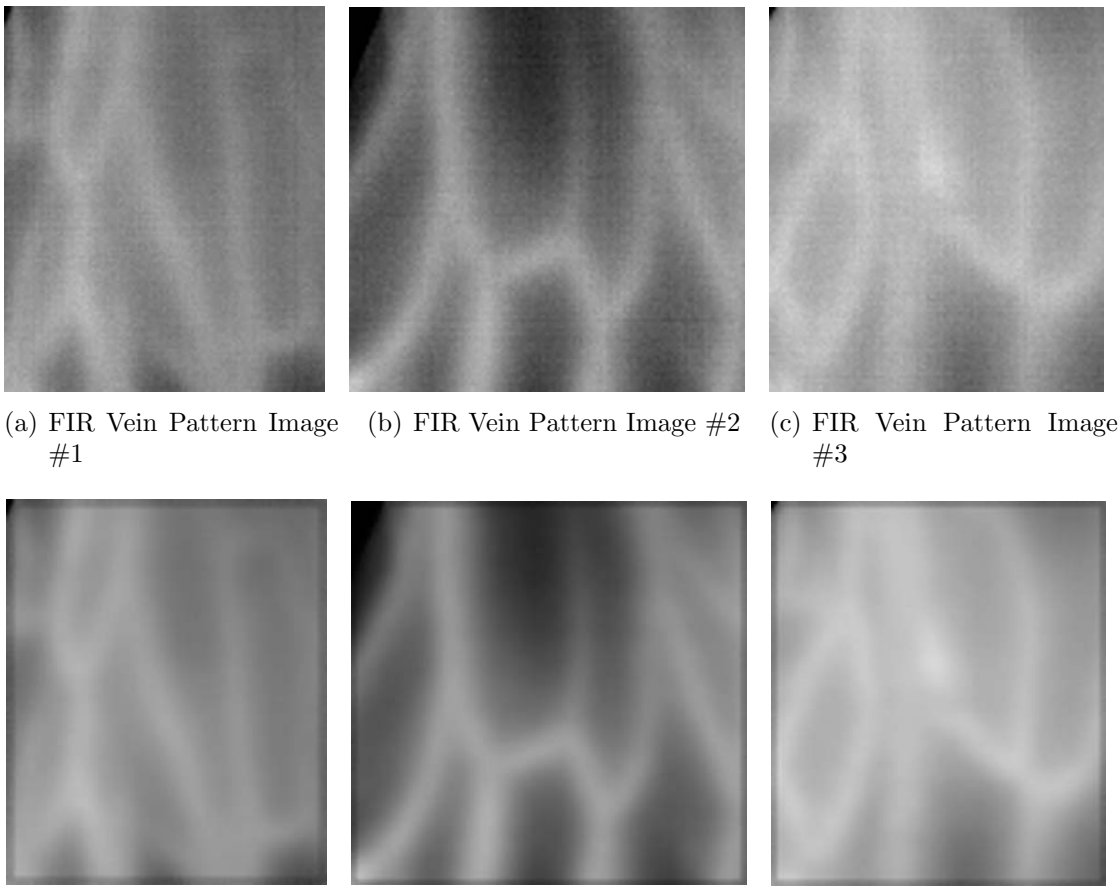

(a) FIR Vein Pattern Image #1 (b) FIR Vein Pattern Image #2 (c) FIR Vein Pattern Image #3

(d) After LLMMSE filtering for Figure 4.6(a) (e) After LLMMSE filtering for Figure 4.6(b) (f) After LLMMSE filtering for Figure 4.6(c)

Figure 4.6: De-noising results for the FIR vein pattern images using LLMMSE filter with parameters derived with 2 images. (Upper row: the original noisy images; Lower row: the filtered images.)

4.4 Post-processing of the De-noised Vein Pattern Image

4.4.1 Image Normalization

After removing the noise, the vein pattern images were normalized to have pre-specified mean and variance values. The normalization process further reduces the possible imperfections in the image due to the sensor noise and other effects. The nor-

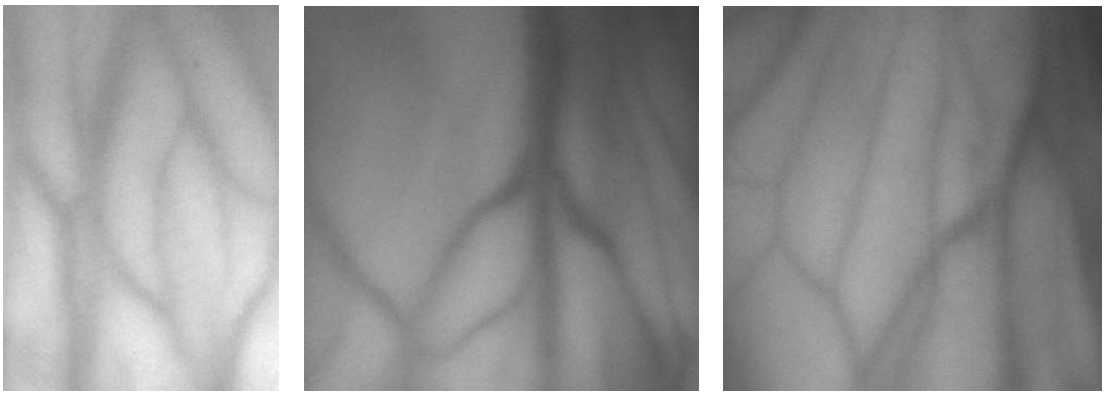

(a) NIR Vein Pattern Image #1 (b) NIR Vein Pattern Image #2 (c) NIR Vein Pattern Image #3

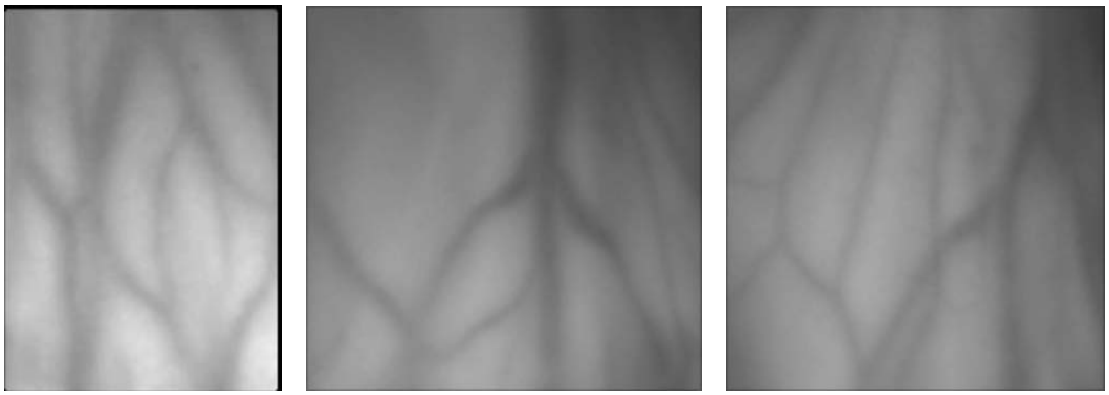

(d) After LLMMSE filtering for Figure 4.7(a) (e) After LLMMSE filtering for Figure 4.7(b) (f) After LLMMSE filtering for Figure 4.7(c)

Figure 4.7: De-noising results for the NIR vein pattern images using LLMMSE filter with parameters derived with 2 images. (Upper row: the original noisy images; Lower row: the filtered images.)

malization method employed in this work are similar to the one suggested by Hong et. al. (Hong et al., 1998). Let $I(x, y)$ denote the intensity value at position (x, y) in a vein pattern image. The mean and variance of the image are denoted as μ and σ^2 respectively. Then for an image sized $N \times M$, the normalized image $I^{'}(x, y)$ is obtained using the pixel-wise operations in Equation 4.29, where μ_d and σ_d^2 are the desired values for mean and variance respectively (in our case, these two values were set empirically based on evaluation of a number of sample images).

$$I^{'}(x,y) = \begin{cases} \mu_d + \sqrt{\frac{\sigma_d^2 \cdot (I(x,y)-\mu)^2}{\sigma^2}}, & I(x,y) > \mu \\ \mu_d - \sqrt{\frac{\sigma_d^2 \cdot (I(x,y)-\mu)^2}{\sigma^2}}, & \text{Otherwise} \end{cases} . \tag{4.29}$$

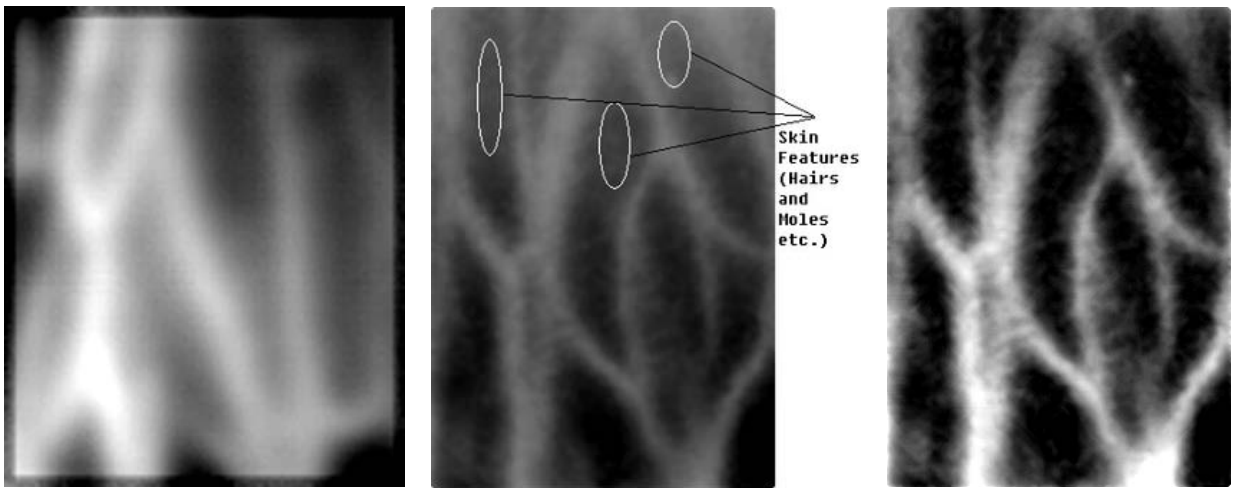

(a) FIR Vein Pattern Image After Normalization for Figure 4.6(d)

(b) NIR Vein Pattern Image After Normalization (Skin Features are Observable in the Image)

(c) Removal of Skin Features in NIR Images with Morphological Top-Hat Operation

Figure 4.8: Post-processing results for the vein pattern image.

Figures 4.8(a) and 4.8(b) show the FIR and NIR vein pattern image after enhancement respectively. It can be seen that the quality of the image has been improved significantly. However, for some NIR images, the defects on the skin surfaces such as hairs and moles are also visible in the image (as shown in Figure 4.8(b)). these skin features will potentially create problems when come to extraction of vein patterns in the later stage. Therefore, proper measures have to be carried out to eliminate these

features as much as possible.

4.4.2 Skin Features Removal in NIR Images Using Morphological Top-Hat Operation

For the NIR images, the skin features such as hairs, moles are also visible together with the veins in the image. These artifacts usually disrupt the vein patterns and cause errors in the later vein pattern extraction stage. Due to the fact that these skin defects are usually small in size, to remove these artifacts, one can apply the morphological *Top-Hat* operation with a structural element *SE*.

The morphological *Top-Hat* operation essentially gives the the image minus the morphological opening of the image. Mathematically, it is defined as

$$TopHat(F, SE) = F - (F \bigcirc SE) \tag{4.30}$$

where the "$\bigcirc$" is the morphological opening (erosion followed by dilation) operator, and F and SE are the original image and the structure element respectively. Figure 4.8(c) shows the result after the application of the morphological *Top-Hat* operation (where the structure element SE here was chosen as disc shape with size 36). It can be seen that the skin defects between the vein patterns have been eliminated substantially, and the image is cleaner in the visual sense.

However, the morphological *Top-Hat* operation will often disrupt the vein itself. It is observed in Figure 4.8(c) that the continuity of a slight portion of the veins has been disrupted by this *Top-Hat* operation. In this case, currently, manual intervention is required to restore the vein pattern continuity in the image. In fact, for the NIR vein pattern images, at the current stage, they require frequent human intervention for the removal of skin features, which creates a problem for building an automatic

vein pattern biometric system. Hence, at the later matching stage in Chapter 6, we focused on the experiment with the FIR vein pattern image data. Additional work will be carried out specially for solving the skin features removal problem from the NIR image in the future research.

4.5 Summary

This chapter presents the preprocessing process of both FIR and NIR vein pattern images. Two key issues and solutions in this process were addressed in the chapter. The first major issue is to define a size invariant region of interest. In this research, the ROI is located by firstly extracting the hand contour using an edge detector; and then via calculating the distance profile between the contour points and the mid-point of the wrist-line, the hand landmark points (two valley points between fingers in this case) were found, which were then used to define a rectangular region (with $height = 1.4 * width$)as the ROI. Defining the ROI in this manner ensures all the regions of interest are referencing to the same area of the hand, meanwhile it covers the majority part of the vein patterns in the back of the hand. Most importantly, the size of the ROI is determined by the distance between the finger valley points, which ensures the ROIs are invariant to the change of hand size.

Then this chapter continues to improve the quality of the vein pattern images. The noise model of the image was investigated, and it is found to be signal dependent noise. This research propose to use the LLMMSE filter to remove the SDN, which is commonly accepted for its superior performance in removing SDN whilst preserving the original image features. However, traditional LLMMSE filter requires *priori* knowledge (or assumption) of the noise parameter σ_n^2 and the imaging gamma value γ, which is not always available or hard to predict. We propose a novel technique

to construct the LLMMSE filter by automatically estimating its filter parameter using two image instances of the noisy scene. Experimental results show our proposed method outperformed others' approaches in removing SDN for generic image noise removal applications. In the meantime, the LLMMSE filter constructed by our method performed effectively in de-noising the signal dependent noise in both FIR and NIR vein pattern images.

Additional efforts were made to post-process the de-noised FIR and NIR images. These include image normalization, which is to further suppress other noise factors. Special care were taken to the NIR images, where the skin surface features were partially eliminated via morphological *Top-Hat* operation. Nevertheless, due to the fact that the it is difficult at the current stage to remove the skin features entirely from the NIR vein pattern images, we chose to use the FIR vein pattern images for matching in the later part of the thesis.

After this preprocessing process, we now can obtain an enhanced ROI image of the vein pattern, which is ready for the next step where the vein pattern is to be extracted.

The work done in this chapter for the ROI definition was reported in the paper (Wang & Leedham, 2005), whilst the technique for signal dependent noise removal in images was presented in another paper (Wang et al., 2007a, 2008).

Chapter 5

Vein Pattern Shape Estimation

It was stated in Chapter 2 that the vein patterns in the human body parts will grow in a predictable manner like fingerprints. However, according to a technical report (Sweeney, 1998) by a British research group, the shape of the vein patterns will remain very stable invariant to the temporal change. This implies the geometrical shape of the vein pattern can be used as the sole feature for person recognition.

The type of representation used in describing shape can have a significant impact on the effectiveness and efficiency of the recognition strategy for the vein pattern. There are mainly two ways for representing an object's shape: skeleton representation, and contour representation.

5.1 Skeleton-based Versus. Contour-based Shape Descriptor

The skeleton representation of an object is a powerful shape descriptor that captures both boundary and region information of the object. The skeleton of a shape is a representation composed of idealized thin lines that preserve the connectivity or topology of the original shape. On the other hand, the contour based approach represents the shape with a chain of ordered boundary points of the object. These two shape de-

scriptors are widely used for many applications. Sebastian & Kimia (Sebastian & Kimia, 2005) carried out an in-depth comparison between the contour- and skeleton-based shape descriptors in the applications of object recognition. They examined the tradeoff between robustness and computational complexity for contour- and skeleton-based representation, and indicated that, compared to contour-based representation, the additional computational effort required in skeleton-based recognition is worthwhile in the presence of large amount of object variation, in particular those involving the presence of articulation or rearrangement of parts.

In the context of vein pattern images, articulation movement and rearrangement of parts for the same vein pattern in different images is minimal due to the temporal stability nature of the vein patterns. However, for FIR images, due to uneven heat distribution, some parts of the veins will be occluded in some images. Similarly for NIR images, due to uneven illumination, some parts of the veins will be invisible in some images. The occlusion of the object parts will degrade the accuracy of any shape recognition algorithms, and the impact of the occlusion effect is much more significant for the contour-based shape recognition than the skeleton-based recognition (Sebastian & Kimia, 2005).

Two other factors also contribute to the disadvantages of the contour serving as the vein pattern shape descriptor. Firstly, since the vein patterns grow with age, which implies the size of the vein pattern will constantly change with time. Secondly, in the vein pattern images, in particular the FIR images, the veins are surrounded by many faint white regions having similar gray-scale intensity to the vein itself. This makes it difficult to determine the actual position of the boundary points of the veins. The uncertainty of the boundary points caused by these two factors will lead to substantial undesired variation of the contour itself. On the contrary, the skeleton-

based descriptor relies on the medial axis of the veins and remains relatively unaffected by the uncertainty of the boundary points, which makes it capable of representing the vein pattern shape more consistently.

Therefore, in this chapter, we will look into extracting the vein pattern's shape in its skeleton form. The traditional binary-based skeletonization method was firstly attempted and is described in the following section.

5.2 Binary-based Vein Pattern Skeletonization

Traditional skeletonization algorithms work by iteratively peeling off the boundary points of the object until a single pixel wide skeleton remains. Before this process is applied, the object has to be segmented from the image. In this work, the vein patterns were separated from the background using the gray-scale thresholding approach.

5.2.1 Image Binarization with Local Adaptive Thresholding

The philosophy of thresholding is based on the assumption that the gray level distribution for object points and background points are in two separate regions in the gray-level histogram of the image. Because of its intuitive properties and simplicity of implementation, image thresholding enjoys a central position in applications of image segmentation. There are generally two types of thresholding techniques, namely *Global Thresholding* and *Local Adaptive Thresholding*.

Global Thresholding

When an image has a bimodal histogram for its gray-scale intensity, a global thresholding technique can usually be utilized to separate objects from the background. The threshold is defined as

$$f'(i,j) = \begin{cases} 1, & f(i,j) \geq T \\ 0, & \text{otherwise} \end{cases} . \tag{5.1}$$

where T is the threshold value, and $f(i,j)$ and $f'(i,j)$ are the original gray-scale image and the resulting binary image respectively. The selection of T is important to minimize the probability of error. One famous method was proposed by Otsu (Otsu, 1979), which maximizes the between-class variance of the background and foreground. Many other algorithms can also be found in the literature (Brink, 1995; Solihin & Leedham, 1999). Global Thresholding is computationally simple and fast, however, it does not work effectively under low-contrast and noisy conditions, and it also fails to perform well when the background intensity varies significantly across the image.

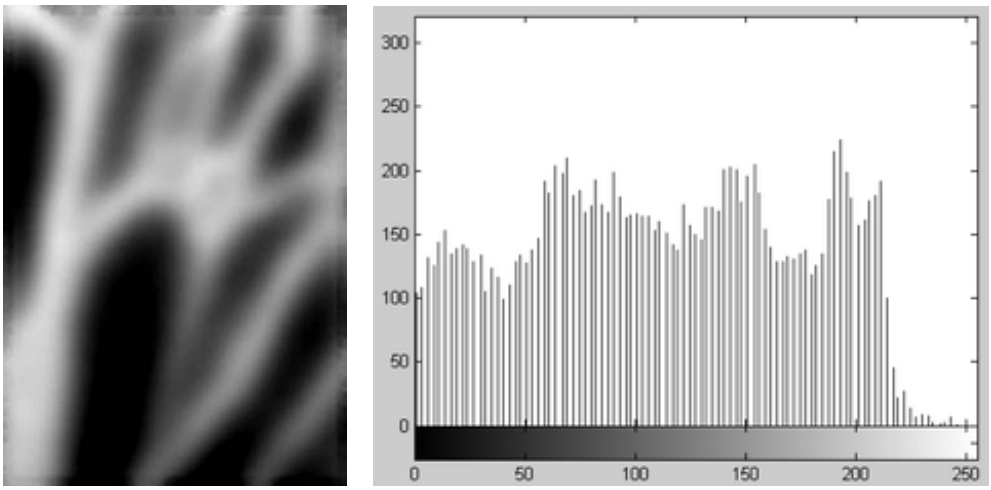

(a) ROI Image in Figure 4.3(a) After Normalization (Non-uniform Intensity is Obvious)

(b) Gray Level Histogram

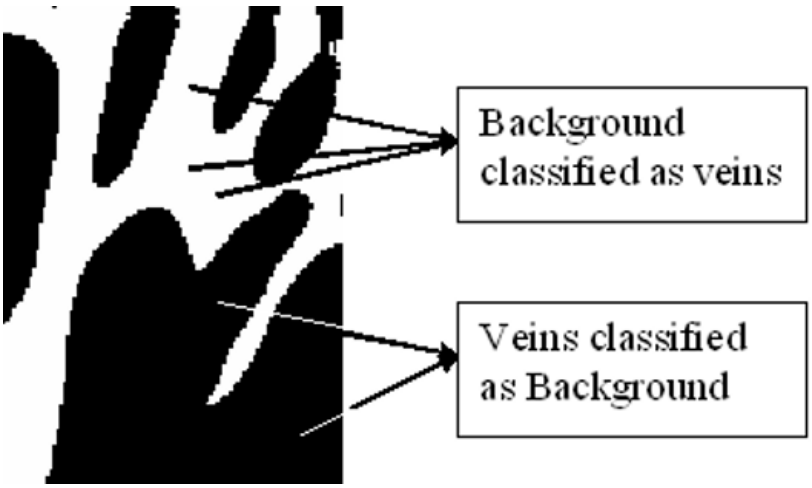

(c) Otsu's Algorithm

Figure 5.1: Vein Pattern Segmentation using Global Thresholding.

By carefully examining the the hand vein image data obtained in this project, it apparent that the gray level intensity of veins is not uniform for all locations in the image. An example is given in Figure 5.1(a) where the intensity value of the diffusion area around one part of the vein is higher than the intensity of another part of the vein. Figure 5.1(b) shows the histogram of the gray level distribution of the image, and it can be seen that the histogram does not have a bimodal shape. Therefore, we can expect that global thresholding techniques will not perform adequately in segmenting vein patterns from the images. The experiment using Otsu's global thresholding algorithm further proves our presumption. In the resulting images (as in Figure 5.1(c)), we can see that not only the weak parts of the vein are lost after thresholding, but also the diffusion areas around the veins are classified as part of the vein, which results in a greatly distorted vein size. It was concluded that global thresholding is not a good option for vein pattern segmentation.

Local Adaptive Thresholding

Unlike global thresholding, local thresholding methods use different threshold values for pixels at different location in the images. Typically, a local thresholding algorithm splits an image into sub-images and calculates the thresholds for each sub-image. Usually, these sub-images shall be large enough to contain both the object of interest and the background. The determination of a threshold value is dependent on the distribution of the gray level histogram of the sub-image: if the histogram is bimodal, the threshold is chosen to be the valley point between the two dominant peaks, whilst for uni-modal histograms, the threshold value is interpolated amongst adjacent thresholds. However, it is difficult to determine the number of sub-regions the image should be divided into, and usually requires user intervention. Nevertheless, some recent work (Chen & Leedham, 2004, 2005) in this area to allow automatic region definition

has been attempted.

We investigated several local adaptive thresholding algorithms, and it was found that an algorithm that combines global and local adaptive thresholding: local thresholding with global reduction, gives a more satisfactory result for segmenting the vein patterns from the background. Instead of dividing the image into several subregions, the algorithm chooses different threshold values for every pixel in the image based on the analysis of the gray-scale statistics of its surrounding neighbors. For every pixel in the image, its threshold value is set as the regional mean value subtracted by a global offset. The thresholding process is mathematically expressed in Equation 5.2, where μ_{ij} is the mean value for its 13×13 neighborhood, and $T_g = 5$ is a common offset for all the pixels. The neighborhood size and global offset value T_g are chosen on a trial-and-error basis whereby various values of the neighborhood size and T_g were attempted to several images, and the final values were determined by visual comparison.

$$I^{'}(i,j) = \begin{cases} = 1, & \text{if } I(i,j) \geq (\mu_{ij} - T_g) \\ = 0, & \text{otherwise} \end{cases} . \tag{5.2}$$

(a) Local Thresholding with Global Reduction for Figure 4.3(a)

(b) After Morphological Closing

(c) Misclassified background pixels (The circled areas)

Figure 5.2: Vein Pattern Segmentation using local thresholding with global reduction.

This adaptive thresholding technique is more capable of handling situations where the background or the foreground has non-uniform intensity values in the image. Figure 5.2(a) shows the thresholded vein patterns using this method. After removing the isolated residues in the image using morphological closing, we can see that the weak parts of the vein and other fine details are well preserved, and we have a much better binary vein pattern image compared to the global thresholding, which is illustrated in Figure 5.2(b).

But it can also been seen from Figure 5.2(c) there are also many misclassifications of background pixels being classified as vein pixels, especially for those pixels near the edge of the veins. This is because the intensity thresholding method suffers from errors due to image inhomogeneities and the partial volume effect (Yim et al., 2000). Furthermore, the choice of threshold level is subjective, and might not be optimum for all images.

The misclassification errors introduced by this binarization process will be propagated to the next stage, and may be magnified by the skeletonization algorithm, as is elaborated in the following section.

5.2.2 Binary Based Skeletonization

Many skeletonisation algorithms can be applied to the binary images obtained from the previous segmentation stage. We use the popular thinning algorithm proposed by Guo and Hall (Guo & Hall, 1992) as provided by the standard Matlab library. Figure 5.3 shows the skeleton of the vein pattern extracted by the thinning algorithm. It can be seen that the skeletons of the vein pattern are successfully extracted and the shape of the vein pattern is preserved relatively well.

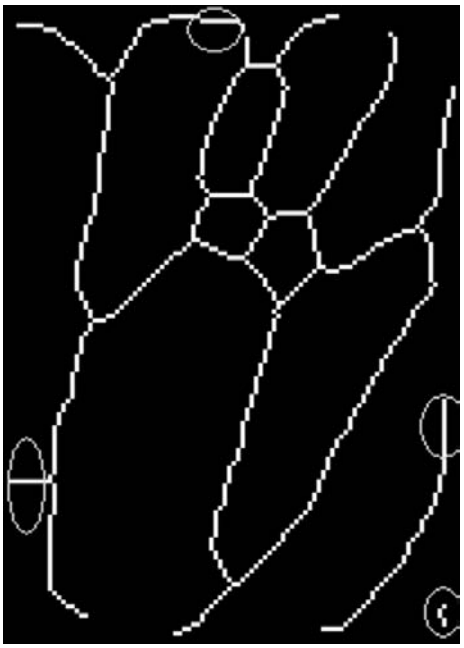

Figure 5.3: Skeletons of the vein pattern using binary-based skeletonization, where the shape of the vein pattern is overall well preserved, but the false branches (in the circled area) are also numerous.

5.2.3 Discussion

It is clear from Figure 5.3 that the misclassification points in the binarization stage have led to numerous spur branches as well as isolated segments of skeletons. These false branches will, in turn, degrade the accuracy of the matching process. Whilst some pruning processes can be taken to remove some of the small artifacts, they generally have some negative impacts to the original skeletons.

In addition, during the binarization process, for the thresholding algorithm, the threshold selection strategy might not be optimum for all images, and the size of the neighborhood used for evaluating the gray-scale statistics is chosen empirically, which when applied to some images, will not produce the optimum performance. Errors in the binarization stage will be propagated to the subsequent skeletonization stage, and may be magnified and in turn will degrade the performance of the later recognition accuracy.

In order to minimize the errors introduced by the segmentation process, it is

preferable to eliminate the segmentation stage. This implies the skeletonization will be performed directly on the gray scale images, for which, we proposed a new scheme by using the watershed concept for object skeletonization in both gray-scale and binary images.

5.3 Gray-Scale Skeletonization using Watershed Algorithm

5.3.1 The watershed principle

The watershed concept is based on visualizing an image in three dimensions: the two spatial coordinates versus the gray level for each pixel, through which any gray-scale image can be considered as a topographical surface. The basic idea of the watershed algorithm is a simulation of the immersion process (Bieniek & Moga, 2000; Gonzalez & Woods, 2002) as shown in Figure 5.4 (Beurcher, 2007) : At first, holes are pierced in all regional minima of the relief (connected plateaus of constant altitude from which it is impossible to reach a location of lower altitude without having to climb). Then by sinking the whole surface slowly into a lake, water springs through the holes and progressively immerses the adjacent walls. To prevent streams of water coming from different holes to intermingle, a dam is set up at the meeting locations. The flooding will eventually reach a stage when only the tops of the dams are visible above the water-line. These dam boundaries correspond to the divide lines of the watersheds.

Mathematically, this immersion process can be established by the definition of a geodesic distance, geodesic influence zone and the concept of the catchment basins (Yu, 2004).

Definition 3 *The geodesic distance $d_A(x, y)$ between two pixels x and y in A is the*

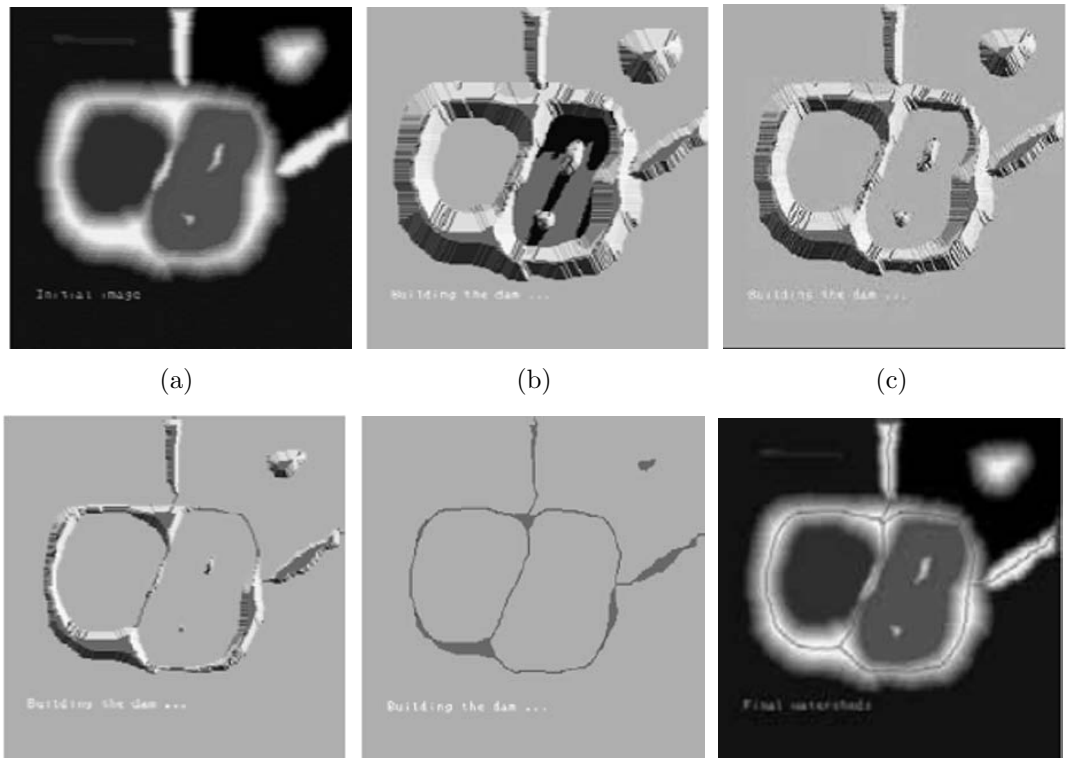

(a) (b) (c)

(d) (e) (f)

Figure 5.4: The simulated immersion process for the watershed algorithm. (source: "http://cmm.ensmp.fr/ beucher/wtshed.html")

infimum length of the paths P which join x and y and are totally included in A (Equation 5.3).

$$d_A(x,y) = inf\{l(P)\} \tag{5.3}$$

Definition 4 *geodesic influence zone is defined as: Suppose A contains a set B consisting of several connected components B_1, B_2,...,B_k. The geodesic influence zone $iz_A(B_i)$ of a connected component B_i of B in A is the locus of the points of A whose geodesic distance of B_i is smaller than their geodesic distance to any other component of B, which is expressed in Equation 5.4.*

$$iz_A(B_i) = \{p \in A, \forall j \in [1,k]/\{i\}, d_A(p,B_i)\} \tag{5.4}$$

Definition 5 *The set of catchment basins of the gray-scale image I is equal to the*

set X_{hmax} obtained after the following recursion:

$$X_{h_{min}} = T_{h_{min}(I)}, \ \ where\ T_h(I) = \{p \in D_I, I(p) \leq h\} \tag{5.5}$$

$$\forall h \in [h_{min}, h_{max} - 1], X_{h+1} = min_{h+1} \bigcup iz_{T_{h+1}(I)}(X_h) \tag{5.6}$$

The immersion process is implemented by recursively expending the catchment basins until they remain unchanged for two consecutive recursions, whereby the final catchment basins for the image I are found. The watersheds for the image I essentially correspond to the set of points D_I which do not belong to any catchment basins in the image.

5.3.2 Watersheds Algorithmic Skeletonization for Both Gray-scale and Binary Objects

Traditionally, the watershed algorithm has been used to find the contour of the objects for segmentation purposes. Therefore, it is usually applied to the gradient images, and the resulting watersheds will correspond to the edges of the object of interest. However, if the object of interest in the image divides the background into several unconnected subregions, we can apply the watershed concept to extract the skeleton of the object.

Watershed-based Skeletonization for Gray-scale Image

Given a gray-scale image, if the object of interest in the image divides the background into several unconnected subregions, the whole image can be visualized as several lakes separated by many "dams" as shown in Figure 5.5(b). Applying an edge detector on the gray-scale image will only result in finding the contour of the object because of the thickness of the object in the gray-scale image (see Figure 5.5(c)). Instead, when using the immersion process of the watershed concept, the edge pixels of the object

will be peeled off recursively for each iteration of expanding the catchment basins. The process will stop once there are two catchment basins about to merge with each other. The meeting point of the two catchment basins is then set as the watershed point, which is usually the local highest gray-scale intensity point located centrally in a local neighborhood of the object. This immersion process continues until none of the catchment basins can expand further. This will result in a set of watershed points that are located centrally along the object's shape, and are usually the highest gray-level intensity pixel along the object's shape. This sequence of points essentially corresponds to the skeleton points of the gray-scale object in the image as shown in Figure 5.5(d)).

To produce the final skeleton of the object, we used a polynomial curve fitting algorithm to generate curves based on the watershed points obtained by the immersion process: Given a set of sampling points $\{X(i), Y(i)\}$, it can be used to construct a smooth curve that is an estimate of the original curve by applying a polynomial curve fitting process. The X values and the Y values are firstly represented in parametric forms: $x = p_x(s)$ and $y = p_y(s)$, where s is the sampling point. Then the polynomial curve fitting process finds the coefficients p_{xn} (and p_{yn}) respectively of a polynomial $p(x)$ (and $p(y)$) of degree n that fits the data $p(x(i))$ (and $p(y(i))$) to $s(i)$, in a least squares sense (as shown in Equations 5.7 and 5.8). With these coefficients p_{xn} (and p_{yn}) obtained, the new values for $x(i)$ and $y(i)$ are found accordingly.

$$p_x(s) = p_{x1}s^n + p_{x2}s^{n-1} + ... + p_{xn}s + p_{x(n+1)} \tag{5.7}$$

$$p_y(s) = p_{y1}s^n + p_{y2}s^{n-1} + ... + p_{yn}s + p_{y(n+1)} \tag{5.8}$$

In our experiment, the degree n of the polynomial is set to 5, and Figure 5.8(d) shows that, with the watershed points obtained, the polynomial curve fitting algorithm

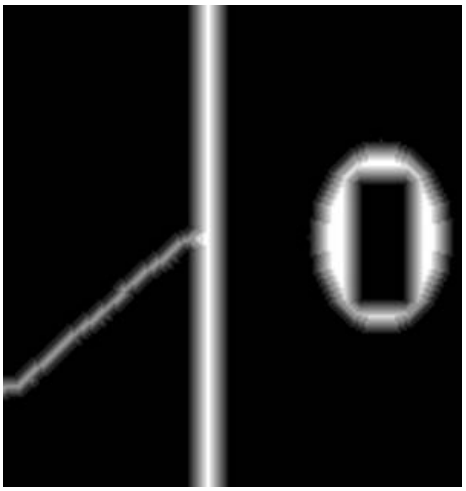

(a) A gray scale image

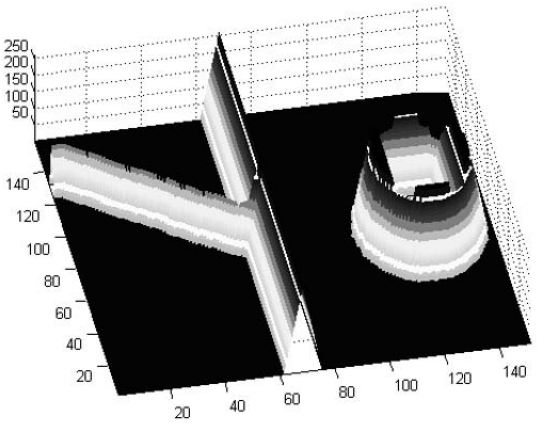

(b) 3 dimensional visualization of (a)

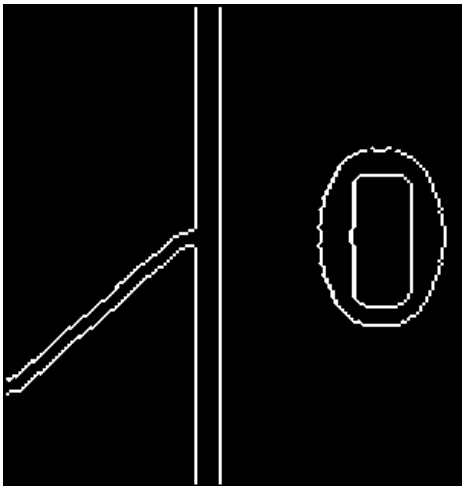

(c) Canny edge detector applied to (a)

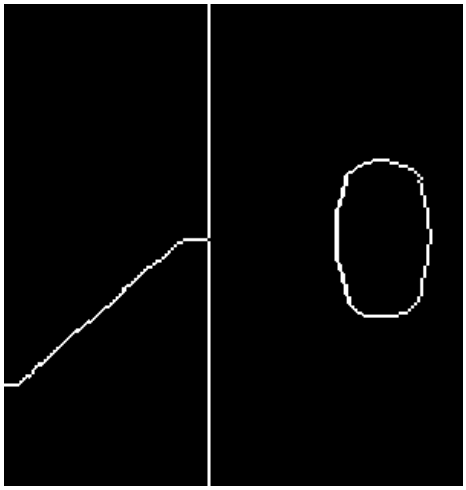

(d) The skeleton of (a) extracted using the watershed algorithm

Figure 5.5: Watershed algorithm applied to gray scale skeletonization

produced smooth skeletons for the object in the gray-scale image.

Watershed-based Skeletonization for Binary Image

It is possible to apply the watershed algorithm directly to binary images to extract a skeletal representation of the object. However, due to the fact that the intensity value for the object remains constant (values equal logic 1) throughout the image, this indifference of the edge pixels and the pixels near the medial-axis of the object will result in a distorted skeletal representation of the object when applying the watershed immersion process. This is illustrated in the example shown in Figure 5.6(b).

To overcome the problems faced by the binary image, we can transform the bi-

(a) A binary image for a bird

(b) Skeletons obtained by direct application of the watershed immersion

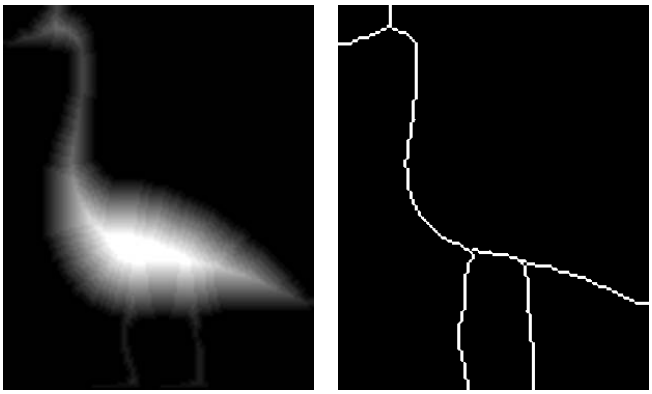

(c) The Euclidian distance transform map for the binary image

(d) Skeleton obtained by watershed immersion process applied on the distance transform map

Figure 5.6: Skeletonization using the watershed algorithm for a binary image

nary image into a gray-scale image by computing the *Euclidian Distance Transform*. This Euclidian distance transform of a binary image calculates the Euclidian distance from every pixel to the nearest nonzero-valued pixel. An example is shown in Figure 5.7 where a small binary image is on the left and its computed Euclidian distance transform is on the right. The skeleton then lies along the singularities (i.e. creases or curvature discontinuities) in the distance transform, and the watershed immersion process can be applied to this distance transform map to obtain the final skeleton of the object.

Figure 5.6 shows an example of the process for extracting skeletons from a binary image. By using the Euclidian distance transform, we can obtain the skeleton for that

1	1	0	0	0
1	1	0	0	0
0	0	0	0	0
0	0	0	0	0
0	1	1	1	0

0.00	0.00	1.00	2.00	3.00
0.00	0.00	1.00	2.00	3.00
1.00	1.00	1.41	2.00	2.24
1.41	1.00	1.00	1.00	1.41
1.00	0.00	0.00	0.00	1.00

Figure 5.7: The Euclidian distance transform (right) of a binary image (left).

object that are closer to the actual skeleton that humans perceive.

5.3.3 Watershed Algorithm for the Vein Pattern Skeletonization

When we apply the watershed algorithm directly to the gray-scale vein pattern images, it is capable of locating the skeletons of the veins. The image in the center of Figure 5.8 shows the result of applying the watershed algorithm to the thermal vein pattern image. It is clear that the result contains too many false ridges, and this is commonly referred to as over-segmentation, and is due to noise and other local irregularities. Many researchers have addressed the over-segmentation problem for the watershed algorithm. Markers, for example, are widely used to reduce the effect of over-segmentation. In our approach, we perform morphological opening followed by closing operations to suppress the noise and local irregularities in the image prior to the application of the watershed algorithm (Equation 5.9). The image in Figure 5.8(c) shows the result using our approach, and it can be easily seen that the single pixel wide skeleton of the vein pattern is successfully extracted, and the number of false branches is significantly reduced.

$$I' = (I \circ B) \bullet B; \ \textit{where } B \textit{ is the structuring element.} \tag{5.9}$$

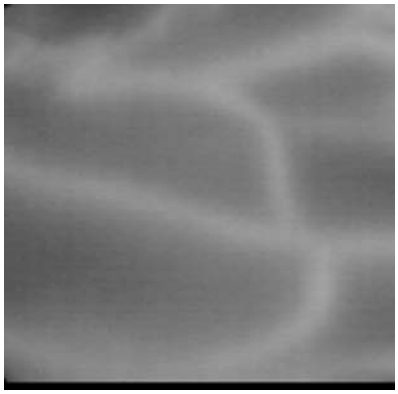

(a) A vein pattern image

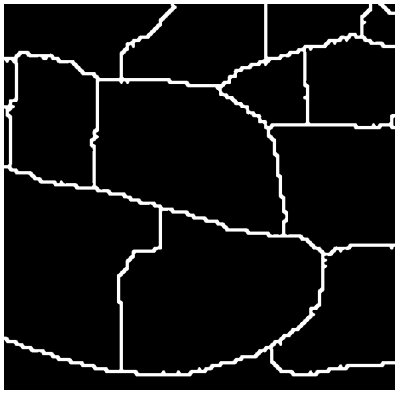

(b) Skeleton obtained by direct application of the watershed algorithm, where over-segmentation is apparent

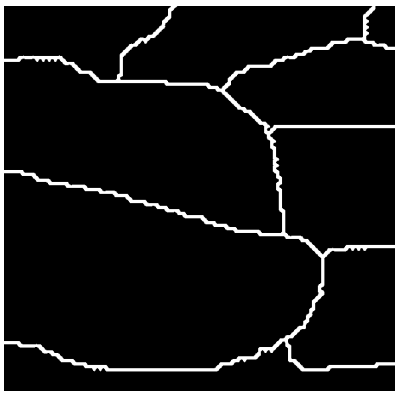

(c) Skeleton obtained by applying morphological opening and closing first followed by the watershed algorithm

(d) After polynomial curve fitting

Figure 5.8: Skeletonization using the watershed algorithm

The watershed algorithm was investigated for gray-scale skeletonization on our thermal hand vein patterns database. Around 70% of the vein pattern images can produce the proper smooth skeleton without losing any connectivity (as shown in the examples in Figure 5.9). However, there are some situations (about 30% of the vein pattern images) where the watershed algorithm fails to skeletonize the vein patterns properly: when the veins have floating endpoints in the image, the watershed algorithm is unable to extract this type of lines, as is shown in Figure 5.10. This is caused by the nature of the watershed immersion process: the "dam" (the watershed pixel) will only be built when two circular catchment basins are about to merge. This

property of the watershed immersion algorithm leads to any island- or peninsular- like of object parts being flooded without any "dams" being built during the immersion process, and hence the skeleton of that part of the object will be lost. This remains an issue to be tackled in the future for the watershed immersion algorithm to be more robust in the application of skeletonizing objects of any shapes.

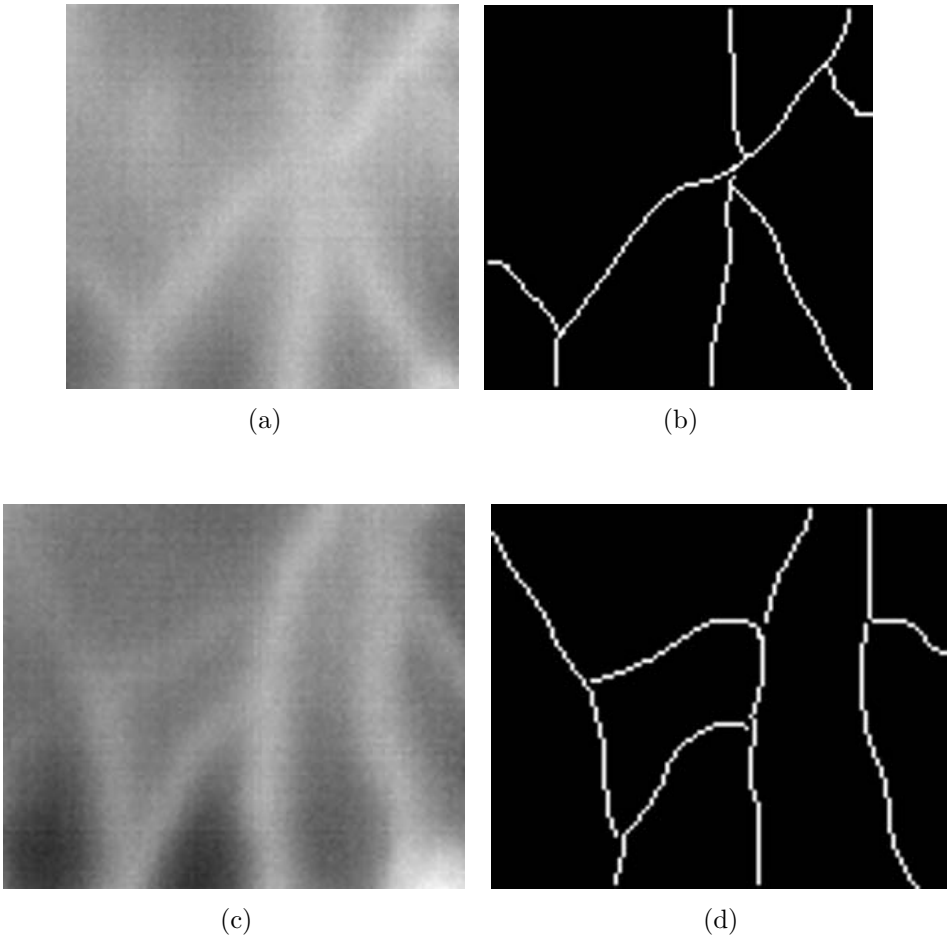

(a) (b)

(c) (d)

Figure 5.9: Additional experiments for the watershed algorithmic skeletonization with vein pattern images

5.4 Summary

This chapter discussed the process of extracting the vein pattern shape from the enhanced ROI images. At first, the choice of shape descriptors is analyzed. Two types of shape descriptors are investigated: the skeleton-based and contour-based shape representation. It was found that there is a trade off between robustness and

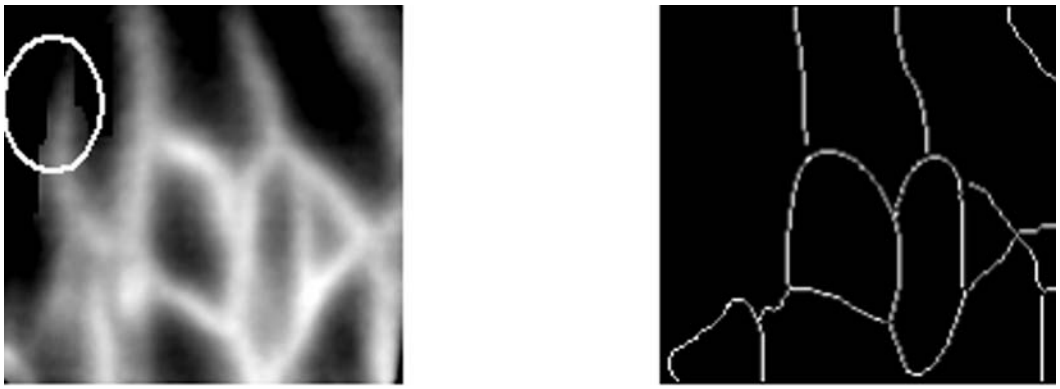

Figure 5.10: Situation where the watershed algorithm fails to extract the proper skeletons: the vein patterns have a floating end point

computational complexity for these two shape descriptors. However, compared to the contour-base descriptor, the skeletal representation of the objects are more robust against any potential shape variation for the object, and is relatively less affected by the uncertainty of the object's boundary points. Therefore, a decision was made to represent the vein pattern's shape in its skeletal form.

We started by firstly investigating the traditional binary-based skeletonization. The binary-based skeletonization operates on binary images. In the context of IR vein pattern images, due to the fact that the gray-scale intensity for the veins is not uniform throughout the image, the global thresholding technique does not provide satisfactory results. Therefore, we utilized a technique of local adaptive thresholding with global offset to perform the binarization process. The resulted binary images were passed to a classic thinning algorithm. Experimental results showed that the traditional binary-based skeletonization is able to extract the skeletons that are approximately close to the shape of the vein patterns. However, because of the additional binarization stage, errors (misclassification pixels) introduced will be propagated to and possibly magnified at the skeletonization stage.

To overcome the problem faced by the traditional binary skeletonization algorithms, we proposed a watershed algorithmic skeletonization approach that works

directly on the gray-scale images. The algorithm imitates the water immersion process that peels of the boundary points of the object recursively by expanding the catchment basins. A "dam" (watershed pixel) is built at the meeting point of two catchment basins before they are about the merge. The final resulting watershed corresponds to the skeleton of the object. This approach works directly on the gray-scale images, and by eliminating the binarization process, it prevents errors being propagated to and magnified by the skeletonization process. The watershed algorithmic skeletonization approach can also work on the binary images. To produce more accurate skeleton for the object, the Euclidian distance transform for the binary image is firstly computed; and the water immersion process is then carried out on this distance transform map to obtain the final skeletons for the object.

Experimental results on both generic and IR vein pattern images showed that the watershed algorithmic skeletonization approach is capable of extracting the skeletons of the objects, and the shape of the object is preserved relatively well. However, this approach faces the problem that for the objects have floating end points, the skeletons of that part of the object will be lost after the water immersion process. This will cause a loss of information in the shape of the vein patterns, and remains a major issue to be tackled in the future research.

The works on the watershed algorithmic skeletonization approach proposed in this chapter were presented in several papers (Wang & Leedham, 2007b, 2007a) listed in the reference.

Chapter 6

Vein Pattern Features and Matching

Though various vein pattern biometric systems have been developed, there are few published research studies specifically addressing the issue of the selection of features to recognize the vein patterns. Cross and Smith (Cross & Smith, 1995) used the medial axis representation as the feature of the vein pattern, and applies the "constrained sequential correlation" to match the patterns. Lin and Fan (Lin & Fan, 2004) proposed the use of multi-resolution analysis features to analyze the palm-dorsa vein patterns. Miura et al (Miura et al., 2004) utilized "template matching" to recognize the vein patterns in the finger. Fujitsu's (Fujitsu-Laboratories-Ltd, 2003) palm vein verification product has reported high accuracy (1% FRR and 0.5% FAR), but to the best of our knowledge, the features used are not disclosed in any published research articles. Whilst these authors claim the features they use to recognize the vein patterns can reach a high level of accuracy, there is a lack of agreement on the commonly acceptable features that can best represent the shape of the vein patterns. In addition, there is scant research which focuses on the distribution of the features in the vein patterns as well as the negative impacts brought to the matching stage

due to the potential errors occurring in the preprocessing stages.

Correct selection of features is vital to any vein pattern biometric systems. This chapter is therefore motivated to investigate the possible features that can best represent the shape of the vein patterns, as well as their tolerance to potential preprocessing errors. In addition, matching algorithms were also proposed for the recognition of the feature set. Inspired by the well-established techniques used in fingerprint biometrics, we started with investigation of salient point features (SPF) of the vein pattern.

6.1 Salient Point Features

In finger print biometrics, a fingerprint pattern can be well represented by a number of critical points in the finger print image: the ridge endings and ridge bifurcations. These critical points are commonly referred as minutiae, and they are widely used as the feature to match a pair of fingerprints, and hence to identify a person (Jain et al., 1997). Buddaharaju (Buddaharaju et al., 2007) demonstrated the use of minutiae in the application of recognizing the thermal patterns of a face. Intuitively, we could use a similar set of salient points to represent the vein pattern. Typically, in the vein pattern, the branching points and the ending points in the vein pattern skeleton image are the two types of crucial salient points to be extracted.

6.1.1 Salient Points Extraction

Extracting the salient points from the skeletons of the vein patterns is a trivial task. To obtain the junction points from the skeleton of vein patterns, we run the following pixel-wise operation commonly known as the Cross Number (CN) concept (Halici

et al., 1999): For a 3×3 region,

P_1	P_2	P_3
P_8	P_0	P_4
P_7	P_6	P_5

if P_0 is 1, and the number of transition N_{trans} between 0 and 1 (and vice versa)from P_1 to P_8 is greater than or equal to 6, then P_0 is a junction point. Mathematically, this can be expressed by the Equation 6.1.

$$N_{trans} = \sum_{i=1}^{8} |P_{i+1} - P_i|, \text{ where } P_9 = P_1 \tag{6.1}$$

A similar approach can be applied to find the ending points. The difference is that the number of transition N_{trans} for an ending point is now exactly 2. However, due to the fact that the vein pattern is a network of blood vessels, there are very few ending points for the veins. Therefore, the ending points extracted here are endings of vein skeleton curves which reside mostly at the edge of the image as a result of cropping of the ROI from the images, instead of the true ending points of the veins. The reason why we take these ending points as a complement minutiae feature to the bifurcation points is because, though not the true vein endings, they do contain geometrical information about the shape of the skeletons of the vein pattern. Figure 6.1(c) shows the salient points extracted from the skeleton image of the vein pattern. Due to the fact that the size of the hands are different from subject to subject, the size of the ROIs varies. In order to cater for the change of the size of the ROIs, the salient points of all the vein pattern images are centrally aligned in a 180×180 pixel region. This alignment ensures the accurate relative measurement of two SPF sets. It is apparent that any changes to the ROI will lead to displacement to the salient points, especially the ending points which resulted from cropping of ROI from the

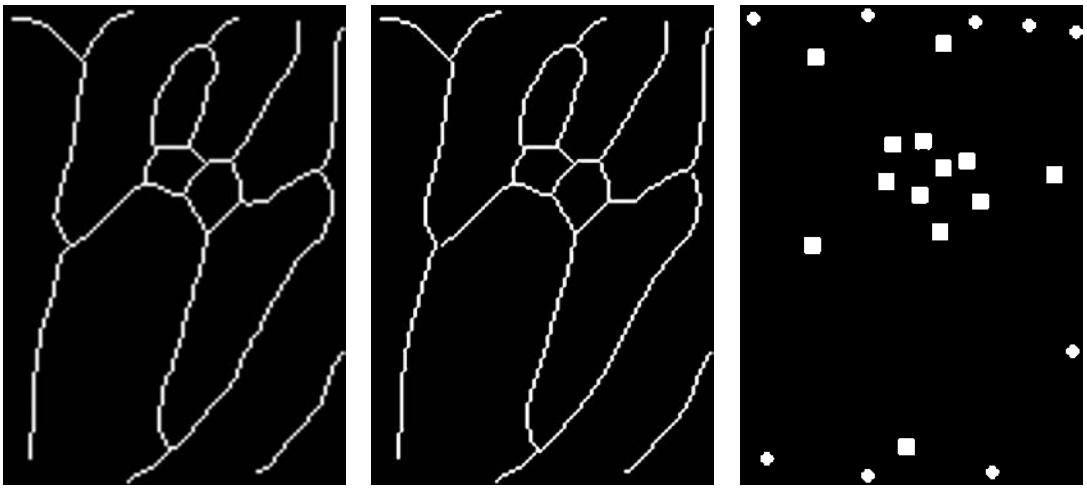

(a) Skeletons of the Vein Pattern

(b) After Polynomial Curve Fitting

(c) The Salient Points of the Vein Pattern (Square for Bifurcation Points; Round for Ending Points)

Figure 6.1: Skeleton and Salient Points of the Vein Pattern

image. The effect of changes to the ROI is studied in detail in Section 6.1.4.

Experiments were carried out on our FIR vein pattern database and the results for the analysis of the distribution of the number of salient points for each vein pattern image are shown in Figure 6.3, together with the distribution of the number of bifurcation and ending points in Figure 6.2(a) and Figure 6.2(b) respectively. It can be seen that for each vein pattern image, there is a trend that the average number of bifurcation points is 7, whilst the average number of ending points is 6, and overall, the total number of salient points is 13. The number of salient points is relatively small for vein patterns in the back of the hand. Nevertheless, for personal verification applications within a reasonable sized population, these salient point features are still capable of providing strong discriminating power, as will be shown in Section 6.1.3.

6.1.2 Salient Points Evaluation

To evaluate the usefulness of the two types of salient points, namely bifurcation and ending points, we carried out 3 sets of personal verification experiments: firstly with the bifurcation points only, and then with ending points only, and finally the combina-

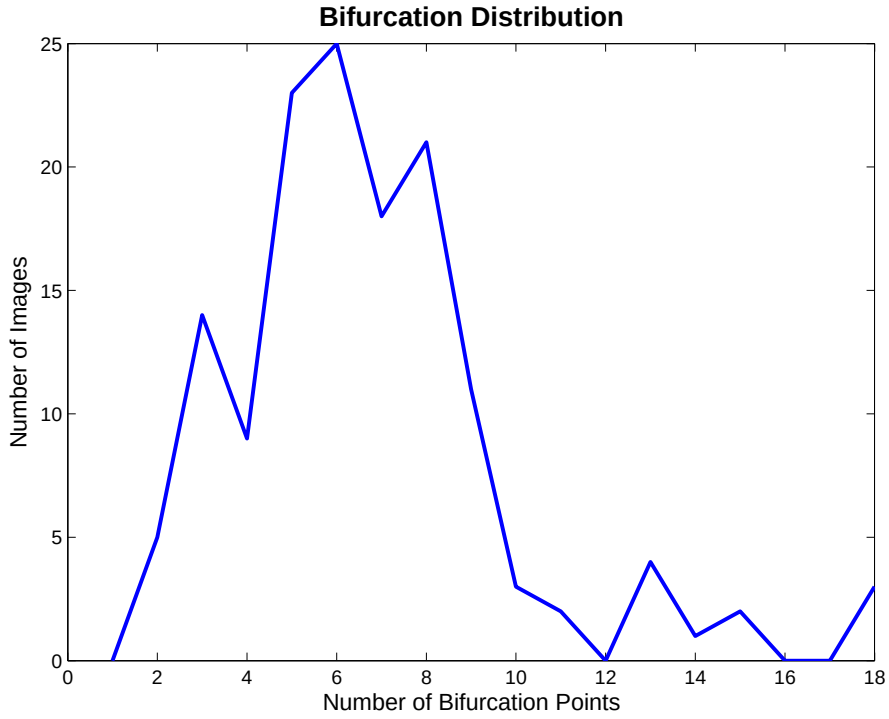

(a) Bifurcation Point Distribution (Mean=7)

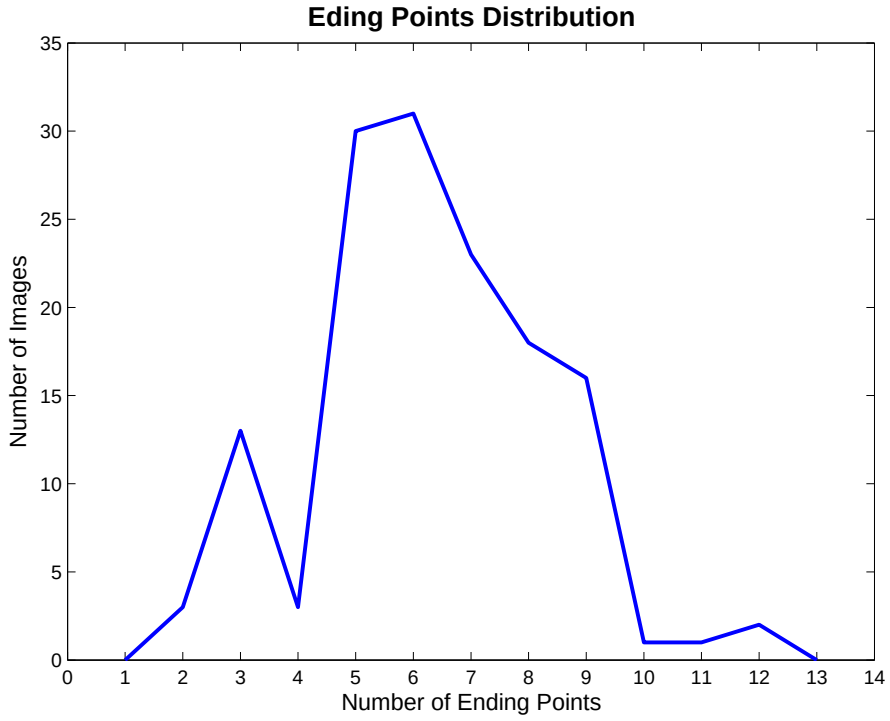

(b) Ending Point Distribution (Mean=6)

Figure 6.2: Distribution of the Number of Bifurcation and Ending Points

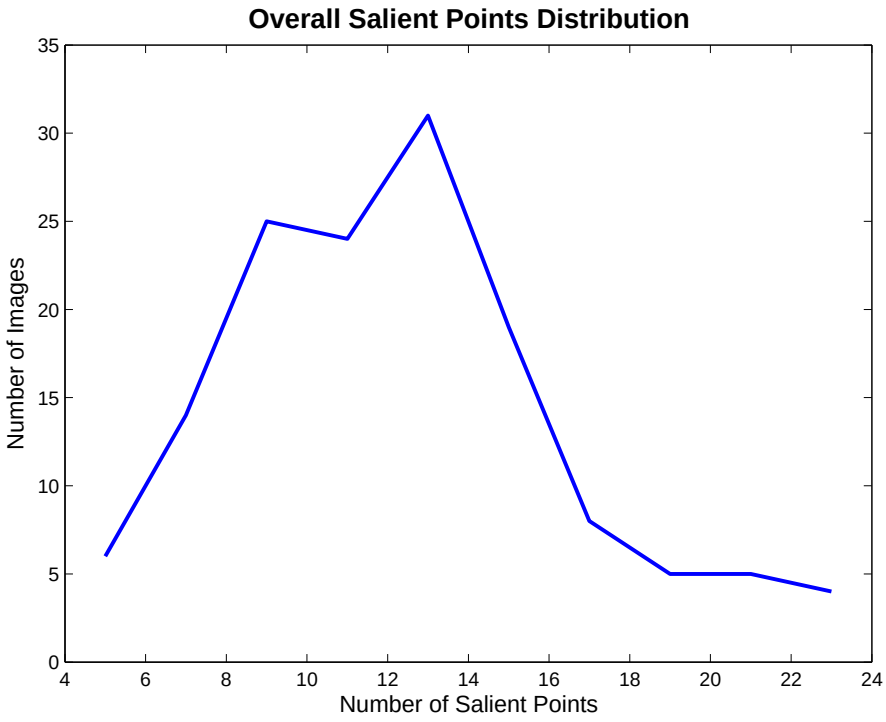

Figure 6.3: Distribution of the Total Number of Salient Points (Mean=13)

Table 6.1: Salient Point Feature Evaluation Using Modified Hausdorff Distance

	Equal Error Rate	Threshold Value Found
Bifurcation Points Only	2.1%	11.5
Ending Points Only	2%	11
Combination of Both Salient Features	0%	10

tion of the two salient point types. The 3 sets of experiments utilize the same modified Hausdorff distance (this is described in section 6.1.3) to measure the similarity. Table 6.1 contains the results of the evaluation, which shows that while the bifurcation and ending points can reach relatively high recognition accuracy, the combination of the two types of salient points can further increase the accuracy, which is advantageous especially when high feature discriminating power is desired for a large population group.

6.1.3 Similarity Measure of the Salient Point Features with the Modified Hausdorff Distance

Many techniques can be applied to the analysis of salient point features of vein pattern in a similar manner to those applied to fingerprint minutiae. However, due to the fact that the number of SPF for the vein pattern is relatively small compared to those for fingerprints, analysis based on geometrical information is preferred to statistical features. Since the vein pattern is represented as a set of 2 dimensional points, matching of a pair of such pattern can be achieved by measuring the Hausdorff distance between the two SPF sets.

In many applications, for example the SPF matching in our case, due to occlusion and noise, not all points from set M have a corresponding point in set T. More typically, the two point sets are of different size, and thus no one-to-one correspondence exists between all points. Under this circumstance, the Hausdorff distance is often one of the optimum measures for comparing similarity of shapes.

The Hausdorff distance is a distance measure between two point sets. Unlike most of the shape recognition techniques that need a one-to-one correspondence between the template and the testing data, the Hausdorff distance can be found without explicit point correspondence (Ruchlidge, 1997). According to Huttenlocher et al. (Huttenlocher et al., 1993), the Hausdorff distance for binary image matching is more tolerant to perturbations in the locations of points than binary correlation techniques since it measures proximity rather than exact superposition. On the other hand, the images to be matched shall be roughly aligned.

For two point sets $M^p = \{m_1^p, m_2^p, ..., m_k^p\}$ and $T^p = \{t_1^p, t_2^p, ..., t_n^p\}$, the *directed* Hausdorff distance $h(M^p, T^p)$ is defined as the lowest upper bound (supremum) over

all points in M of the distances to T as in equation 6.3:

$$h(M^p, T^p) = \sup_{m_i^p \in M} \inf_{t_j^p \in T} d(m_i^p, t_i^p), \tag{6.2}$$

with $d(m_i^p, t_i^p)$ the underlying distance, which often is the Euclidean distance $||m_i^p - t_i^p||$. $h(M^p, T^p)$ identifies the point $m_i^p \in M^p$ that is farthest from any point of T^p and measures the distance from m_i^p to its nearest neighbor in T^p. The Hausdorff distance $H(M^p, T^p)$ is then the maximum of $h(M, T)$ and $h(T, M)$:

$$H(M^p, T^p) = \max\left(h(M^p, T^p), h(T^p, M^p)\right), \tag{6.3}$$

which measures the degree of mismatch between two sets by measuring the distance of the point of M^p that is farthest from any point of T^p and vice versa. The smaller the value of H, the more similar the two point sets are. For two finite point sets with size k and p respectively, the Hausdorff distance H can be computed using Voronoi diagrams with time complexity equals to $O((k+p)log(k+p))$ (Alt et al., 1995).

However, this original form of the Hausdorff distance is very sensitive to outlier points. A few outlier points can perturb the distance greatly, though the two point sets might be very similar (Gao & Leung, 2002b). Our experiments on the database of 47 distinct objects shows the direct application of the original form of Hausdorff distance performs poorly for SPF recognition. Figure 6.4 shows the False Acceptance Rate and False Rejection Rate curves, from which it can be seen that when the threshold value for the distance measure H is 25, the EER is approximately 7.2%, which is not acceptable in any security applications.

To Overcome the weakness of the Hausdorff distance, Dubuisson and Jain (Dubuisson & Jain, 1994) investigated many forms of different Hausdorff distance measures, and indicated that a modified Hausdorff distance measure is less sensitive to outlier

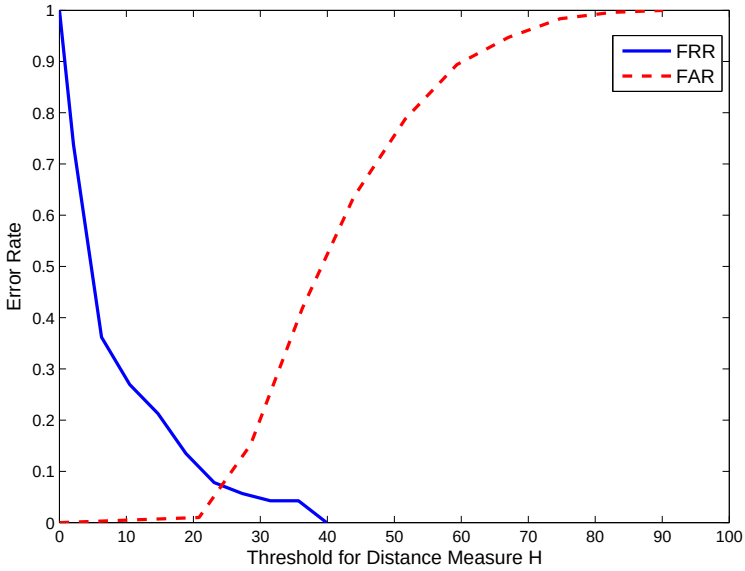

Figure 6.4: Error Rate Curves for Salient Point Features Recognition Using the Original Form of Hausdorff Distance (EER=7.2% where the threshold is observed to be 25)

points, and gives the best performance. Unlike the original form, the directed modified Hausdorff distance $h(M^p, T^p)$ is defined as in Equation 6.4, where N_m^p stands for the number of points in M^p. An experiment with the MHD was carried out on the same data set, and the algorithm achieves 0% EER (as shown in Figure 6.5) when the threshold value for the distance measure H was set to 10. This result supports our decision to use the modified Haudorff distance measure to recognize the salient point features of vein patterns.

$$h(M^p, T^p) = \frac{1}{N_m^p} \sum_{m_i^p \in M^p} \min_{t_j^p \in T^p} \| m_i^p - t_j^p \| . \tag{6.4}$$

6.1.4 Tolerance to Errors

Tolerance to Loss of Features

Occasionally, some minutiae points will be missing due to inadequate image preprocessing in the stages before matching. To assess the tolerance of the MHD al-

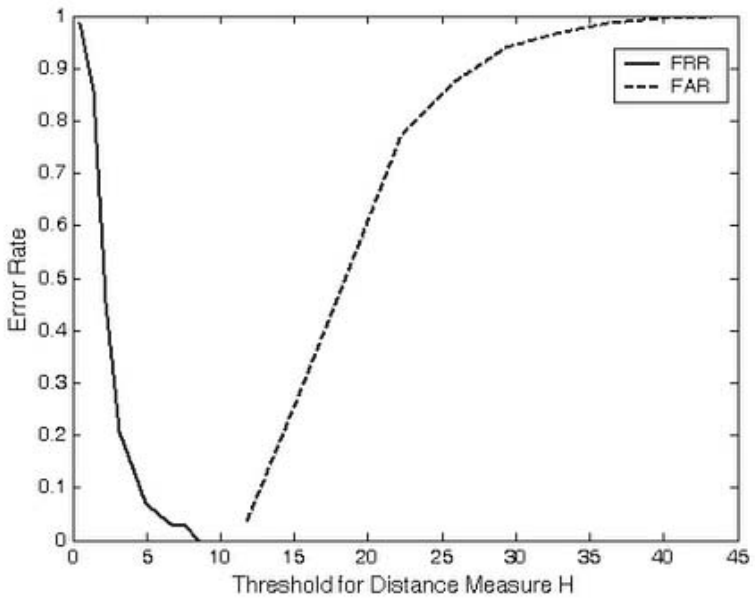

Figure 6.5: Error Rate Curves for Salient Point Features Recognition Using the Modified Hausdorff Distance (EER=0% where the threshold is 10)

gorithm to this circumstance, we simulate the loss of salient points by randomly removing several salient points from the extracted SPF data for each subject. We started testing the MHD algorithm with one salient point missing for each subject, then we gradually increased the number of lost salient points to 13, which is the average number of salient points for all the vein patterns. Figure 6.6(a) shows the change of recognition accuracy with the increase of the number of lost salient points. It can be seen that the error rate increases slowly when the number of missing minutiae is small, and when the number of missing salient points is greater than 4 (which is equivalent to 20% of the total number of salient points), the error rate starts to increase rapidly. This is what we have intuitively predicted, as the average number of minutiae points is relatively small for the vein patterns, therefore, a number of missing salient points (such as 20%) could easily cause a significant loss of information, which will eventually adversely affect the recognition accuracy.

Tolerance to Geometrical Displacement

For the experiments carried out in our research, with the full cooperation from the participants, we restrict the position where they can place their hands so that all the hand images are well aligned. However, for real life applications, users generally place their hands at places that are slightly displaced from the desired position. This may lead to errors when detecting hand landmarks, and hence causes shifting of the regions of interest. As a result, the salient points extracted in the later stage will be shifted. Mathematically, the shifting can be formulated using a geometrical affine transformation, as expressed in Equation 6.5 with the transformation matrix indicating the salient points are rotated by an angle of θ followed by a translation with an offset of (t_x, t_y) along the X and Y axes respectively.

$$\begin{bmatrix} x' \\ y' \\ 1 \end{bmatrix} = \begin{bmatrix} \cos\theta & -\sin\theta & t_x \\ \sin\theta & \cos\theta & t_y \\ 0 & 0 & 1 \end{bmatrix} \begin{bmatrix} x \\ y \\ 1 \end{bmatrix} \tag{6.5}$$

To simulate the effect of geometrical transformation, we apply the affine transformation of Equation 6.5 to the salient point feature data with the randomly generated θ value within the range of $-10°$ to $10°$ and the offset value in the range of -5 to 5 pixels respectively. The transformed minutiae data was analyzed again by the MHD algorithm, and the result in Figure 6.6(b) shows the EER was found to be 15% where the threshold value for distance measure H was observed to be 13. This result indicates that minutiae analysis using the MHD algorithm is quite sensitive to the geometrical transformation. This is expected as the modified Hausdorff distance measures the similarity between two point sets based on their spatial information. When geometrical transformation is applied to the point sets, the coordinate values for the points are distorted significantly, and hence prevents the modified Hausdorff distance from

measuring the similarity accurately.

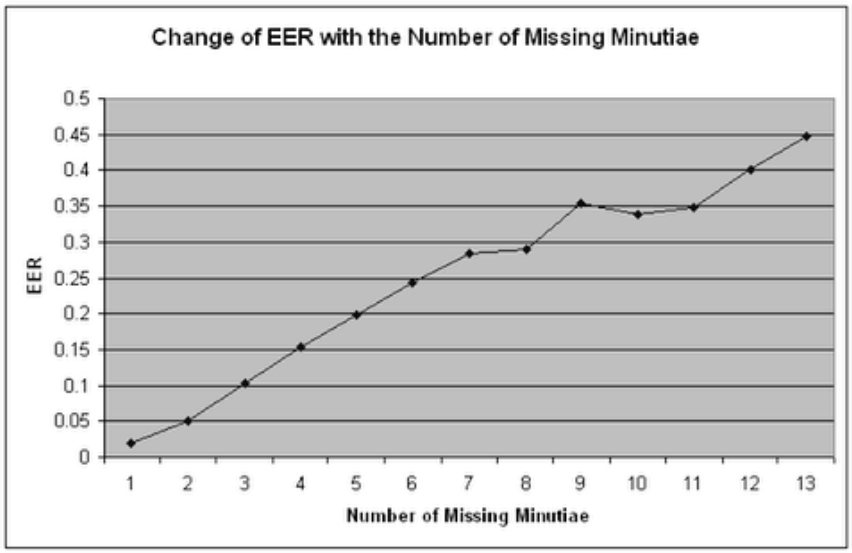

(a) Equal Error Rate (EER) Versus Number of Missing Salient Points

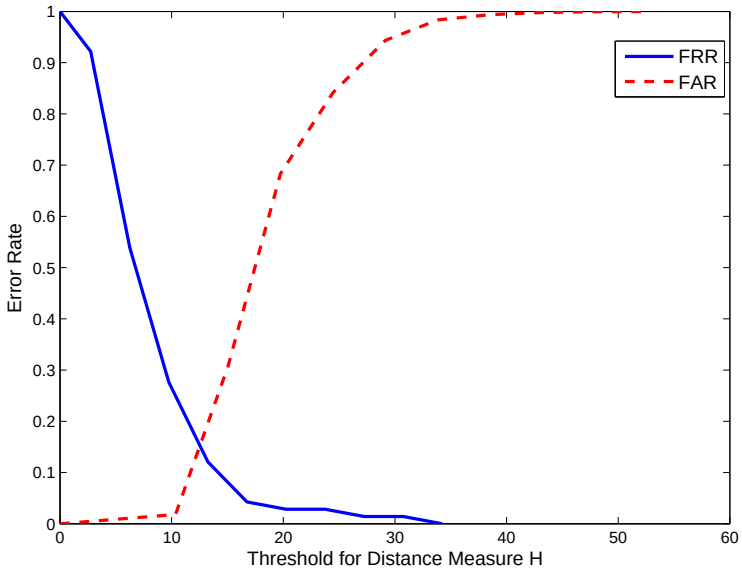

(b) Error Curve After Geometrical Transformation with Random θ and Offset (EER=15%)

Figure 6.6: Tolerance of the Salient Point Features Against Errors

6.2 The Line Edge Maps

The salient point features are powerful in providing discriminating features for the vein patterns. However, it still suffers from several weaknesses: First, it uses the spatial information of the vein pattern, but it lacks local structure representation such

as orientation information. There is a possibility that two vein patterns are totally different, and yet the two vein patterns give very similar salient points. Secondly, the number of salient points are relatively small, and the discriminating power of such salient point feature could decreases adversely as the population size increases. Lastly, as stated in Section 6.1.4, the salient point features have low tolerance against the loss of feature points. All these weakness of the salient point features will prevent them from being used as a strong discriminating feature in large scaled person identificaiton/verification applications.

6.2.1 Building the Line Edge Map

To overcome the weakness of the salient point features, instead of extracting a few crucial points from the vein pattern, we proposed to construct the Line Edge Map (LEM) for each of the vein pattern and use it as a feature for recognition. The Line Edge Map refers to splitting the individual curve of the skeleton of the vein pattern into multiple line segments, and the resultant line segments set is used to represent the shape of the vein pattern. The major advantage of LEM over salient point features is that the LEM (which is a line segment set) provides much richer information about the local structure (including positions and orientation) of the object's shape than the salient points do. This is more desirable when higher discriminating power for features is required.

To construct the LEM from the skeletons of the vein patterns, we apply the Hough Line Transform iteratively to extract line segments from each curve segment in the vein pattern skeleton image.

The Hough transform is a general technique for identifying the locations and orientations of certain types of features in a digital image. The simplest form of the

Hough transform is the Hough line transform. Mathematically, a representation of a line is the slope-intercept form:

$$y = m \cdot x + b, \tag{6.6}$$

where m is the slope of the line and b is the y-intercept. However, this representation is not very stable, as lines get more and more vertical, the values of m and b grow towards infinity. A more useful representation of a line is its normal form:

$$x \cdot \cos\theta + y \cdot \sin\theta = \rho. \tag{6.7}$$

This equation specifies a line passing through (x, y) that is perpendicular to the line drawn from the origin to (ρ, θ) in polar space. For each point (x, y) on a line, θ and ρ are constant. Therefore, for any given point (x, y), the lines passing through that point can be obtained by solving for ρ and θ. By iterating through possible angles for θ, we can solve for ρ by Equation 6.7 directly. A Hough Line Transform effectively finds all the lines in the polar space that pass every point in the image. By applying a voting algorithm, the lines that passing many points in the original image can be obtained. Details about the Hough Line Transform can be found in the reference (Duda & Hart, January 1972). Figure 6.7(b) shows the longest line segment detected on a curve in Figure 6.7(a) by using the Hough Line Transform.

To construct the LEM for the vein patterns using Hough Line Transform, we run the following algorithm:

Step 1: Divide the vein pattern skeletons into individual curve segments $\{C_1, C_2, \ldots, C_n\}$.

1.a Detect the branch points and ending points in the vein pattern skeleton image.

(a) A curve

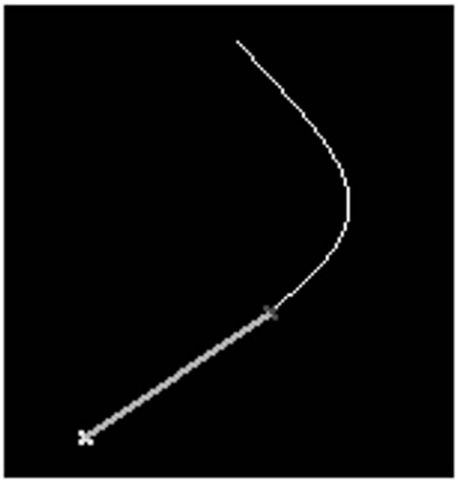

(b) The longest line segment in the curve detected by Hough line transform

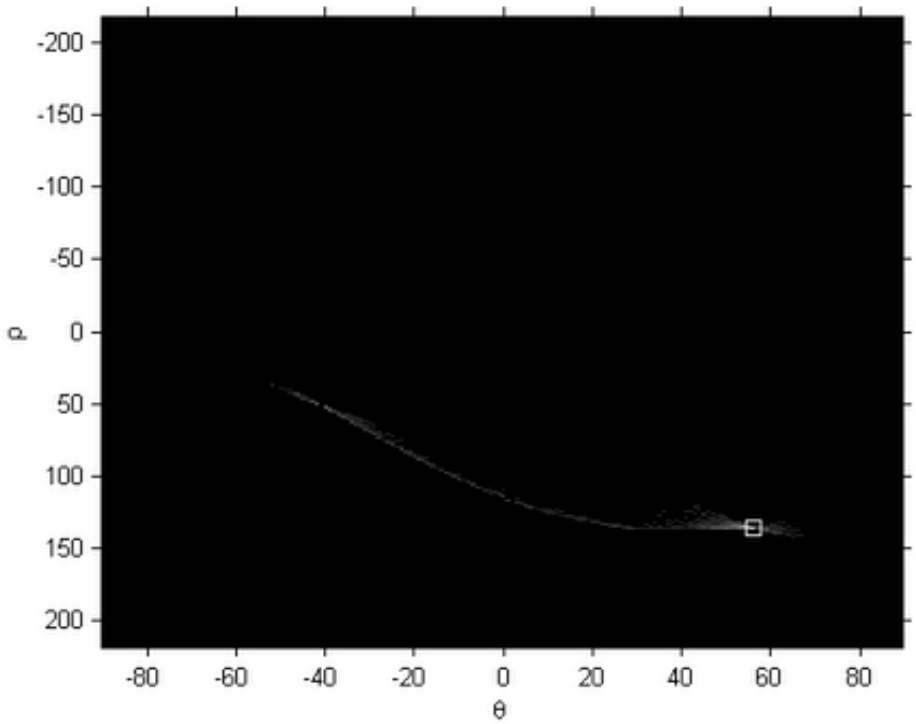

(c) The Hough Transform of the curve (the square indicates the line that gets the most votes)

Figure 6.7: An example of Hough Line Transform on detecting the longest line segment on a curve

1.b Starting from each ending point, run a line tracing algorithm to group the skeleton pixels into individual curve segments until another ending point or branch point is met.

1.c For circles or loops in the vein pattern skeleton image, break the loop at an arbitrary position so that it becomes a curve segment.

Step 2: Build line segment representation for each curve segment.

For $C_i = C_1$ to C_n:

2.a Apply Hough line transform to the current curve segment C_i to obtain the current longest line segment L_{ij}.

2.b Store the two ending points of L_{ij} into a file for representation of this line segment.

2.c Remove the line segment L_{ij} from the current curve segment C_i.

2.d Repeat step 2.a until no more skeleton pixels are remaining, and thus, the curve segment C_i is now represented by a set of line segments $\{L_{i1}, L_{i2}, \ldots, L_{im}\}$, where m is the number of line segments extracted from C_i.

After running the above algorithm, we would obtain the line edge map for the vein pattern skeleton image, which consists of a large set of line segments. Figure 6.8 shows the line edge map extracted from several vein pattern skeleton images.

6.2.2 The Line Segment Hausdorff Distance with Line Edge Maps

To match shapes that are described by a set of line segments, we can calculate the Line-segment Hausdorff Distance (LHD) between two line-segment sets. The LHD

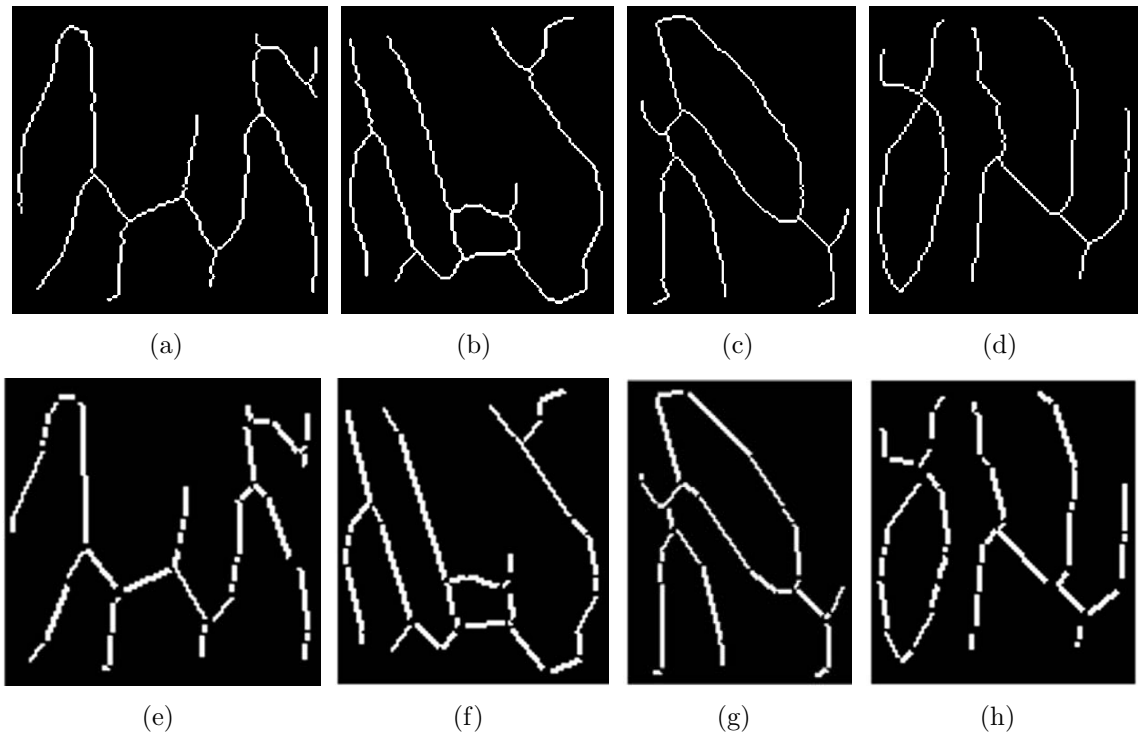

Figure 6.8: The Line Edge Maps (e)-(h) Extracted from vein pattern skeleton images (a)-(d)

was firstly proposed by Gao & Leung (Gao & Leung, 2002a) in a application of face recognition.

Given two finite line segment sets $M^l = \{m_1^l, m_2^l, ..., m_p^l\}$ and $T^l = \{t_1^l, t_2^l, ..., t_p^l\}$, the LHD is built on the vector $\overrightarrow{d}(m_i^l, t_j^l)$ representing the distance between the two line segment sets, and the vector is defined as

$$\overrightarrow{d}(m_i^l, t_j^l) = \begin{bmatrix} d_\theta(m_i^l, t_j^l) \\ d_\parallel(m_i^l, t_j^l) \\ d_\perp(m_i^l, t_j^l) \end{bmatrix}^T \tag{6.8}$$

where $d_\theta(m_i^l, t_j^l)$, $d_\parallel(m_i^l, t_j^l)$ and $d_\perp(m_i^l, t_j^l)$ are the *angle distance, parallel distance and perpendicular distance* respectively, and they are defined as:

$$d_\theta(m_i^l, t_j^l) = f\left(\theta(m_i^l, t_j^l)\right), \tag{6.9}$$

$$d_\parallel(m_i^l, t_j^l) = min\left(l_{\parallel 1}, l_{\parallel 2}\right), \tag{6.10}$$

$$d_{\perp}(m_i^l, t_j^l) = l_{\perp}, \tag{6.11}$$

where $\theta(m_i^l, t_j^l)$ is the smallest intersecting angle between lines m_i^l and t_i^l. $f(\bullet)$ is a non-linear penalty function to map the angle to a scalar, and generally, the tangent function is used.

Gao & Leung illustrated the designs of the parallel and perpendicular displacements with a simplified example of two parallel lines, m_i^l and t_i^l, as shown in Figure 6.9. $d_{\parallel}(m_i^l, t_j^l)$ is defined as the minimum displacement to align either the left end points or the right end points of the lines. $d_{\perp}(m_i^l, t_j^l)$ is simply the vertical distance between the lines. When m_i^l and t_i^l are not parallel, one can rotate the shorter line with its midpoint as rotation center to the desirable orientation before computing $d_{\parallel}(m_i^l, t_j^l)$ and $d_{\perp}(m_i^l, t_j^l)$. Figure 6.10 shows 3 typical rotations. The purpose of rotation is to calculate $d_{\parallel}(m_i^l, t_j^l)$ and $d_{\perp}(m_i^l, t_j^l)$. Among the three rotations of Figure 6.10(b), (c) and (d), (b) is found to give measures of $d_{\parallel}(m_i^l, t_j^l)$ and $d_{\perp}(m_i^l, t_j^l)$ closest to the original values by human observers. In order to cater for the effect of broken

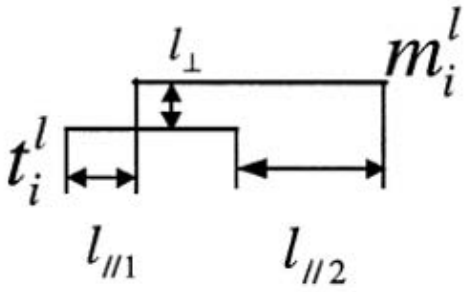

Figure 6.9: Line Displacement Measure. (Source: Gao & Leung 2002)

lines caused by segmentation error, and alleviate the effect of adding, missing and shifting of feature points (i.e. end points of line segments) caused by inconsistency of feature point detection, the parallel shifts $l_{\parallel 1}$, and $l_{\parallel 2}$, are reset to zero if one line is within the range of the other as shown in Figure 6.11. Finally, the numerical value

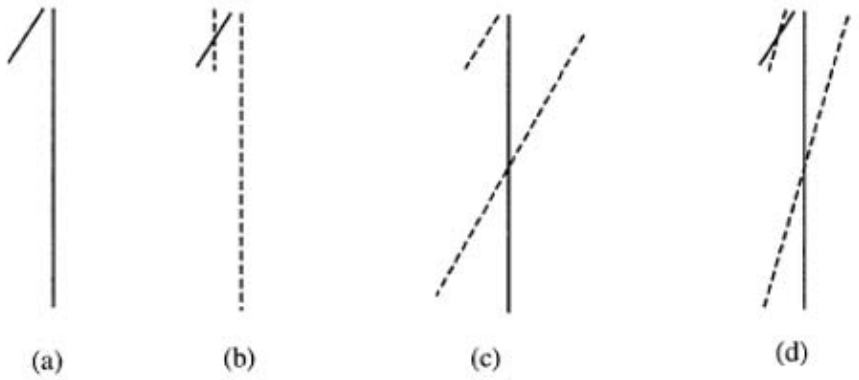

Figure 6.10: The rotation effect of two lines. (a) The original line pair. (b) Rotate the shorter line. (c) Rotate the longer line. (d) Rotate both lines with half of their angle difference in opposite directions. Solid lines represent lines before rotation. Dashed lines represent lines after rotation. (Source: Gao & Leung 2002)

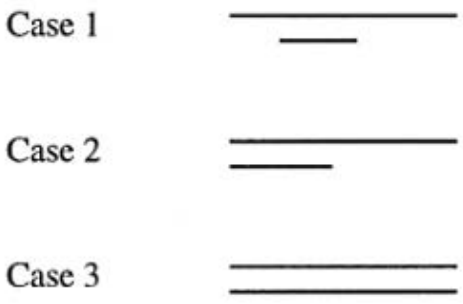

Figure 6.11: Cases where $d_{\parallel}(m,t) = 0$. (Source: Gao & Leung 2002)

of the distance is given by Equation 6.12.

$$d(m_i^l, t_j^l) = \sqrt{(W_a \cdot d_\theta(m_i^l, t_j^l))^2 + d_\parallel^2(m_i^l, t_j^l) + d_\perp^2(m_i^l, t_j^l)} \tag{6.12}$$

where W_a is the weight for angle distance which is usually determined by empirical studies. The directed and undirected LHDs are defined in Equations 6.13 and 6.14, where $l_{m_i^l}$ is the length of line segment m_i^l.

$$h_l(M^l, T^l) = \frac{1}{\sum_{m_i^l \in M^l} l_{m_i^l}} \sum_{m_i^l \in M^l} l_{m_i^l} \cdot \min_{t_j^l \in T^l} d(m_i^l, t_j^l) \tag{6.13}$$

$$H_l(M^l, T^l) = \max(h_l(M^l, T^l), h_l(T^l, M^l)) \tag{6.14}$$

Testing was carried out on same Far-Infrared vein pattern image database. As there are 47 distinct subjects with a total of 141 distinct images, there will be $P\begin{pmatrix} 141 \\ 2 \end{pmatrix} = 19740$ possible access attempts, out of which 423 access attempts are genuine, and the remaining 19317 are intruder attempts. Figure 6.12 shows the distribution of the genuine and intruder accesses against the value H. It can be easily seen from Figure 6.12 that the smaller H is, the higher the probability the vein pattern belong to the genuine class. By choosing $H = 6.4$ to be the threshold value, the system achieves 0% false acceptance rate (FAR) and 0.015% false rejection rate (FRR) for all the access attempts made. It is clear that the performance of the LEM is comparable to the one of the minutiae features (with 0% of EER) in terms of accuracy.

6.2.3 Tolerance to Errors

Tolerance to Occlusion

For minutiae features, one of the major concern for errors is the loss of minutiae points due to preprocessing errors, whilst for the LEM, the cause of loss of line segments in

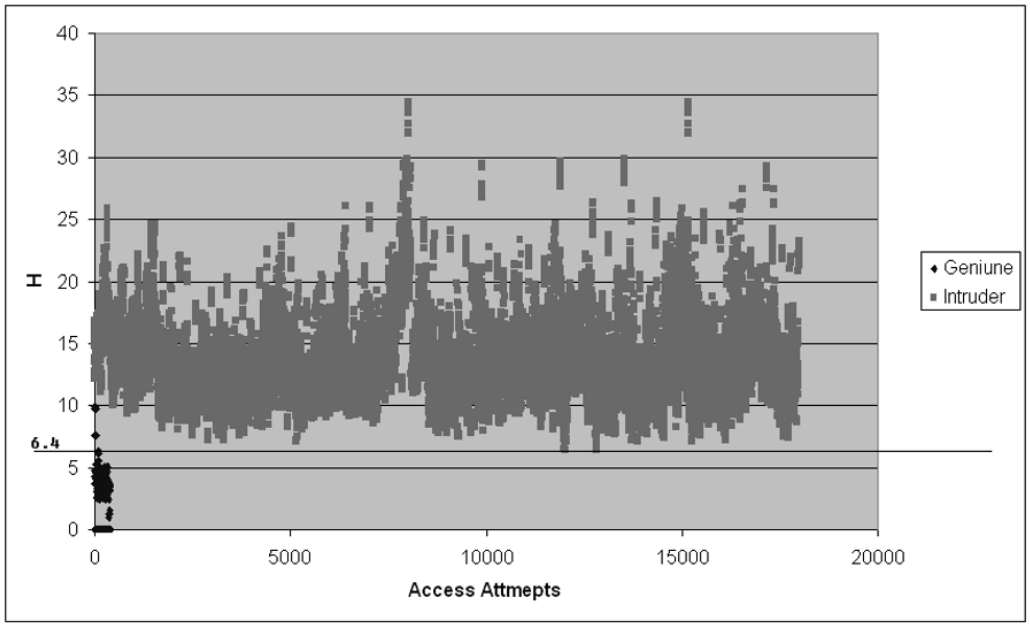

Figure 6.12: Distribution of genuine and intruder accesses against similarity measure H' for the FIR image data

the LEM is usually by occlusion. In order to simulate the occlusion effect, we created a rectangular image mask with random size between 7 and 30, and applied this mask to the vein pattern skeleton image at a random position. Figure 6.13 shows a vein pattern skeleton image occluded by a random mask created. It can be seen that some parts of the skeleton of the vein pattern have been missing due to occlusion, including some important junction areas. By applying the same LHD measurement to the occluded LEMs, we observed that the matching accuracy remains very stable: at threshold $H_L = 5.7$, the equal error rate increased to around 0.028%. This is illustrated in Figure 6.14. This result demonstrates the a significant advantage of LEM over the minutiae feature in terms of tolerance to loss of features.

Tolerance to Geometrical Displacement

Analysis of tolerance of the method of matching LEMs using the LHD measurements against geometrical displacement was carried out on the transformed vein pattern skeleton images. The experiment was performed in the same way as in the second

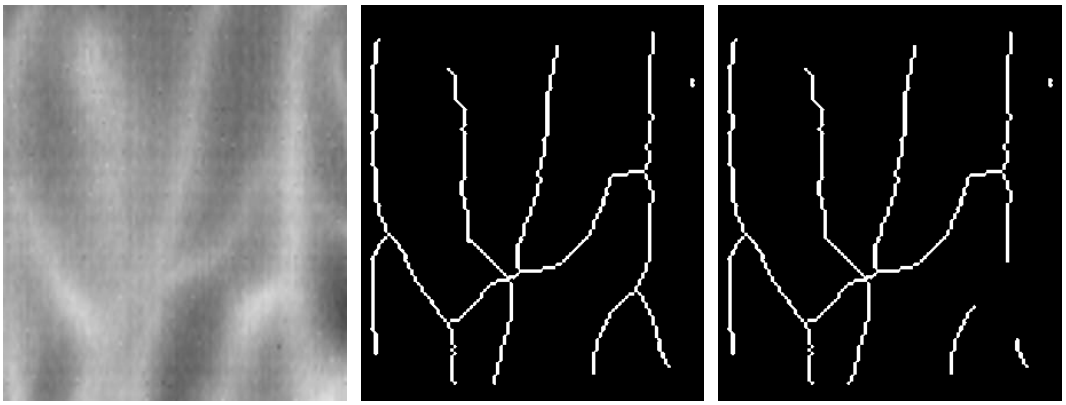

(a) An FIR Vein Pattern Image

(b) The Skeleton of the Vein Pattern

(c) The Skeleton After Occlusion by an Image Mask (the Junction Area on the Right is lost)

Figure 6.13: An vein pattern skeleton image occluded by an image mask

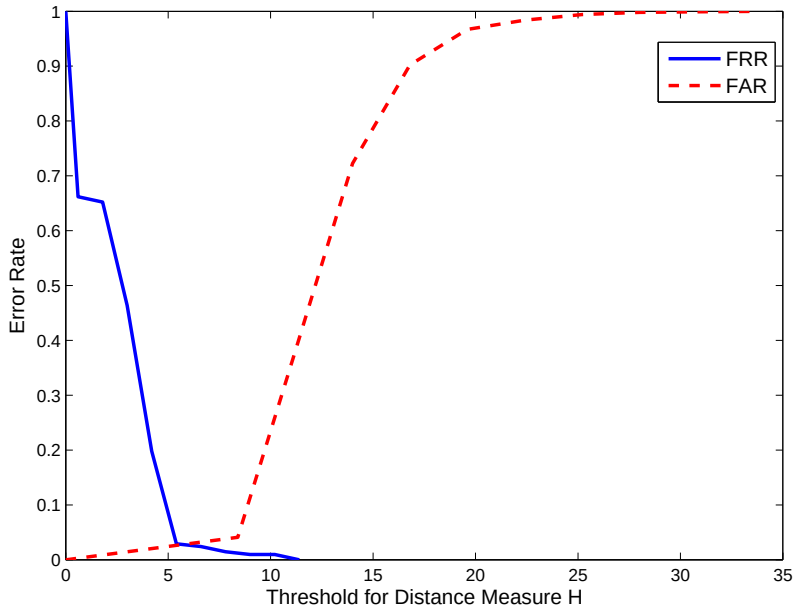

Figure 6.14: Error Rate Curves for the LEMs Occluded by a Random Image Mask

part of Section 6.1.4. We simulated the geometrical displacement by applying the affine transformation in Equation 6.5 to each of the vein pattern skeleton images. The rotation angle θ and the offset values in the x and y axis were randomly generated within the range of $-10°$ to $10°$ and -5 to 5 pixels respectively, in the same way as in the analysis of the minutiae features. The experimental result shown in Figure 6.15 shows that the EER reaches 10%, where the threshold value for H_L is observed to be 8.5. This is a significant increase compared to the matching result (where EER nearly equals to 0%) obtained previously for the experiments with original vein pattern skeleton images before geometrical transformation. The accuracy of LEM with LHD measurement degrade gracefully with geometrical displacement (having EER equal to 10%), as compared to the minutiae features having EER equal to 15% under the same circumstance. Whilst this is an improvement over the minutiae feature, the error rate that LEMs with LHD measurement have is intolerable for any applications. This, in fact, is the major issue for the LEMs with LHD measurement. Resolving this issue requires close alignment of the skeleton images. In fact, image alignment in object matching is still an unsolved problem in many applications.

6.3 Summary

This chapter presents the features used for matching of vein pattern shapes.

Inspired by the popular minutiae features commonly used in fingerprint analysis, we firstly defined some crucial points in the vein pattern skeleton images as the salient features for vein patterns. Similar to fingerprints, these salient features include branch points and ending points, however, the ending points are not the *true* ending points of the vein pattern, instead, they are the result of by cropping the ROI from the image. Analysis of the distribution of these salient points showed a trend that, on average,

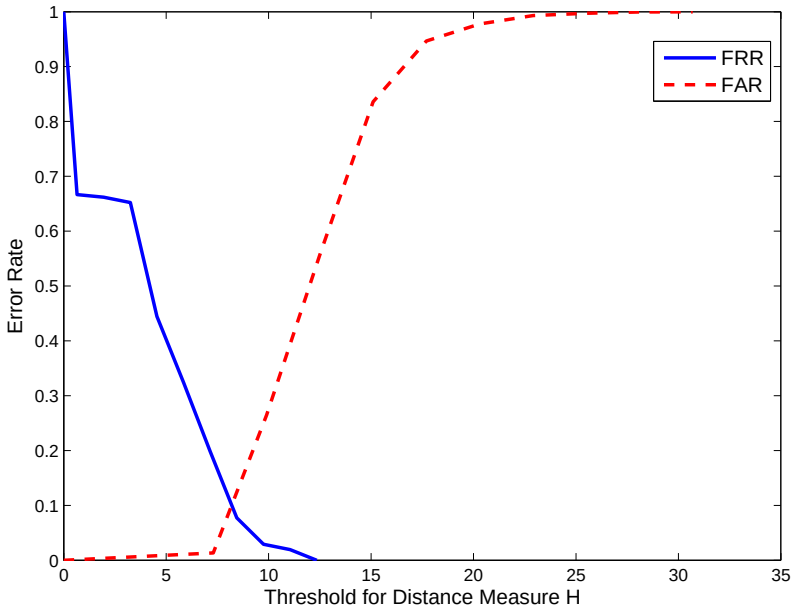

Figure 6.15: Error Rate Curves for the LHD Measurement of LEMs with Random Geometrical Displacement ($-10° \leq \theta \leq 10°$, and offsets lie between -5 to 5 pixels)

there are 13 salient points in each vein pattern ROI image, amongst which 7 are branch points and 6 are ending points. We evaluated the efficacy of these two types of salient points, and it was found that whilst each individual type of salient points can provide satisfactory performance for person verification purposes, the combination of the two types of salient points gives higher discriminating power. In order to use the extracted salient features to perform personal verification tasks, we propose to use the modified Hausdorff distance (MHD) algorithm to measure the spatial similarity between the minutiae sets. Experiments showed encouraging results as the equal error rate (EER) reaches 0%. This result indicates the salient point features in the vein patterns can be used as a feature set in personal verification applications efficiently. We further analyzed the tolerance of the salient point features against the loss of feature points and geometrical transformation. Results show that the recognition accuracy drops rapidly when a large number of minutiae are lost. In addition, the recognition accuracy decreases with the geometrical transformation, which indicates the MHD algorithm

is sensitive to the geometrical transformation, and proper alignments of images are necessary.

In order to overcome the weakness faced by the salient point features, we proposed the use of a Line Edge Map as the feature set representing the vein pattern. A LEM is defined as a line segment set, of which the line segments are split from each curve segment in the skeleton image of the vein pattern. Unlike the salient point features, the LEM is rich in local structure information, including position and orientation, which provides stronger discriminating power when the size of the population group grows tremendously. The LEMs are constructed using the Hough Line Transform, where the longest line segment in each curve segment is extracted each time iteratively. To perform matching on two LEMs, we propose to use the Line-segment Hausdorff distance measurement. The LHD measurement does not rely on one-to-one correspondence of line segments (which is a major advantage over other matching technique), and it provides superior performance on matching line segment sets. Experimental results showed that the LEM with LHD measurement gives very high matching accuracy and is comparable to the one by salient point features. However, the LEM outperforms the salient point features under the circumstances of object occlusion (which means loss of salient points for salient point features, and loss of line segments for LEMs). It is found that the LEM with LHD measurement is quite robust against object occlusion. However, in terms of tolerance to geometrical displacement, due to the nature of the LHD replying on spatial information, the performance of LEM with LHD measurement degrades, though more gracefully compared to the salient point features. This remains a major challenge for the matching algorithm to be more robust against misalignment.

The work on the salient point feature analysis is reported in paper (Wang &

Leedham, 2005), and the analysis of LEMs with LHD measurement of vein patterns can be found in our other paper (Wang et al., 2007b)

Chapter 7

An Initial Study of Vein Pattern Biometrics for Identical Twins

It is always a crucial topic to study the hereditary relationship for any type of biometric features. Amongst these hereditary studies, an investigation into the similarity of identical twins in their biometrics is one of most challenging tasks.

7.1 Identical twin studies

There are two types of twins, dizygotic and monozygotic twins. Dizygotic twins result from two different fertilized eggs resulting in different deoxyribose nucleic acid (DNA). Monozygotic twins, also called identical twins, are the results of a single fertilized egg splitting into two individual cells and developing into two individuals. Therefore, identical twins have the same genetic expressions. According to Nora and Fraser (Nora & Fraser, 1994), the frequency of identical twins is about 0.4% across different populations, and some researchers (Phillips et al., 2000) believe this is the upper limit for the performance of certain biometrics, such as face recognition.

Since the identical twins have the same genetic expression, this closest genetics-based relationship makes it questionable on the level of similarity between a pair of

identical twins' biometric traits. Not all biometrics can provide sufficient distinctive information to classify identical twins, such as faces. Whilst there has been research in iris, face, voice, fingerprint, palm prints (Kong et al., 2006) verification for identical twins, there is scant work on the analysis of the identical twins' vein patterns. During our vein pattern image database collection, we have collected images data for 3 pairs of identical twins; it is therefore important and possible for us to carry out an initial study with the image data from the 3 pairs of identical twins to examine the vein patterns' similarity and their genetic relationships.

Twin pairs 1 and 2 are male participants, whilst twin pair 3 are female participants. All the 3 pairs of twins are in the age band 10 to 20 years. Figures 7.1, 7.2, 7.3, shows the raw FIR vein pattern images of both left and right hands for the 3 pairs of twins respectively. It is apparent that each twin pair's vein patterns are distinguishable and different to our human vision. Nevertheless, it is important to establish a computational evidence for this.

To evaluate the similarity between a pair of identical twins' vein patterns, we run the same processing to the vein pattern images of the twins as stated in the previous chapters 4, 5. After we obtain the skeletons for the vein patterns; we then extract their salient point features as well as construct the LEMs. We will use both types of features to evaluate the genetic relationship of the vein patterns between identical twins.

Testing was firstly carried out to analyze the intra-class distance with the salient point features. The intra-class distance is defined as the MHD between two SPF sets extracted from two difference vein pattern images of the same hand of the same twin individual. Then we proceed to analyze the inter-class distance with the salient point features. The inter-class distance is defined as the MHD between two SPF sets

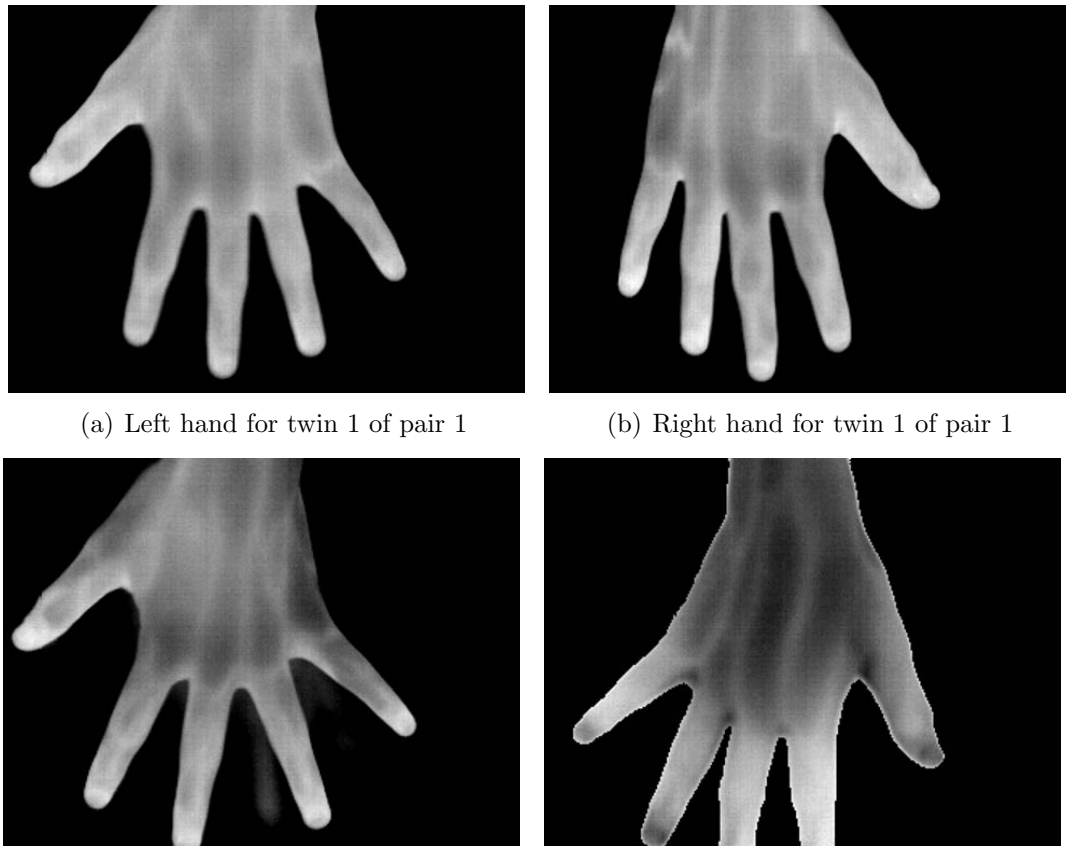

(a) Left hand for twin 1 of pair 1

(b) Right hand for twin 1 of pair 1

(c) Left hand for twin 2 of pair 1

(d) Right hand for twin 2 of pair 1

Figure 7.1: Vein Pattern Images for the Left and Right Hands of Twin Pair 1

extracted from two difference vein pattern images of the same side of hands from the two individuals of the same twin pair. Tables 7.1 and 7.2 show the intra- and inter-class distance of the vein patterns for identical twins using the MHD measurement. It can be seen that the values of the intra-class distance are distributed in the range of $[0 \sim 9.301]$, with averaged value of 3.136. On the other hand, the inter-class distances are in the range of $[14.252 \sim 27.818]$, with averaged value of 19.926. It is easy to see that the distributions of the intra- and inter-class distances are clearly separated. Therefore, by choosing a threshold value between $[9.301 \sim 14.252]$ for the MHD H' (it was chosen to be 10, same as the threshold value used in Chapter 6), we can classify the genuine and intruder , even if the imposter is their identical twin counterpart.

Similar testing was carried out with the LEM features, and now we calculate the LHD values for the LEM sets instead of the MHD as for the SPF sets. Tables 7.3 and

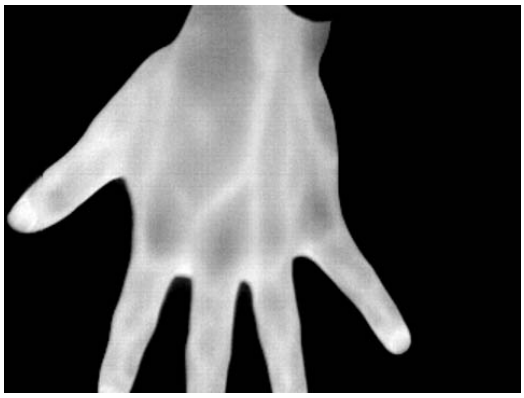

(a) Left hand for twin 1 of pair 2

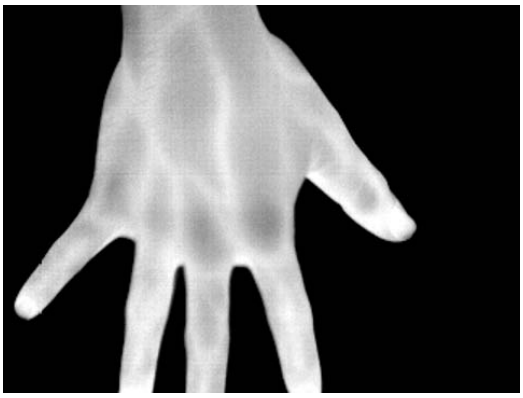

(b) Right hand for twin 1 of pair 2

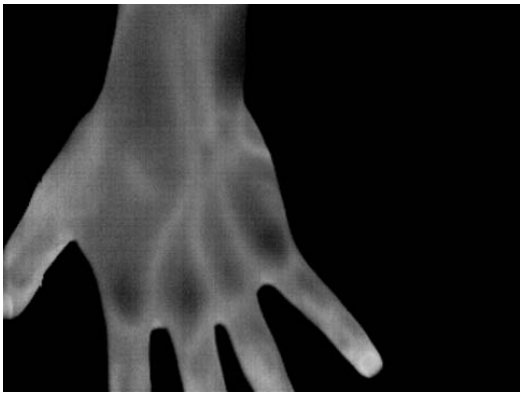

(c) Left hand for twin 2 of pair 2

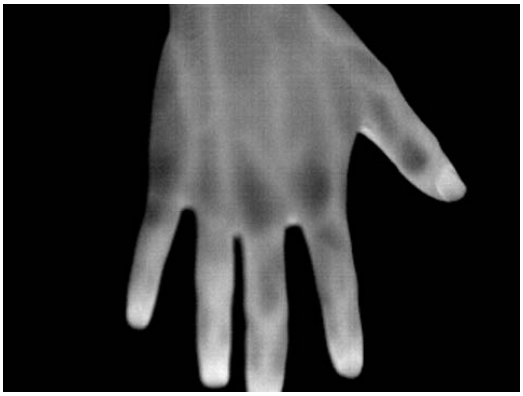

(d) Right hand for twin 2 of pair 2

Figure 7.2: Vein Pattern Images for the Left and Right Hands of Twin Pair 2

Table 7.1: Intra-Class Distance for Each Twin Individual with the Salient Point Features

Individual	Left Hand			Right Hand		
	Min	Max	Average	Min	Max	Average
Twin11	0	4.046	2.098	0	5.072	2.922
Twin12	0	5.639	3.485	0	4.279	2.496
Twin21	0	9.030	4.320	0	8.907	4.541
Twin22	0	3.456	2.021	0	4.079	1.898
Twin31	0	7.692	3.801	0	3.148	1.665
Twin32	0	6.721	3.324	0	9.301	5.062
Overall	0	9.030	3.175	0	9.301	3.097

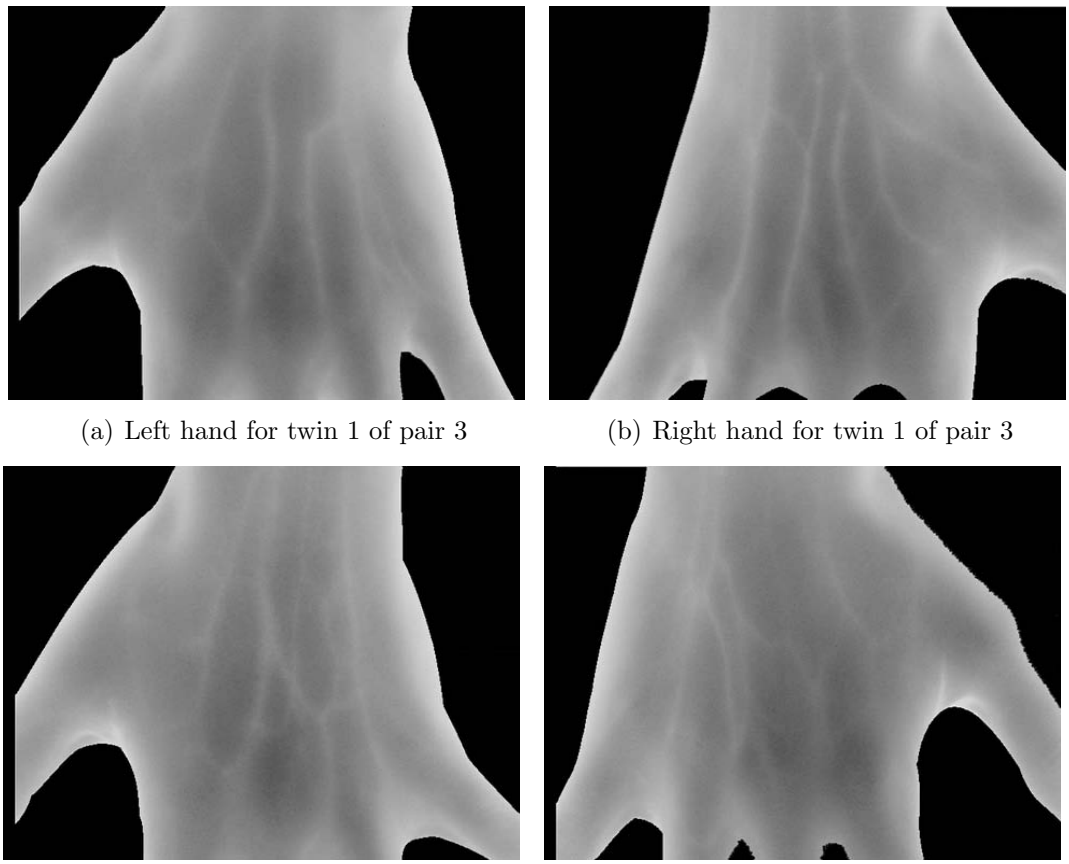

(a) Left hand for twin 1 of pair 3

(b) Right hand for twin 1 of pair 3

(c) Left hand for twin 2 of pair 3

(d) Right hand for twin 2 of pair 3

Figure 7.3: Vein Pattern Images for the Left and Right Hands of Twin Pair 3

Table 7.2: Inter-Class Distance for Each Twin Individual with the Salient Point Features

Twin Pair	Left Hand			Right Hand		
	Min	Max	Average	Min	Max	Average
Pair1	16.630	20.400	18.359	14.252	16.991	15.850
Pair2	15.963	19.244	17.246	18.684	25.787	22.042
Pair3	21.981	24.408	23.602	19.091	27.811	22.452
Overall	15.963	24.408	19.736	14.252	27.811	20.115

Table 7.3: Intra-Class Distance for Each Twin Individual with the LEM Features

Individual	Left Hand			Right Hand		
	Min	Max	Average	Min	Max	Average
Twin11	0	4.407	2.412	0	5.640	3.566
Twin12	0	5.321	3.164	0	4.686	2.753
Twin21	0	3.670	2.230	0	5.108	3.563
Twin22	0	5.007	2.853	0	4.962	2.480
Twin31	0	4.202	2.507	0	5.770	3.068
Twin32	0	5.586	3.566	0	4.835	2.883
Overall	0	5.586	2.789	0	5.770	3.052

Table 7.4: Inter-Class Distance for Each Twin Individual with the LEM Features

Twin Pair	Left Hand			Right Hand		
	Min	Max	Average	Min	Max	Average
Pair1	6.680	10.348	7.787	9.850	11.947	10.851
Pair2	10.605	11.709	11.033	8.603	13.866	11.318
Pair3	9.938	10.760	10.284	8.072	8.869	8.536
Overall	6.680	11.709	9.701	8.072	13.866	10.235

7.4 show the LHD values for the intra- and inter-class distances. It can be seen the intra-class distances are in the range of $[0 \sim 5.770]$ with averaged value of 2.921, whilst the inter-class distances are in the range of $[6.680 \sim 13.866]$ having the averaged value of 9.968. This means the genuine and intruder can be linearly separated by having a threshold values for the LHD to be somewhere between $[5.770 \sim 6.680]$ (we used 6.4, the same value used in Chapter 6). This experimental result depicts efficacy of the LEM feature in classifying identical twins' vein patterns in the back of the hand.

The experiments with the vein pattern images of the identical twins using the SPF and LEM features have shown encouraging results. It has been shown that,

within an identical twin pair, the distributions of intra-class distance and inter-class distance are separable by a hard-decision threshold value. This means that even if two persons are identical twins, they have different hand vein patterns that can be classifiable. Whilst the twin vein pattern image data is currently too limited to draw any conclusion on the uniqueness of vein patterns between identical twins, this initial study does demonstrate the potential of the hand vein pattern being genetically independent across identical twins. In order to provide stronger quantitative evidence on the uniqueness issue, a more comprehensive twin vein pattern image data set is needed, which requires another round of data collection that specifically focuses on twin participants.

7.2 Additional Issues of Vein Pattern Biometrics

Apart from the identical twins, there are several other genetic related issues requiring analysis to determine the uniqueness of hand vein patterns. One of them is the hereditary issue. Whilst the genetic information from an ancestor will pass down to the subsequent generations by inheritance, a similar question can be raised for hand vein patterns: what is the relationship between the vein patterns of different generations from the same family? It is an interesting topic to study the similarity and the potential evolvement (if any) between the vein patterns of different generations of the same family. On the other hand, it is also necessary to carry out study on siblings, even though they are not twins, for a more conclusive analysis on genetic relationship issues of the hand vein patterns.

Additional issues on the uniqueness study of vein patterns include establishing a stronger quantitative evidence for the temporal stability of the hand vein patterns. Currently, researchers believe the vein patterns will grow in a predictable manner like

fingerprints in a reasonable time span. However, this requires a more statistically sound scientific evidence, which is too large to be tackled in this study and remains an issue to be tackled in the future.

7.3 Summary

In this chapter, we mainly focus on the analysis of the similarity of hand vein patterns between identical twins. We carried out an initial study with image data from 3 pairs of identical twins. The image data showed the vein patterns in the back of the hand are visually discernible for each identical twin. Further analysis was carried out to establish computational evidence for the distinctiveness of hand vein patterns between identical twins. Separate experiments were attempted with the SPF and LEM features extracted from the vein pattern images respectively. The results showed that both types of features are capable of providing clearly separated distributions of intra- and inter-class distances. This implies the hand vein patterns between identical twins are genetically independent, and have the potential of being computationally distinguishable, even though the identical twins have the same genetic expression. Whilst the data with 3 twin pair is limited and does not lead to a firm conclusion in a strict sense, this initial study in the chapter does provide an encouraging start for the analysis of uniqueness of hand vein patterns between identical twins.

This chapter also identified several other research issues related to the uniqueness of hand vein pattern biometrics. These include a hereditary study of vein patterns within a family (both across generations and amongst siblings), as well as temporal study for the evolvement (if any) for the hand vein patterns. All these will lead to an extension of the current research topic and are of interest for the future research.

Chapter 8

Conclusions and Future Research

This chapter summarizes the work carried out and reported in this thesis. The limitations of the current approaches are also discussed. Finally, the major research issues remaining and their possible solutions are suggested for further study in the future.

8.1 Summary

The goal of this research is to investigate the potential of vein patterns being used as a biometric feature in personal verification applications. The research identifies and investigates several major issues regarding the vein pattern biometrics. These research issues are: (i). Collectibility of the vein pattern data; (ii). Processing of the vein pattern images; (iii). Identification of features for matching the vein patterns; (iv). The discriminating power of the vein patterns in biometric applications.

1. **Collectibility of the vein pattern data.**

   This thesis has investigated several imaging technologies for the purpose of acquiring vein pattern images. These include the X-ray angiogram, ultrasonic scanning, as well as infrared imaging. All three imaging technologies are capable of capturing the blood vessel images. However, the X-ray angiogram is invasive as it requires injection of contrasting agents into the blood vessels,

whilst for the ultrasonic scanning, it requires the application of a gel to the surface of the skin and the images are of lower resolution. Such constraints limit these two imaging technologies to medical practices and are not acceptable for general purpose biometric applications.

However, it is found that the IR imaging is capable of capturing images that visibly record the vein pattern structure in a non-intrusive way. The IR imaging techniques investigated in this thesis use the Far- and Near-infrared spectral ranges. These two techniques are based on different mechanisms and exhibit different properties in the images. The Far-infrared imaging captures the vein pattern images based on the fact that, in general, the blood in the veins is warmer than the surrounding tissue, and hence there is more FIR radiation emitted from the veins. Therefore, the veins in the image appear brighter than the surrounding tissue. Near-infrared imaging, however, operates on the fact that the hemoglobin in the blood absorbs more incident infrared radiation in the near-infrared range than the surrounding tissue, which results in the veins appearing darker in color than the surrounding tissue.

System setups and acquisition processes were carefully analyzed and designed for both Far- and Near-infrared imaging techniques to collect vein pattern image data for various parts of the hand, including the back of the hand, the palm, and the wrist area. The image data collected showed that Far-infrared imaging is capable of capturing the major blood vessels in the back of the hand. However, due to heat radiation and merging of IR emitted from small closely spaced veins, it has difficulty in capturing the fine vein pattern structure in the palm side and the wrist area. In addition, the FIR imaging is sensitive to ambient and body conditions. All these drawbacks make the FIR imaging only applicable to the

image acquisition of the major vein patterns in the back of the hand, and they also lead to a relatively low success rate for vein pattern capturing.

For the Near-infrared imaging technique, it can capture the vein patterns in various parts of the hand effectively with a very high success rate, including the major veins in the back of the hand, as well as the small vein structures in the palm side and the wrist area. However, it faces the problem that the images obtained are often corrupted by some visible skin features such as crease lines, hairs and scars, especially at the palm side. These unexpected skin features create problems for automatic separation of vein patterns from the images, and currently remains an issue to be tackled in the future research.

2. **Processing of the vein pattern images.**

   The processing of the vein pattern images covers the region of interest selection, image enhancement and vein pattern skeleton extraction. Several new image processing algorithms were proposed in this portion of the work.

   A methodology based on the hand landmark points described in section 4.2 was proposed to define the region of interest that is invariant to the change of hand size, which ensures the region of interest refers to the same region of different hands. Then, due to the presence of the signal dependent noise, a LLMMSE filter was utilized to remove the signal dependent noise in the infrared vein pattern images in Chapter 4. In this part of the work, we proposed a novel technique to construct the LLMMSE filter by deriving the filter parameters automatically using two image instances of the same scene, which is a major advantage over the traditional techniques that rely on a *priori* knowledge of the noise parameters. The proposed method not only can be used to remove the signal dependent noise in the vein pattern images, but also can be used in signal

dependent noise removal for any generic images.

For vein pattern skeletonization, attempts were firstly made using traditional binary skeletonization, which requires the vein pattern to be separated from the background and binarized. However, this will have the problem that the errors occurring at the binarization stage will be propagated to the subsequent skeletonization stage. In order to tackle the problem, we proposed in Chapter 5 a watershed based skeletonization algorithm to extract the skeletons of vein patterns directly from the gray-scale images. This eliminates the vein pattern image binarization stage, and hence prevents the potential errors introduced in this binarization process being propagated to the subsequent processing stages. The proposed method simulates a water immersion process over the 3-D visualized gray scale image, and it finds the skeletons of the object by building "dams" between different catchment basins. This method works well for the images with object curves separating the background into different unconnected regions. However, it is incapable of accurately extracting the skeleton of the object curve which have floating endpoints in the image.

3. **Identification of features for matching the vein patterns.**

Inspired by the fingerprint biometrics, the research firstly investigated the salient point features for the vein patterns, as similar to the traditional minutiae features for fingerprints. Extraction of the SPF is a trivial process by applying the Cross Number concept. The experiments in this work found a trend that, on average, there are 7 branch points and 6 ending points in each vein pattern image, which sum up to be 13 salient points for each vein pattern image of the back of the hand. The analysis showed the combination of the junction points and ending points provides a better performance at the matching stage

than each single type does, and the recognition accuracy reaches 0% EER on our Far-infrared hand vein pattern image database. However, the number of salient points in the vein pattern images are very much limited, which could prevent it from being used in applications with a large population. Meanwhile, its tolerance to missing salient points and geometrical displacement is low.

To overcome the weaknesses faced by the salient point features, we then proposed to use a new type of features to represent the vein patterns, which is the Line Edge Maps. The Line Edge Map is a line segment set used as a representation of the skeleton shape of the vein pattern, and is constructed by splitting each curve segment in the skeleton image of the vein pattern into individual line segments. The Line Edge Maps is richer in local structural information compared to the salient point features. The matching of two Line Edge Maps is done by calculating the Line-segment Hausdorff Distance to determine the similarity of two vein patterns. The experimental results showed that the LEM provides a high discriminating power that is comparable to the salient point features, and at the meantime, it is more tolerance to object occlusion occurred in the images. Therefore, the LEM is more preferable to the salient point features to be utilized in personal verification applications. Nevertheless, it also faces the problem of being sensitive to geometrical displacement.

4. **The study on the discriminative power of hand vein patterns in biometric applications.**

   We studied the discriminating power of the vein patterns through assessing the accuracy of general person verification with hand vein patterns. A hand vein pattern image database was carefully designed and constructed to provide a statically representative subset of the population. The experiments with this

database gave results that the verification accuracy is very high (with EER almost reaching 0%). This showed that the vein patterns do exhibit very high discriminating power in the context of person verification applications. Further efforts were taken to analyze a more advanced issue for the hand vein pattern genetic relationship study: the identical twin study. In Chapter 7, we carried out an initial study for the vein pattern similarities between identical twins. Whilst the data from twins are very limited in the experiment, the study gives a very encouraging result showing a trend that two persons' vein patterns are genetically independent and potentially computational distinguishable, even if they are otherwise visually identical twins.

Overall, the work reported in this thesis shows that the vein pattern (in the back of the hand in our work) can provide strong discriminating power for personal verification purpose and it has a very high potential to become another major biometrics, particularly when used in conjunction with other biometrics such as hand geometry, fingerprints and palm prints.

8.2 Future Research

Though promising results have been achieved on several key issues in the investigation of the potential of vein pattern biometrics, many possible extensions exist to further improve the five individual processing stages of the system defined in Section 2.6.3.

1. First of all, continuous efforts are to be put into the construction of a larger vein pattern image database to make it more representative for all possible population groups.
2. The quality of image data is vital for the application; hence more work is needed in the data preprocessing stage. The current image enhancement techniques is

not sufficient to improve the Near Infrared image quality significantly, especially when the images are heavily corrupted by many skin features such as hairs and palm prints. It is a necessary step to obtain the high quality image before the NIR vein pattern image data being used in the verification application similar to the FIR vein pattern images that have been investigated in this thesis.

3. In Chapter 5, a watershed based skeletonization algorithm is proposed to extract the skeletons of the vein patterns directly from the gray-scale images. Whist this algorithm can prevent the errors introduced at the binarization stage being propagated to the subsequent stages, it has several limitations as stated in that chapter. Further efforts are required to improve the proposed watershed based skeletonization algorithm so that, whilst retaining its capability of gray-scale skeletonization, it can also detect the skeletons for those object curves having floating endpoints in the image.
4. In Chapter 6, though the LHD measurement for the LEMs can achieve high recognition accuracy, it has the problem of having low tolerance against geometrical transformation. This imposes a requirement for us to improve the algorithm in the future so that it will be more robust in response to the variations that the feature data can have.
5. In Chapter 7, we studied the similarity of vein patterns between twins. However, additional data is required to establish a stronger computational evidence for the study. In addition, further effort is required to analyze other genetically related aspects, such as hereditary issues. Lastly, works have to be done to carry out analysis on the temporal effect on the evolvement of vein patterns.
6. Finally, attempts shall be made to integrate the vein pattern biometrics with other types of biometrics to become a multi-modal biometric system. Those

candidate biometric technologies under current investigation include hand geometry and palm-print recognition.

References

Aiazzi, B., Alparone, L., & Baronti, S. (1997). A robust method for parameter estimation of signal-dependent noise models in digital images. In *Proceedings of IEEE international conference on digital signal processing* (p. 601-604). Santorini, Greece.

Ali, J. M., & Hassanien, A. E. (2003). An iris recognition system to enhance e-security environment based on wavelet theory. *Advanced Modeling and Optimization*, *5*(2), 93-104.

Alt, H., Behrends, B., & Blomer, J. (1995). Approximate matching of polygonal shapes. *Annals of Mathematics and Artificial Intelligence*, 251-265.

Argenti, F., Torricelli, G., & Alparone, L. (May 2002). Signal-dependent noise removal in the undecimated wavelet domain. In *Proceedings of IEEE international conference on acoustics, speech, signal processing* (Vol. 4, p. 3293-3296). Orlando, USA.

Ashbourn, J. (2000). *Biometrics: Advanced identity verification.* London: Springer-Verlag.

Beurcher, S. (2007, June). *The watershed transformation page: Image segmentation and mathematical morphology.* Online (Accessed June 2007): http://cmm.ensmp.fr/ beucher/wtshed.html.

Bicz, W., Gurnienny, Z., & Pluta, M. (1995). Ultrasound sensor for fingerprints recognition. *Proceedings of SPIE: Optoelectorinc and Electronics Sensors*, *2634*, 104-111.

Bieniek, A., & Moga, A. (2000). An efficient watershed algorithm based on connected components. *Journal of Pattern Recognition*, *33*(6), 907-916.

Boles, W., & Boashash, B. (1998). A human identification technique using images of the iris and wavelet transform. *IEEE Transactions on Signal Processing*, *46*(4), 1185-1188.

Bolle, R., Connell, J., Pankanti, S., Ratha, N. K., & Senior, A. W. (2004). *Guide to biometrics.* New York: Springer-Verlag Inc.

Brink, A. (1995). Minimum saptial entropy threshold selection. *IEE Proceedings of Vision, Image and Signal Processing*, *142*(3), 128-132.

Brunelli, R., & Falavigna, D. (1993). Face recognition: Features versus templates. *IEEE Transaction on Pattern Analysis and Machine Intelligence*, *15*(10), 1042-1052.

Buddaharaju, P., Pavlidis, I., Tsiamyrtzis, P., & Bazakos, M. (2007). Physiology-based face recognition in the thermal infrared spectrum. *IEEE. Transaction on Pattern Analysis and Machine Intelligence*, *29*(4), 613-626.

Burckhardt, C. (1978). Speckle in ultrasound b-mode scans. *IEEE Transaction on Sonics and Ultras.*, *SU025*(1), 1-6.

Chellappa, R., Wilson, C., & Sironhey, S. (1995). Human and machine recogntion of faces: A survey. *Proceedings of IEEE*, *83*(5), 705-740.

Chen, Y., & Leedham, G. (2004). The multistage approach to information extraction in degraded document images. In *Proceedings of IEEE 17th international conference on pattern recognition* (p. 445-448). Cambridge, England, UK.

Chen, Y., & Leedham, G. (2005). Decompose algorithm for thresholding degraded historical document images. *IEE Proceedings on Vision, Image and Signal Processing*, *152*(6), 702-713.

Clarke, R. (1994). Human identification in information systems: Management challenges and public policy issues. *Information Technology & People*, *7*(4), 6-37.

Coetzee, L. (1992). *Fingerprint recognition.* Unpublished master's thesis, Faculty of Electronic and Computer Engineering, University of Pretoria.

Cross, J., & Smith, C. (1995). Thermographic imaging of subcutaneous vascular network of the back of the hand for biometric identification. In *Proceedings of the IEEE 29th international carnahan conference on security technology.* Sanderstead, Surrey, England.

Curlander, J., & McDonough, R. (1991). *Synthetic aperture radar: Systems & signal processing.* New York: John Wiley & Sons.

Daugman, J. (2001). Statistical richness of visual phase information: Update on recognizing persons by iris patterns. *International Journal of Computer Vision*, *45*(1), 25-38.

Dolfing, J., & Aarts, E. (1998). On-line signature verification with hidden markov models. In *Proceedings of the international conference on pattern recognition.* Tarrytown, New York, USA.

Dubuisson, M., & Jain, A. (1994). A modified hausdorff distance for object matching. In *Proceedings of 12th international conference on pattern recognition* (p. 566-568). Jerusalem, Israel.

Duda, R., & Hart, P. (January 1972). Use of the hough transformation to detect lines and curves in pictures. *Comm. ACM*(1), 11-15.

Fantini, S., & Franceschini, M. A. (2002). Frequency-domain techniques for tissue spectroscopy and imaging. *Handbook of Optical Biomedical Diagnostics*, 405-453.

Faraji, H., & MacLean, W. (2006). Ccd noise removal in digital images. *IEEE Transaction on Image Processing*, *15*(9), 2676-2685.

Frost, V., Stiles, J., Shanmugan, K., & Holtzman, J. (March, 1982). A model for radar images and its application to adaptive digital filtering for multiplicative noise. *IEEE Transaction on Pattern Analysis and Machine Intelligence*, *PAMI-4*, 157-166.

Fujitsu-Laboratories-Ltd. (2003, March 31). *Fujitsu laboratories develops technology for world's first contactless palm vein pattern biometric authentication system.* Online: http://pr.fujitsu.com/en/news/2003/03/31.html.

Gao, Y., & Leung, M. (2002a). Face recognition using line edge map. *IEEE Transaction on Pattern Analysis and Machine Intelligence*, *24*(6), 764-779.

Gao, Y., & Leung, M. (2002b). Line segment hausdorff distance on face matching. *Pattern Recognition*, 361-371.

Gonzalez, R., & Woods, R. (2002). *Digital image processing.* New Jersey: Prentice-Hall, Inc,.

Guo, Z., & Hall, R. (1992). Fast fully parallel thinning algorithms. *Comput. Vision Graphics Image Process: Image Understanding*, *55*, 317-328.

Halici, U., Jain, L., & Erol, A. (1999). An introduction to fingerprint recognition. In L. Jain, U. Halici, I. Hayashi, S. Lee, & S. Tsutsui (Eds.), *Intelligent biometric techniques in fingerprint and face recognition* (p. 3-34). Florida: CRC Press.

Harrick, N. (1962). Techniques to improve binary joint transform correlator performance for fingerprint recognition. *Applied Optics*, *33*, 2774.

Harris, D. (1992). *Infrared window and dome materials.* Bellingham, WA: SPIE.

Hawkes, P., & Clayden, D. (1993, September). *Veincheck research for automatic identification of people.* Presented in The Hand and Fingerprint Seminar at NPL.

Healey, G., & Kondepudy, R. (1994). Radiometric ccd camera calibration and noise estimation. *IEEE Transaction on Pattern Analysis and Machine Intelligence*, *16*(3), 267-276.

Hong, L., Wan, Y., & Jain, A. (1998). Fingerprint image enhancement: Algorithm and performance evaluation. *IEEE Transaction on Pattern Analysis and Machine Intelligence*, *20*(8), 777-789.

Huttenlocher, D., Klanderman, G., & Rucklidge, W. (1993). Comparing images using the hausdorff distance. *IEEE Transaction on Pattern Analysis and Machine Intelligence.*, *15*, 850-863.

Im, S.-K., Park, H.-M., Kim, S.-W., Chung, C.-K., & Choi, H.-S. (2000). Improved vein pattern extracting algorithm and its implementation. *Digest of technical papers of International Conference on Consumer Electornics.*

Jain, A. (1989). *Fundamentals of digital image processing.* Englewood Cliffs: Prentice Hall.

Jain, A., Bolle, R., & Pankanti, S. (1999). *Biometrics: Personal identification in networked society.* Dordrecht: Kluwer Academic Publishers.

Jain, A., & Duta, N. (1999). Deformable matching of hand shapes for user verification. In *Proceedings of the international conference on image processing (icip)* (p. 857-861). Kobe, Japan.

Jain, A., Hong, L., Pankanti, S., & Bolle, R. (1997). An identity authentication system using fingerprints. *Proceedings of IEEE*, *85*(9), 1365-1388.

Jain, A., Pankanti, S., Prabhakar, S., & Ross, A. (2001). Recent advances in fingerprint verification. *Lecture Notes Comput. Sci*, *2091*, 182-190.

Jain, A., Prabhakar, S., Hong, L., & Pankanti, S. (2000). Filterbank-based fingerprint matching. *IEEE Transaction on Image Process.*, *9*(5), 846-859.

Jain, A., Ross, A., & Pankanti, S. (1999). A prototype hand geometry-based verification system. In *Proceedings of the 2nd international conference on audio- and video-based biometric person authentication (avbpa)* (p. 166-171). Washington D.C., USA.

Janesick, J. (2001). *Scientific charge-coupled devices.* Bellingham, WA: SPIE.

Kong, W., Zhang, D., & Lu, G. (2006). A study of identical twins' palmprints for personal verification. *Pattern Recognition*, 2149-2156.

Kuan, D., Sawchucli, A., Strand, T., & Chavel, P. (1985). Adaptive noise smoothing filter for images with signal-dependent noise. *IEEE Transaction on Pattern Analysis and Machine Intelligence*, *7*(2), 165-177.

Lay, Y. L. (2000). Hand shape recognition. *Optics and Laser Technology*, *32*, 1-5.

Lee, J. (May 1986). Speckle suppression and analysis for synthetic aperture radar images. *Optical Engineering*, *20*, 636-643.

Lin, C.-L., & Fan, K.-C. (2004). Biometric verification using thermal images of palm-dorsa vein patterns. *IEEE Transaction on Circuits and Systems for Video Technology*, *14*(2), 199-213.

Luis-Garcia, R. de, Alberola-Lopez, C., Agahzout, O., & Ruiz-Alzola, J. (2003). Biometric identificaiton systems. *Signal Processing*, *83*(12), 2539-2557.

MacGregor, P., & Welford, R. (1991). Veincheck: Imaging for security and personnel identification. *Advanced Imaging*, *6*(7), 52-56.

Miura, N., Nagasaka, A., & Miyatake, T. (2004). Feature extraction of finger-vein patterns based on repeated line tracking and its application to personl identification. *Machine Vision and Applications*, *15*, 194-203.

Nalwa, V. (1997). Automatic on-line signature verification. *Proceedings of IEEE*, *85*(2), 215-239.

Nanavati, S., Tieme, M., & Nanavati, R. (2002). *Biometrics: Identity verification in a networked world, a wiley tech brief.* New York: John Wiley & Sons, Inc.

Newham, E. (1995). *The biometric report.* New York: SJB Services.

NIST. (2000). *American national standard for information systems - data format for the interchange of fingerprint, facial, and scar mark and tatto (smt) information* (Vol. 1-2000). ansi-itl.

Nora, J., & Fraser, F. (1994). *Medical genetics: Principles and practice* (4th ed.). Philadelphia: Lea & Febiger.

Oden, C., Ercil, A., & Buke, B. (2003). Combining implicit polynomilas and geometric features for hand recognition. *Pattern Recognition Letters*, *24*, 2145-2152.

Ong, M. G. K., Connie, T., Jin, A. T. B., & Ling, D. N. C. (2003). A single-sensor hand geometry and palmprint verification system. In *Proceedings of the 2003 ACM SIGMM workshop on biometrics methods and applications.* Berkeley, California, USA.

Otsu, N. (1979). A threshold selection method from gray-level histograms. *IEEE Transaction on Systems, Man and Cybernetics*, *9*(1), 62-66.

Paranjape, R., Mahovsky, J., Benedicenti, L., & Koles, Z. (2001). The electoencephalogram as a biometric. In *Proceedings of the canadian conference on electrical and computer engineering* (p. 1363-1366). Winnipeg, Manitoba, Canada.

Phillips, P. (1999). Support vector machines applied to face recognition. In *Technical report, nistir 6241.* National Institute of Standards and Technolgoy.

Phillips, P., Martin, A., Wilson, C., & Przybocki, M. (2000). An introduction to evaluating biometric systems. *Computer*(2), 56-63.

Pratt, W. (1991). *Digital image processing.* New York: J. Wiley.

Ratha, N., Chen, S., & Jain, A. (1995). Adaptive flow orientation based feature extraction in fingerprint images. *Pattern Recognition*, *28*(8), 799-813.

Ratha, N., Senior, A., & Bolle, R. (2001). Tutorial on automated biometrics. In *Proceedings of international conference on advances in pattern recognition.* Rio de Janeiro, Brazil.

Reynolds, D. (2002). Automatic speaker recognition: Current approaches and future trends. In *Proceedings of IEEE autoid 2002* (p. 103-108). Tarrytown, New York, USA.

Ruchlidge, W. (1997). Efficiently locating objects using hausdorff distance. *International Journal of Computer Vision*, *24*, 251-270.

Samaria, F., & Harter, A. (1994). Parameterisation of a stochastic model for human face identification. In *Procceedings of 2nd IEEE workshop on application s of computer vision.* Sarasota FL.

Sebastian, T. B., & Kimia, B. B. (2005). Curves vs. skeletons in object recognition. *Signal Processing*, *85*, 247-263.

Sijbers, J., Dekker, A. den, Audekerke, J. V., Verhoye, M., & Dyck, D. V. (1998). Estimation of the noise in magnitude mr images. *Magnetic Resonance Imaging*, *16*(1), 87-90.

Solihin, Y., & Leedham, C. G. (1999). Integral ratio: A new class of global thresholding techinques for handwriting images. *IEEE Transaction on Pattern Analysis and Machine Intelligence*, *21*(8), 761-768.

Srihari, S., H. Cha s., Arora, H., & Lee, S. (2002). Individuality of handwriting. *Journal of Forensic Sciences*, *47*(7), 1-17.

Stosz, J., & Alyea, L. (1993). Automated system for fingerprint authentication using pores and ridge structure.

Sweeney, E. (1998). Veincheck - a technical perspective. *Information Security Techincal Report*, *3*(1), 47-51.

Turk, M., & Pentland, A. (1991). Eigenfaces for recognition. *Journal of Cognitive Neuro Science*, *3*(1), 71-86.

Veres, G., Nixon, M., & Carter, J. (2006). Is enough enough? what is sufficiency in biometric data? *Lecture Notes Computer Science, Image Analysis and Recognition*, *4142*, 262-273.

Wang, L., & Leedham, C. G. (2005). A thermal hand vein pattern verification system. In S. Singh, M. Singh, C. Apte, & P. Perner (Eds.), *Pattern recognition and image analysis* (Vol. 3687, p. 58-65). Springer.

Wang, L., & Leedham, C. G. (2006). Near- and far- infrared imaging for vein pattern biometrics. In *Proceedings of IEEE international conference on advanced video and signal based surveillance* (p. 52). Sydney, Australia.

Wang, L., & Leedham, C. G. (2007a). An improved smoothed watershed algorithm for gray-scale skeletonization of thermal vein patterns. In *International workshop on advanced image technology.* Bangkok, Thailand.

Wang, L., & Leedham, C. G. (2007b). A watershed algorithmic approach for gray-scale skeletonization in thermal vein pattern biometrics. In Y. Wang, Y. Cheung, & H. Liu (Eds.), *Lecture notes in artificial intelligence* (Vol. 4456, p. 935-942). Berlin Heidelberg: Springer-Verlag.

Wang, L., Leedham, C. G., & Cho, S.-Y. (2007a). Deriving filter patermeters using dual-images for image de-noising. In *Proceedings of the IEEE 2007 international symposium on intelligent signal processing and communication systems (ispacs 2007).* Xiamen, China. (Accepted)

Wang, L., Leedham, C. G., & Cho, S.-Y. (2007b). Minutiae feature analysis for infrared vein pattern biometrics. *Pattern Recognition.* (Accepted)

Wang, L., Leedham, C. G., & Cho, S.-Y. (2008). Automatic signal-dependent noise removal for infrared vein pattern images. *Machine Vision and Applications.* (Under Review)

Wayman, J. (1997). Generalized biometric identification model. In *Proceedings of the 31st IEEE asilomar conference on signals, systems and computing.* Pacific Grove, CA.

Wong, L., & Shi, P. (2002). Peg-free hand geometry recognition using hierarchical geometry and shape matching. In *Proceedings of the IAPR workshop on machine vision applications* (p. 281-284). Nara, Japan.

Woodward, J., Orlans, N., & Higgins, P. (2003). *Biometrics: Identity assurance in the information age.* New York: McGraw-Hill/Osborne.

Yim, P., Choyke, P., & Summers, R. (2000). Gray-scale skeletonization of small vessels in magnetic resonance angiography. *IEEE Transaction on Medical Imaging*, *19*(6), 586-576.

Yu, H. (2004). *Morphologcail image segmentation for co-aligned multiple images using watersheds transformation.* Master Thesis. The Florida State University.

Appendix A

Infrared Vein Pattern Image Data Collection Protocol

A.1 Overview

The Forensics and Security Laboratory in the Nanyang Technological University (NTU) Singapore has multiple projects in progress in the field of biometrics. In order to evaluate and improve the methodologies utilized in these projects, the author and 2 other colleagues proposed and organized a series of biometric data collection events in the NTU campus during April 2006. The focus of the data collection events aimed to collect the infrared hand vein pattern images from the participants, and in the meantime, to collect facial expression and palm-print images to support two other projects that are currently in progress in the FORSE Lab.

Throughout process of the hand vein pattern image collection, the author will attempt to accomplish the following:

1. To collect the FIR images for the vein patterns in the back of the hand.
2. To collect the NIR images for the vein patterns in the back of the hand, the palm, the wrist region.
3. To assess the capability of FIR imaging in capturing the vein patterns in other

parts of the hand.

A.2 Data Collection Procedures

A.2.1 The Venue

The choice of the location for data collection is limited by many factors such as cost, time and labors. In this project, the data collection was carried out on the main campus of NTU. A positive aspect of NTU to the project is that the university has a large community of international students and staffs, with over 7800 students from more than 80 countries, accounting for nearly 1/3 of the overall student population in the university. This provides a good opportunity to study the vein patterns in a larger racial mix. The specific venue of the data collection is in the main building (a normal office environment with air conditioning) of the School of Computer Engineering, next to the school's general office, where the pedestrian flow is heavy.

A.2.2 The Time

The data collection practice lasted for a week's time between 9th to 15th April 2006.

A.2.3 The Sample

The samples were chosen by randomly inviting the volunteers from pedestrians passing by our data collection station. Veres et. al. (Veres et al., 2006) propose a computational approach to estimate the subject size for statical significance. Their paper provides mathematical equations to calculate the sample and subject size. Nevertheless, the parameters in these equations are estimated from existing large databases. This is a problem for constructing the vein pattern database, because there are no publicly available database on vein pattern images. Therefore, we try to collect as

many samples as possible, and due to the time constraint, the target for the minimum number of subjects is set to 150 participants.

A.2.4 Instruments

The instruments prepared for the data collection include the imaging devices, a meta data recording program, and consent forms.

The Imaging Devices:

1. The Equipments. There are two sets of equipments used for data collection. One is for capturing FIR images, and the other is for NIR images.

    - For FIR imaging, the equipments include: *(i).* an NEC Thermo Tracer TS7302; *(ii).* A "Hama" brand copy-stand; *(iii).* A thermo Workbench software for conversion the temperature information into images. (iv). A workstation for receiving and storing the image data.
    - For NIR imaging, the equipments used are: *(i).* A Hitachi KP-F2A infrared CCD camera; *(ii).* Three pieces of infrared filters with cutoff frequencies $720nm$, $800nm$ and $900nm$, where the one with $800nm$ are used for data collection and the other two are experimental purposes. *(iii).* A "Hama" brand copy-stand; *(iv).* Two infrared LED lamps peaked at $800nm$. *(v).* A Matrox Meteor-II/Digital frame grabber card. *(vi).* A workstation for receiving and storing the image data.

2. The systems' setup.

    - For FIR imaging, the thermal camera is mounted to the copy-stand, and is adjusted to a height of approximately $30cm$ above the base of the copy-stand. The camera is connected to the workstation for data transmission.

- For NIR imaging, the two infrared lamps are fixed to both sides of the lamp handles of the copy-stand; then the camera with the 800nm filter mounted in its front is mounted to the copy-stand and adjusted to the position that is approximately 60cm above the base of the copy-stand. The camera is then connected to the station for data transmission.

The Meta Data Recording Program:

We have developed a MS Access based programming to record the meta data for the participants' particulars. The main information we collected from the participants are: *(i).* The name; *(ii).* Gender; *(iii).* Age range; *(iv).* Occupation; *(v).* Race group; *(vi).* Matriculation/IC number. The participants are to key in those information prior to the data collection, and a non-repeating number will be automatically generated by the program as a unique ID for the participant and his/her image data. Figure A.1 shows the user interface of the program.

Consent Forms:

This form is to serve as the legal document giving the author the right to use the image data collected. Each participant will have to sign the form before the enrollment process, and he/she has to indicate whether they wish to have his/her image data published in any form of publication. A sample consent form is shown in Figure A.2.

A.2.5 Time Frame for Data Collection

1. Initiation of the data collection practice.

   Data Collection Team:

   - Installation of image acquisition systems;
   - Assign responsibilities for FIR/NIR imaging systems, meta data recording

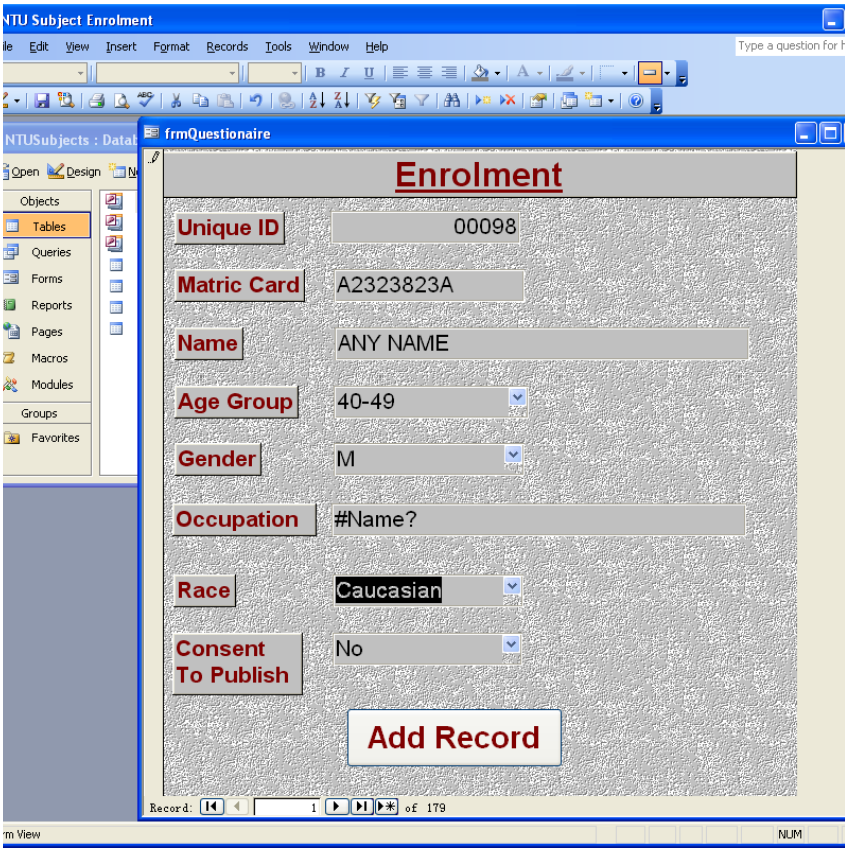

Figure A.1: The user interface of the meta data recording program.

and consent forms;

- Inviting the participants from the pedestrians.

2. Meta data input.

   Participants: The participant keys in the personal particular.

3. Signing consent forms.

   Participants: The participant signs the consent form.

4. Taking FIR images.

   Participants:

   - The participant approaches the FIR image collection station with hands dry.
   - The participant places the left hand on the base of the copy-stand with the

Participant Consent Form

The purpose of this data collection study is to evaluate the design of the techniques and algorithm for numerous projects at Forensics and Security Research Laboratory in Nanyang Technological University, Singapore. We are interested in collecting images of hands and faces from volunteers. The session is not designed to test/evaluate your ability in any manner. Please be advised that there are no risks associated with participation in this session.

During this session, you will be photographed for collecting images of hands and faces. This includes optical, near and far infra-red images of both sides of your hands and wrist area as well as face images. The whole process takes less than 10 minutes per person using four sets of imaging equipment.

If for any reason you are uncomfortable during the session and do not want to complete a task, you may say so and we will move on to the next task. In addition, if you do not want to continue, you may end the session and leave at any time.

Approximately 200 people will participate in this study. The data collected will be used for experiments for investigating novel biometric and security projects. Your name and ID is used on the collection stage only to ensure there are no double entries in the database and will not be included in the report nor will your name be associated with any session data collected.

If you wish to speak with someone about your participation in this study, or if you feel you were not treated as described above, please contact Vladimir at vpervouchine@gmail.com.

I, _____, have read and fully understand the extent of the study and any risks involved. All of my questions, if any, have been answered to my satisfaction. My signature below acknowledges my understanding of the information provided in this form and indicates my willingness to participate in this data collection session. I allow my collected data to be used for research purposes and be included in publications of research results. I have been given a blank copy of this consent form for my records.

☐ I **DO NOT** wish to have the face images collected to be published in any form of publications.

Signature:_____ Date:_____

Figure A.2: The consent form to be filled by the participants before enrollment.

back of the hand facing up.

- The thermal camera captures three images.

5. Taking NIR images.

   Participants:

   - The participant approaches the NIR image collection station.
   - The participant places the left hand on the base of the copy-stand with the back of the hand facing up.
   - The NIR camera captures three images for the back of the hand.
   - The participant flips the left hand with the palm side facing up.
   - The NIR camera captures three images for the palm.
   - The participant moves the left hand so that the wrist region is in the center of the base of the copy-stand.
   - The NIR camera captures three images for the wrist region.
   - Repeat the same procedure for right hands.